

An Extensive Study of Soft Materials Containing Carboxylic Acid Moieties to Determine
Hydrogen Bond Energies Using Analytical and Theoretical Methods

by

Amanda C. Sacco

Submitted in Partial Fulfillment of the Requirements

for the Degree of

Master of Science

in the

Chemistry

Program

YOUNGSTOWN STATE UNIVERSITY

August, 2015

An Extensive Study of Soft Materials Containing Carboxylic Acid Moieties to Determine
Hydrogen Bond Energies Using Analytical and Theoretical Methods

Amanda C. Sacco

I hereby release this thesis to the public. I understand that this thesis will be made available from the OhioLINK ETD Center and the Maag Library Circulation Desk for public access. I also authorize the University or other individuals to make copies of this thesis as needed for scholarly research.

Signature:

Amanda C. Sacco, Student

Date

Approvals:

Dr. Ganesaratnam K. Balendiran, Thesis Advisor

Date

Dr. Larry S. Curtin, Committee Member

Date

Dr. Brian D. Leskiw, Committee Member

Date

Dr. Salvatore A. Sanders, Dean of Graduate Studies

Date

©

Amanda C. Sacco

2015

Thesis Abstract

Although the three projects presented within this thesis vary considerably, there is one theme throughout all of them: use of compounds containing carboxylic acids to determine hydrogen bond energies. Carboxylic acids are an important component of various chemicals and the reactions in which they are involved. Understanding the energies of the hydrogen bonds that are a part of carboxylic acid groups is of high importance, since they can greatly influence the affects that drugs have within the body, including at what point a compound may begin to be metabolized. The other substituents within a compound may influence this factor as well, making the entire research problem compound dependent. However, a variety of chemicals involved in this biophysical research will be studied to determine if their physical bonding properties can be classified according to certain characteristics inherent to the molecules themselves or within the situations and environments in which each are observed.

This project uses multiple forms of analytical testing to gather information, including Raman spectroscopy, Fourier transform-infrared spectroscopy, powder x-ray diffraction, nuclear magnetic resonance, and bomb calorimetry. Additionally, a computational modeling approach provided theoretical data with which results can be compared, specifically for the first project presented in this work. It's found that many of the methods observed results that greatly paralleled one another and conclusions could be deduced. Comparison of results to what has been experimentally and theoretically found in the literature give great insight into differences in results amongst methodology as well. Nonetheless, this research project presents various methods with which potential extrapolation of hydrogen bond energies can be performed.

Acknowledgements

I extend my deepest gratitude and appreciation to everyone who has aided me in completing my master's degree and research toward this thesis. I would like to thank Dr. Balendiran for allowing me to work on this intriguing research project and believing in my ability to perform any assigned task. Additionally, I'd like to extend a sincere thank you to Dr. Leskiw for sharing his knowledge of physical chemistry and life in general and passing that on to me; I've truly enjoyed having you as a professor and mentor over the years. Dr. Curtin, I'm very appreciative of you joining my thesis committee as well and for teaching me how to keep a good lab notebook. Dr. Mettee, thank you for instructing me on how to flame seal NMR tubes, how to use the Spartan computer modeling system, and for allowing me to use the bomb calorimeter. These were essential to my research projects, and I'm so grateful for all of your help.

Furthermore, I'd like to thank the Youngstown State University Department of Chemistry for allowing me to utilize their resources and major pieces of equipment needed for my research. I'd also like to thank Ray Hoff for being so helpful with my incessant need to understand and use all of our instrumentation, especially with the NMR. Furthermore, I extend a sincere thanks to Dr. Damodaran Krishnan for his help with my NMR experiments and measurements. Additionally, I am extremely appreciative for the School of Graduate Studies and Research along with the committee awarding the Cushwa/Commercial Shearing Graduate Fellowship for allowing me to further my education while being fully financially supported. Finally, I'd like to acknowledge Grant DK085496 from National Institutes of Health, the Department of Energy/National

Energy Technology Laboratory, and the American Diabetes Association for their funding toward my research projects.

I know that this entire experience would not have been the same had it not been for the entire Balendiran lab and all of my fellow master's students. Heather, I envy your synthesis skills and know that you'll be successful at everything you accomplish in life. Thank you for being a great friend and workout partner. Dan, I appreciate all of the help and advice you gave me throughout my time in this program. DaVena, you are such a fun person, and I will definitely miss our good conversations. Niloufar, you are a very sweet individual and I wish you the best in all that you do. Emeka, you really are the face of the lab! I will miss your crazy antics. Additionally, I'd like to extend a special thanks to all of the undergraduate students who have helped me complete my research projects, especially Victoria Rumph and Victoria Boulos. I really appreciate your support and involvement with the research at hand. You are all wonderful chemists and amazing people.

As for my entire family, I'm very appreciative of your unconditional love and support, especially in my academic career. I'm so grateful for your encouragement throughout my schooling, especially during my undergraduate and master's degrees. It means so much to me. Marcell, you really are my best friend, and I am so lucky to have met you. Thank you for always listening and being there for me. I hope that I have made you all proud, and I hope that you enjoy reading this thesis.

Table of Contents

Title Page.....	i
Signature Page.....	ii
Copyright Page.....	iii
Abstract.....	iv
Acknowledgments.....	v
Table of Contents.....	vii
List of Tables.....	ix
List of Figures.....	x
List of Symbols and Abbreviations.....	xii
Chapter 1 Purpose of the Research Projects.....	1
1.1 An Overview of Hydrogen Bonding	1
1.2 A Background on Carboxylic Acids.....	3
Chapter 2 Statement of the Overall Research Problem.....	8
2.1 Solid State Pharmaceuticals and Their Behaviors.....	8
2.2 Studies on Hydrogen Bonds and Carboxylic Acids.....	10
Chapter 3 Analysis of Aspartic and Glutamic Acids in a Potassium Chloride Matrix Using a Variety of Methods.....	15
3.1 Background Information.....	15
3.2 Raman Spectroscopy.....	22
3.3 Fourier Transform Infrared Spectroscopy.....	25
3.4 Powder X-Ray Diffraction.....	29
3.5 Theoretical Calculations.....	33
3.6 Experimental Methods.....	36

	3.7 Results.....	40
	3.8 Discussion.....	63
	3.9 Future Work.....	71
Chapter 4	NMR Dimerization and Dissociation Studies of Fibrates.....	73
	4.1 Background Information.....	73
	4.2 Fibrate Derivatives.....	75
	4.3 Nuclear Magnetic Resonance	78
	4.4 Experimental Methods.....	91
	4.5 Results.....	95
	4.6 Discussion.....	100
	4.7 Future Work.....	101
Chapter 5	Use of Bomb Calorimetry to Probe Hydrogen Bond Energies and General Energy Comparisons within Fifty Compounds.....	102
	5.1 Background Information.....	102
	5.2 Calorimetry.....	103
	5.3 Experimental Methods.....	117
	5.4 Results.....	122
	5.5 Discussion.....	159
	5.6 Future Work.....	170
Chapter 6	Conclusions and Future Studies on Hydrogen Bonding Energies...	172
Appendix A	Supplementary Material from Praveen Bandarupalli's Thesis.....	173
Appendix B	Use of Spartan '04 Computer Program Input	177
	Works Cited.....	179

List of Tables

Table 3.1 Asp (A) Complex Bond Lengths.....	45
Table 3.2 Asp (B) Complex Bond Lengths.....	46
Table 3.3 Asp (C) Complex Bond Lengths.....	47
Table 3.4 Asp (D) Complex Bond Lengths.....	48
Table 3.5 Glu 1 Bond Lengths.....	49
Table 3.6 Glu 2 Bond Lengths.....	51
Table 3.7 Glu 3 Bond Lengths.....	53
Table 3.8 Glu 4 Bond Lengths.....	55
Table 3.9 Polyaspartic Acid Bond Lengths.....	57
Table 3.10 Polysuccinimide Bond Lengths.....	58
Table 3.11 Pyroglutamic Acid Bond Lengths.....	59
Table 3.12 Polyglutamic Acid Bond Lengths.....	61
Table 3.13 Gibb's Free Energy for Hartree-Fock and Density Functional Theories with Percent Differences.....	62
Table 3.14 Gibb's Free Energy for Prior Suggested Thermal Decomposition Intermediates Using Hartree-Fock and Density Functional Theories with Percent Differences.....	62
Table 4.1 How the Number of Protons and Neutrons effects the Value of I	70
Table 5.1 Average ΔU and ΔH Values of Selected Amino Acids.....	132
Table 5.2 Average ΔU and ΔH Values of Aspartic and Glutamic Acids in a 2:1 Compound to Benzoic Acid Ratio.....	138
Table 5.3 Average ΔU and ΔH Values of Aspartic and Glutamic Acids in a 1:1 Compound to Benzoic Acid Ratio.....	139
Table 5.4 Average ΔU and ΔH Values of Aspartic and Glutamic Acids in a 1:2 Compound to Benzoic Acid Ratio.....	139
Table 5.5 Average ΔU and ΔH Values of Dipeptides.....	141
Table 5.6 Average ΔU and ΔH Values of Fibrate Derivative Compounds.....	143
Table 5.7 Average ΔU and ΔH Values of Borneol and Camphor.....	146
Table 5.8 Average ΔU and ΔH Values of Benzophenone and Biphenyl.....	147
Table 5.9 Average ΔU and ΔH Values of Assorted Analogous Compounds.....	149
Table 5.10 Average ΔU and ΔH Values of Benzimidazole and Imidazole.....	152

Table 5.11 Average ΔU and ΔH Values of Salicylic Acid Based Compounds.....	152
Table 5.12 Average ΔU and ΔH Values of Low Acyl Gellan Gum and Individual Components in a 2:1 Compound to Benzoic Acid Ratio.....	155
Table 5.13 Average ΔU and ΔH Values of Low Acyl Gellan Gum and Individual Components in a 1:1 Compound to Benzoic Acid Ratio.....	156
Table 5.14 Average ΔU and ΔH Values of Low Acyl Gellan Gum and Individual Components in a 1:2 Compound to Benzoic Acid Ratio.....	156
Table 5.15 Average ΔU and ΔH Values of Cellulose, Plastic, and Starch Polymers.....	157
Table 5.16 Average ΔU and ΔH Values of <i>trans</i> -4-Hydroxy-L-Proline and <i>trans</i> -Cinnamic Acid.....	158

List of Figures

Figure 1.1 Example of Double Energy Well Potential.....	3
Figure 1.2 Structure of the Hydronium Ion.....	4
Figure 1.3 Dimerization of Two Carboxylic Acid Functional Groups	5
Figure 1.4 Molecular Structure of Bilirubin.....	7
Figure 3.1 Aspartic Acid (left) and Glutamic Acid (right) Structures.....	16
Figure 3.2 Illustration of Quantum Energy Transitions for Rayleigh and Raman Scattering.....	23
Figure 3.3 Illustrative Process of FT-IR Sample Analysis	27
Figure 3.4 Layout of a Typical FT-IR Spectrometer	27
Figure 3.5 Sample Raman Spectrum for the 237 Asp 50 Mixture.....	41
Figure 3.6 Sample FT-IR Spectrum for the 237 Asp 50 Mixture.....	42
Figure 3.7 Sample Powder XRD Spectrum for the 237 Asp 50 Mixture (x-axis is 2θ and y-axis is intensity).....	43
Figure 3.8 Asp (A) Complex with Minimized Energy before Calculation.....	44
Figure 3.9 Asp (B) Complex with Minimized Energy before Calculation.....	46
Figure 3.10 Asp (C) Complex with Minimized Energy before Calculation.....	47
Figure 3.11 Asp (D) Complex with Minimized Energy before Calculation.....	48
Figure 3.12 Glu 1 Complex with Minimized Energy before Calculation.....	49
Figure 3.13 Glu 2 Complex with Minimized Energy before Calculation.....	50
Figure 3.14 Glu 3 Complex with Minimized Energy before Calculation.....	52

Figure 3.15 Glu 4 Complex with Minimized Energy before Calculation.....	54
Figure 3.16 Polyaspartic with Minimized Energy before Calculation.....	56
Figure 3.17 Polysuccinimide with Minimized Energy before Calculation.....	58
Figure 3.18 Pyroglutamic Acid with Minimized Energy before Calculation.....	59
Figure 3.19 Polyglutamic Acid with Minimized Energy before Calculation.....	60
Figure 4.1 Energy Levels for a Nucleus Having a Spin Quantum Number of $\frac{1}{2}$	80
Figure 4.2 Structure of Clofibric Acid with Peak Assignments (in ppm).....	86
Figure 4.3 ^1H NMR Entire Spectrum of 20 mg Clofibric Acid Sample.....	96
Figure 4.4 ^1H NMR Close-Up of Shifting Peaks of 20 mg Clofibric Acid Sample.....	97
Figure 4.5 ^1H NMR Entire Spectrum of 1:1 Clofibric Acid: Potassium Chloride Sample.....	98
Figure 4.6 ^1H NMR Close-Up of Shifting Peaks of 1:1 Clofibric Acid:Potassium Chloride Sample.....	99
Figure 5.1 Sample of a Bomb Calorimetry Data Graph.....	107
Figure 5.2 General Set-up of a Bomb Calorimeter.....	119
Figure 5.3 Close-Up Illustration of Sample Holder and Fuse Wire.....	120
Figure 5.4 Data Graph for Trial One of Borneol.....	123
Figure A.1 Overlay of PSI Plots of Reaction Rate Profiles of Aspartic Acid Samples versus Temperature.....	173
Figure A.2 Overlay of DSC Plots of Aspartic Acid Samples Showing Heat Flow versus Temperature.....	173
Figure A.3 Proposed Thermal Decomposition Reactions of Aspartic Acid Samples....	174
Figure A.4 Possible Binding modes of K^+ ion to Aspartic Acid Ligand Referring to Asp A through Asp D.....	174
Figure A.5 Overlay of PSI Plots of Reaction Rate Profiles of Glutamic Acid Samples versus Temperature.....	175
Figure A.6 Overlay of DSC Plots of Glutamic Acid Samples Showing Heat Flow versus Temperature.....	175
Figure A.7 Proposed Thermal Decomposition Reactions of Glutamic Acid Samples...	176
Figure A.8 Possible Binding modes of K^+ ion to Glutamic Acid Ligand Referring to Glu 1 through Glu 4.....	176
Figure B.1. Example of Spartan '04 Calculations Prompt Box.....	177

List of Symbols and Abbreviations		cm^{-1}	per centimeter
NMR	Nuclear Magnetic Resonance	VT-NMR	Variable Temperature Nuclear Magnetic Resonance
XRD	X-Ray Diffraction		
FT-IR	Fourier Transform Infrared Spectroscopy	Ccal	Heat Capacity of the Calorimeter
pKa	Acid Dissociation Constant	ΔU	Internal Energy
		Δn	Change in moles
GIBMS	Guided Ion Beam Tandem Mass Spectrometry	ΔH	Heat of Formation
		Asx	Aspartic Acid and Asparagine
ESI	Electrospray Ionization	Glx	Glutamic Acid and Glutamine
HPLC	High Performance Liquid Chromatography		
		SNR	Signal-to-Noise Ratio
DSC	Differential Scanning Calorimetry	Θ	Angle of Incidence of the X-Ray
TGA	Thermogravimetric Analysis	n	Integer
		λ	Wavelength
GC	Gas Chromatography		
HF	Hartree-Fock Theory	d	Spacing between layers of atoms
DFT	Density Functional Theory	ARI	Aldose Reductase Inhibitor
Asp	Aspartic Acid	LDL	Low Density Lipoprotein
Glu	Glutamic Acid	HDL	High Density Lipoprotein
CID	Collision-Induced Dissociation	iPr	Isopropyl
GPC	Gel Permeation Chromatography	I	Nuclear Spin Quantum Number
IRMPD	Infrared Multiple Photon Dissociation	δ	Chemical Shift
		f	Mole Fraction
Å	Angstroms	BA	Benzoic Acid
°C	degrees Celsius	Fe	Iron
nm	nanometers	ΔT	Change in Temperature

Chapter 1: Purpose of the Research Projects

1.1 An Overview of Hydrogen Bonding

To fully appreciate the purpose of these projects, one must realize the importance of hydrogen bonding within (intramolecular) and between (intermolecular) compounds. In fact, is it possible for patterns of hydrogen bonding energies to emerge? For example, it is known that salicylic acid contains intramolecular hydrogen bonding caused by a fairly acidic hydrogen and an electronegative atom. Various analytical methods have been used to prove this concept. However, not all compounds can be as predictable, especially in dilute solutions or in an environment that causes their usual behavior to be atypical.¹ Also, in systems where polar solvents like water are present, competition can occur in order to form the most stabilized three-dimensional structure. Polar solvents cause greater hydrogen bonding when two oppositely charged species are present as a donor and as an acceptor. Specifically, polar protic solvents like water and methanol provide an important contribution to these bonding behaviors.² Generally, hydrogen bonds are characterized by their physical and geometric properties, relying on graph sets to give insight toward many inherent factors, such as molecular configurations.¹ Hydrogen bonds are attractive forces between a proton donor and acceptor, and they contribute to the shape and function of molecules, including water, deoxyribonucleic acid (DNA), proteins, and other large chemical systems. The electrostatic, induction, electron delocalization, exchange repulsion, and dispersion interactions all cause attraction to be present and hydrogen bonding to occur. Usually, the main contributor is electrostatic with the proton donor and acceptor being of similar basicity in order to form the most stable

bond. Additionally, when resonance forms have nearly identical energies, hydrogen bonding adds stabilization which is important especially in biological systems.³

Linus Pauling referred to hydrogen bonds as being “an interaction that directs the association of a covalently bound hydrogen atom with one or more other atoms, groups of atoms, or molecules into an aggregate structure that is sufficiently stable to make it convenient for the chemist to consider it as an independent chemical species.”¹

Additionally, Jeffrey and Saenger noted that “the hydrogen bond is the most important intra- and intermolecular cohesive force determining geometry, mode of recognition and association of biological molecules.”² Therefore, understanding the energies of hydrogen bonds within molecules provides a vast amount of information on both its chemical and physical properties. Structurally, hydrogen bonding should occur with one or two minima present when a hydrogen is in motion between two donor atoms. A potential energy surface showing one minimum indicates a symmetrical hydrogen bond caused by it being directly between the two donor atoms. When two minima are present, the hydrogen atom is considerably closer to one of the donor atoms providing an asymmetry as represented by a double energy well potential. An illustration of this is provided in Figure 1.1 on the next page. This picture shows a double-well potential in which the atom is located at an equilibrium position having minimum energy.⁴ In fact, short, strong hydrogen bonds are present at low barriers with small donor separations causing the added strength. However, experimental evidence more often shows a constant shifting of equilibrium indicating asymmetrical hydrogen bonds in most environments.³

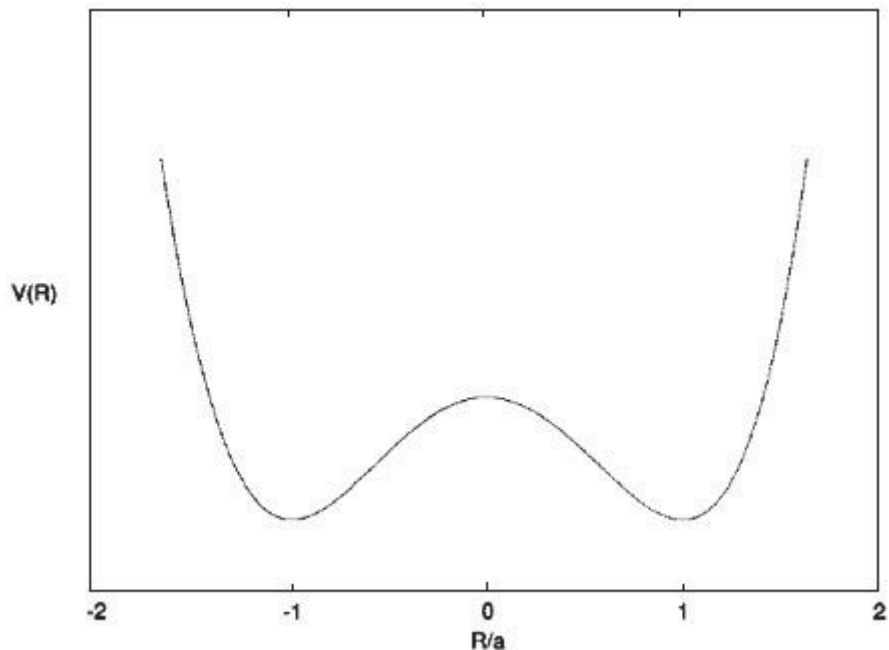


Figure 1.1 Example of Double Energy Well Potential⁴

1.2 A Background on Carboxylic Acids

Carboxylic acids can be used to demonstrate a functional group that can be studied to obtain knowledge on hydrogen bonding, as it's theoretically possible to extrapolate energy contributions from this functional group when a variety of compounds are observed. In general, proton donors like carboxylic acids and amides are almost always involved in hydrogen bonding within crystalline structures.¹ The carboxylic acid moiety, RCO_2H , is an extremely common functional group found in organic compounds. Carboxylic acid derivatives that produce carboxylic acids upon hydrolysis include acyl chlorides, acid anhydrides, esters, and amides. This class of compounds is the most acidic among the organic compounds which contain only carbon, hydrogen, and oxygen atoms, and they have a $\text{p}K_a$ of about five. Carboxylic acid moieties have an inductive effect caused from the electron-withdrawing carbonyl and also delocalize the negative anionic

carboxylate's charge through resonance. Therefore, this means that they are stronger acids than both water and alcohols.⁵

Obviously, one important aspect of a carboxylic acid group is its proton. When speaking of H^+ itself, it is an electron-free fundamental particle having an acidity of roughly 10^{56} times more than a pure H_2SO_4 sample. The hydrogen ion is solvated in a condensed media and almost always bidentate in structure. When the common H_3O^+ species exists, this is called a hydronium ion and has C_{3v} symmetry. Figure 1.2 below gives an illustration of this ionic molecule.⁶

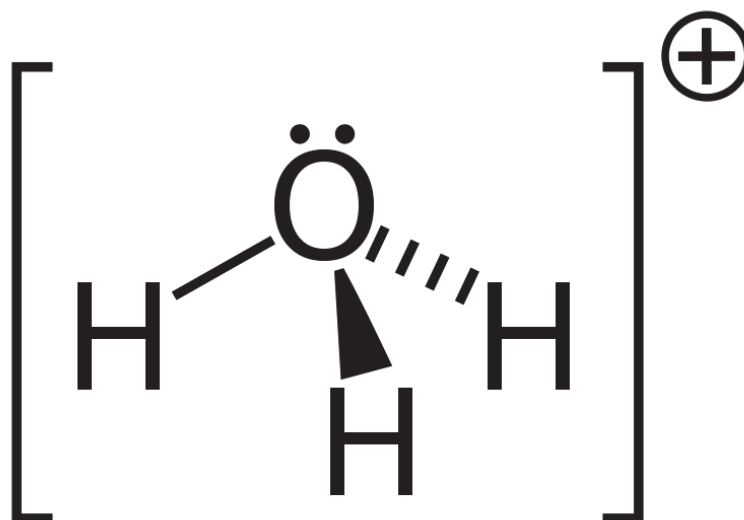


Figure 1.2 Structure of the Hydronium Ion

The H_3O^+ molecule is always trisolvated with one bond being stronger than the other two. Six water molecules solvate H^+ meaning that $H(aq)^+$ is equivalent to the cation $H_{13}O_6^+$.⁶ Its complexity and variability in different compounds and environments makes it a very interesting element to study. Therefore, the hydrogen bonding occurring within carboxylic acids is not well defined overall, especially since it has a vital role in many

organic and biological molecules. This study can delve into the topic of hydrogen bonding and allow for a more complete understanding of its properties through observing the carboxylic acid functional group.

Numerous other properties make carboxylic acid functional groups important in biochemistry and organic chemistry. This class of compounds contains very strong intermolecular attractive forces, having both higher melting and boiling points than compounds comprised of hydrocarbons and oxygen-containing species that are similar in structure. Dimerization is one factor that aids in the strength of this bonding. These kinds of dimers are identical oligomers that form a single molecule through hydrogen bonding.⁷ Figure 1.3 below shows dimerization between two molecules that both contain carboxylic acid functional groups.

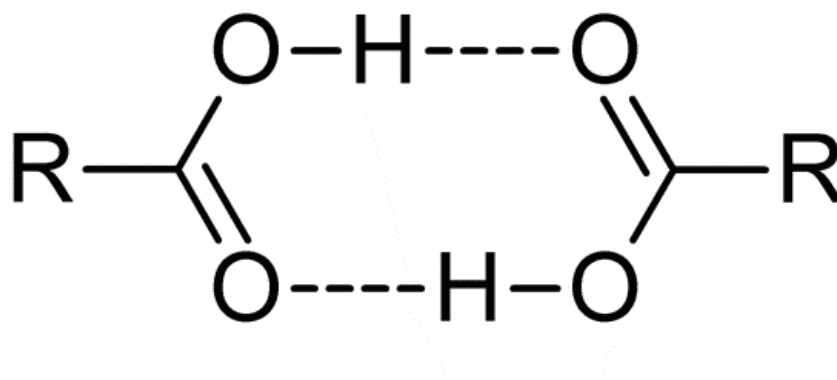


Figure 1.3 Dimerization of Two Carboxylic Acid Functional Groups

Specifically, the hydroxyl group of one of the carboxylic acid's is the proton donor to the oxygen on the carbonyl of the other carboxylic acid; to parallel this, the second one's hydroxyl group acts as the proton donor to the carbonyl of the first carboxylic acid. Therefore, two hydrogen bonds hold this interaction together allowing

for dimerization to occur. This is represented by an O-H---O interaction. In the illustration, R is arbitrary and refers to the rest of the molecule that is not involved in the dimerization. Additionally, it should be noted that when carboxylic acids are in a fluid state, being either a liquid or vapor, they exist primarily in their dimeric form via hydrogen bonding.⁷

Additionally, when amide groups are present within a sample along with carboxylic acid moieties, other bonding patterns may emerge. Strong hydrogen bonds involving nitrogen include N-H---O, O-H---N, and N-H---X, where X is any electronegative element such as fluorine or chlorine. Various biological and chemical processes utilize these types of bonding patterns to become more energetically favorable. These can all cause a varied dimerization interaction to occur and lead to acid-amide and amide-amide bonding possibilities as well.⁸ A study specifically on acid-amide hydrogen bonding capabilities has been performed by Walsh *et al.* (1997) to discuss the possibility of this stable dimer forming in a CDCl₃ solution, while dilutions of this mixture cause an almost solely monomer response to be observed by the NMR. A 2,2-dimethylbutynoic acid having a pyridine terminus was the compound of interest for Walsh *et al.* (1997) and concluded that these types of interactions do occur. One very important acid-amide hydrogen bond is seen in bilirubin, which is a bile pigment that is the product of heme catabolism. A molecular structure of bilirubin is provided in Figure 1.4 below. However, both acid-acid and amide-amide complexes are noted to have been formed in the past; in fact, the amide-amide variety dimer has been found quite often in molecular recognition studies.⁹

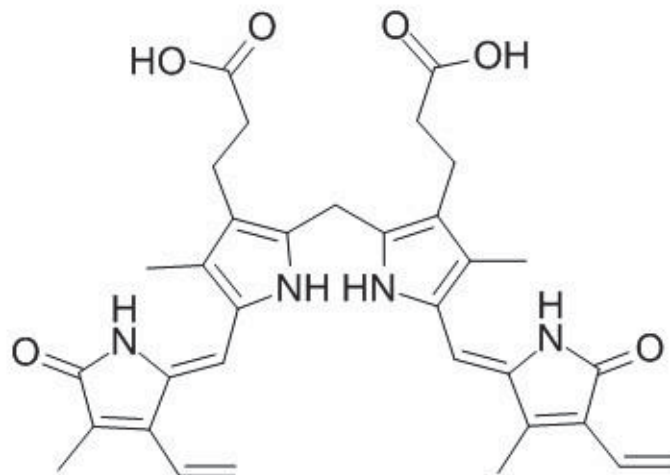


Figure 1.4 Molecular Structure of Bilirubin

The observation of the individual hydrogen bonds within carboxylic acid groups of molecules and in dimerization play a major role in determining properties that impact the physical features of a single molecule or group of molecules. In certain systems, dimerization may not be as favorable as intramolecular interactions or even chelates with a metal ion. Additionally, compounds having more than one type of competing hydrogen bonding, like amine groups or strong electronegative atoms present with carboxylic acids, can exhibit different characteristics than those only possessing one form. Furthermore, these types of molecules can act differently depending upon the conditions to which they are subjected. This basic research can be applied to many facets of science and give insight into various processes. For example, if a mixture is heated to the temperature in which it decomposes, it will have different physical features than an unheated form of the same system. Therefore, being able to understand and explain in what conditions or situations these different processes may occur can provide a wealth of knowledge within the realm of biophysical chemistry and especially in the design of pharmaceuticals.

Chapter 2: Statement of the Overall Research Problem

2.1 Solid State Pharmaceuticals and Their Behaviors

All pharmaceuticals are responsible for affecting an active site within the body, which in turn causes the body to elicit a response due to the entry of this exogenous substance. The exogenous substance should greatly mimic its endogenous counterpart by acting as an agonist or should prevent the activation of the endogenous ligand and their agonists by acting as an antagonist. These are the two main properties in which drug-metabolizing enzymes are principally designed. An active site refers to the location in which a biologically active protein, like an enzyme, can allow a specific reactant molecule to bind. Drug action involves the molecular changes that are produced by a drug-receptor interaction, including a ligand binding to a receptor, while drug effects denote the physiological and psychological changes that can occur. It's important to recognize that the sites of drug action and drug effects can be different as well.¹⁰ The drugs of interest within this research all contain carboxylic acid moieties, which are highly important in determining the functionality and ability of a medicine to perform a certain function. Therefore, the potential extrapolation of hydrogen bond energies for various compounds through excessive experimentation has the ability to provide insight into many areas of science; however, understanding hydrogen bonds specifically within pharmaceuticals gives an interesting approach to this research problem.

Additionally, drugs can undergo protonation and deprotonation depending upon the physiological pH of the body compartment in which the drug is affecting along with the pK_a inherent to the drug itself. When the pH is less than the pK_a , the protonated form of the drug dominates, while the deprotonated form is highly present when the pH is

greater than the pK_a . In general, drugs that are weak acids ionize more readily in an alkaline environment and become less ionized in an acidic environment. Furthermore, this biotransformation can affect drug interactions, since this refers to the metabolism of the parent drug. Often, the drug can be biotransformed into two or more active metabolites, which allows for longer lasting effects within the body.¹⁰

The pharmacokinetics and pharmacodynamics also greatly influence the behavior of a drug and are factors that are considered in drug design. Pharmacokinetics is the body's response to the drug, while pharmacodynamics is the drug's action on the body. In general, pharmacokinetics includes the multiple processes affecting drug bioavailability and the onset of drug action as well. Therefore, it involves the amount of drug available in the blood that's able to freely bind to target sites and how quickly the drug reaches the target site, respectively. Pharmacodynamics handles the affinity, efficacy, and potency of a drug. Affinity is the strength of the chemical bond; if a drug has high affinity, then a low drug concentration is needed to produce the desired effect. Efficacy is the ability of a drug to produce a certain effect within the body, while potency is the amount of drug required to give a specific effect at a preferred intensity.¹⁰ All of these qualities are important when designing drugs, especially considering the factors that are expected to be involved in such a process. Therefore, the work presented in this thesis is a necessary attempt to understand the energetics involved with each compound of interest and specifically on the hydrogen bonding energies being dependent upon the rest of a molecule.

2.2 Studies on Hydrogen Bonds and Carboxylic Acids

Many prior studies have attempted to find hydrogen bond energies using different methods which have been applied here. In fact, it's been presented in the past by Remenar *et al.* (2003) that pharmaceuticals can potentially be engineered to possess the correct stability and bioavailability that will enhance its performance within the body. The morphology and moisture sorption are two crystal form characteristics that have detrimental effects on pharmaceutical research and development efforts.¹¹ Correcting for these aspects can greatly expedite the entire process of drug development, however the ability to control hydrogen bonds impacts the entire functionality of a drug and the ability for it to perform its specific assignment. Theoretically, hydrogen bond energies are between roughly 0.2 and 40 kcal/mol, which includes a wide range of values.¹²

A compound's general physical and chemical properties greatly influence the hydrogen bond energies of those bonds within them. For example, the electronegativity of both the donor and acceptor atoms can impact how strong of a hydrogen bond is present. One project performed by Su *et al.* (2013) used an x-ray diffractometer (XRD) and a mass spectrometer (MS) coupled to a desorption electrospray ionizer (ESI) in an attempt to characterize hydrogen bonds occurring within molecules containing benzothiazole and carboxylic acid groups. These methods complemented each other well, concluding that the hydroxyl bond within the carboxylic acid acts as a stronger donor than N-H bonds within amine groups. Additionally, the carbonyl bond on the carboxylic acid functional group is a weaker accepting group than the nitrogen atom within heterocycles.¹²

Understanding bond dissociation energies can also help with extrapolating hydrogen bond energies. Blanksby and Barney Ellison (2003) used a variety of organic molecules to determine the bond energies and heats of formation of these compounds. Bond dissociation energy corresponds to the depth of the potential energy well with calculations arising from translational, rotational, and vibrational contributions. An illustration of this was shown in Figure 1.1 on page 3 of this thesis. It was found that the C-O bond of methanol is very weak compared to other alcohols, the C-H bond energies in alkanes decrease with more substitution, and aromatic ring structures have increasing bond strengths from ortho- to meta- to para- conformations. Further, by creating new bonds in products or other already stable molecules, the bond enthalpy tends to decrease.¹³ All of this information can be applied to the work here to give more of a depth of knowledge to these general molecular characteristics.

Furthermore, an understanding of the formation of organic molecular nanocrystals is extremely important to pharmaceutical industries due to the importance of their solubility and dissolution rates. It is a key factor in increasing the bioavailability of poorly soluble drugs, as these types of amorphous and nanocrystalline materials can be hard to stabilize for extended periods of time based on their design. Being able to control a crystal's polymorph and even production of nanocrystals is a highly important area of research, however methods of analysis for these processes are not vastly studied. Nanocrystals can form through various methods like spray drying, supercritical fluid crystallization, impinging jets, and microfluidic devices, and these crystals are tested via mainly powder XRD methodology. Yang *et al.* (2014) used differential scanning calorimetry (DSC), solid state nuclear magnetic resonance (NMR), and high-performance

liquid chromatography (HPLC) in order to determine the nanocrystal's properties.¹⁴ This kind of study brings together different aspects of a drug's design from its synthesis to analysis which provides an overall understanding of certain features of the drug that may be useful.

Dimerization of carboxylic acid functional groups is another topic of interest within this thesis. Choi and Ko (2010) observed the pyrolysis of twenty amino acids using gas chromatography/mass spectrometry (GC/MS) and examined the intensity ratios of the peaks from dimerized products using gas chromatography flame ionization detector (GC-FID). Since all amino acids have a carboxylic acid moiety, this study can be correlated with the research performed in this thesis. It was found that some amino acids, such as asparagine, aspartic acid, and serine give dimerized products more than most other amino acids. In fact, the following amino acids were shown to possess the ability to undergo dimerization upon pyrolysis: alanine, asparagine, aspartic acid, cysteine, glycine, isoleucine, leucine, methionine, proline, serine, and valine. Some of these products even contained five- or six-membered rings within them. Interestingly, most also contained fairly short side chains between polar functional groups. Therefore, by analyzing the pyrolysis of these species, possible mechanisms could be established for dimerization and temperature ranges in which these actions occur could be recognized as well.¹⁵

Wolfs and Desseyn (1995) used oxamic, malonic, and succinamic acid to observe hydrogen bonding patterns in the solid state. These compounds have identical functional groups, since they are all derivatives of dicarboxylic acids with one acid group replaced by a primary amide. Possibilities of formations included cyclic acid dimers, acid-acid catamers, and heterogenic associations; vibrational analysis of these compounds can

determine which interactions are occurring. Their hydrogen bonding patterns were found through infrared (IR) and Raman spectroscopy at different temperatures and compared to Hartree-Fock calculations being performed at a 6-31G basis set. The findings from these approaches indicated that there are two different categories with the vibrational energies of malonamic and succinamic acids being very similar to one another but highly different from oxamic acid.¹⁶

Another dimerization-based study used IR spectroscopy methods to observe carboxylic acids and salts in perfluoropolyether (PFPE) media. PFPEs are used as lubricants acting in high-performance applications, and the ones observed by Doan, Koppe, and Kasai (1997) all contained carboxylic acid functional groups. Theoretical calculations showed that acid dimers are formed through hydrogen bonding, while salt dimers are formed through Coulombic interactions of charged constituents. Results indicated a reversible temperature dependence and an instability causing no interconversion between two salt-salt dimer isomers that does occur at room temperature.⁷ Therefore, it can be noted that IR methodology can provide a vast source of information regarding structural differences in a wide range of heated and unheated samples causing dimerization or possibly chelation to be observed within the spectra.

A theoretical approach studied by Nandi, Hazra, and Chakraborty (2005) also looked at the vibrational coupling of carboxylic acid dimers using density functional theory (DFT) calculations, which predict that vibrations from the dimer are mainly caused by combinations of monomer modes. Specifically, this approach observed a benzoic acid dimer and a mixed dimer of benzoic acid and formic acid with the hydrogen bond having the main influence toward binding energies of these systems. These

theoretical methods often try to find energy correlations by looking at the ground and excited state of each dimer. It should be noted that there are many possibilities of excited state energies for these dimers so not all of them can be observed in a single experiment. Therefore, it was found that the excited state dimer appears to be bent compared to the ground state, since the excited benzoic acid then becomes a weaker hydrogen-bond donor; this makes the bond lengths of the two hydrogen bonds different. This study clearly shows the amount of detail involved in executing a purely theoretical research project.¹⁷

Overall, although other projects have observed these kinds of hydrogen bond energies, not many have used the variety of methods and assortment of compounds that have been analyzed in this research. Therefore, the projects presented within this thesis are meant to compare results to other studies in the literature and to the projects presented here, while also being able to draw conclusions in determination of the energies of interest. Although understanding energies of hydrogen bonds are at the heart of this research project, all of the compounds have been selected for comparison purposes. This will allow for a better comprehension of the properties inherent to a compound that influence certain interactions and energies.

Chapter 3: Analysis of Aspartic and Glutamic Acids in a Potassium Chloride Matrix **Using a Variety of Methods**

3.1 Background Information

Analyzing aspartic and glutamic acids in a potassium chloride matrix can be very useful in understanding the solid state structures of many pharmaceutical, cosmetic, and agricultural products.¹⁸ Both of these simple amino acids can be used as a model for more complex systems, keeping in mind that solid dosage forms are made to have acceptable shelf lives to overcome the instability of aqueous solutions. Ionic interactions that can occur in a study such as this are much stronger than typical hydrogen bonding and can dominate a packing pattern; however, hydrogen bonds can also be an important organizational tool within the molecular complex.¹ The observed reaction rates of chemical degradation are dramatically lower in the solid state.¹⁹ In crystalline form, functional groups of amino acids are held together by hydrogen bonds, and solid state amino acids can have structural variations modeling conformationally dependent biological processes.²⁰ Furthermore, amino acids can undergo various degradation steps like decarboxylation, dehydration, deamination, and condensation for example.¹⁸ Aspartic and glutamic acids are both very important compounds to study when trying to understand these processes, are extremely similar structurally, and have a negatively-charged side chain above a pH of 3.²¹ Figure 3.1 on the next page shows their respective structures.

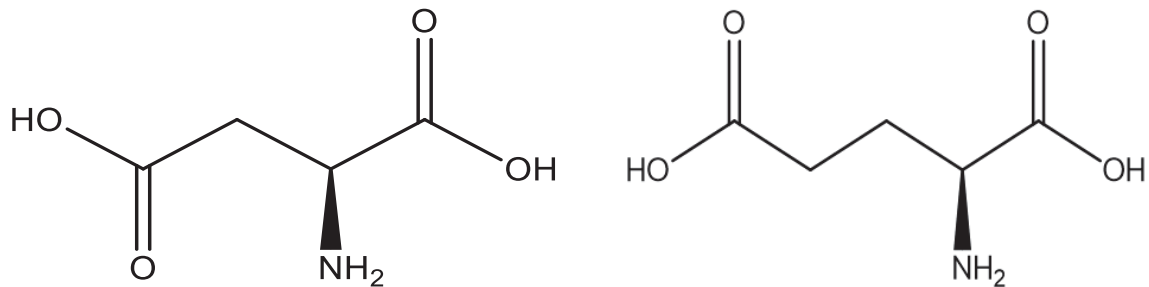


Figure 3.1 Aspartic Acid (left) and Glutamic Acid (right) Structures

Aspartic acid is a non-essential, biologically active molecule that helps to keep the solubility and ionic properties of proteins. Therefore, it can be synthesized and used easily within the body. It can act as both a proton donor and acceptor, which is an advantageous quality in such a molecule.²¹ It's highly important in the urea cycle and DNA metabolism as well. Furthermore, aspartic acid is an excitatory neurotransmitter in the brain, meaning that it will work harder to elicit action potentials that will reach threshold and produce a stimulus.²⁰ The potassium, magnesium, and calcium salts of aspartic acid can act as a mineral supplement. Furthermore, polyaspartate is one common chemical that is biodegradable and can be used as a super-absorber. Therefore, its applications are apparent in pharmaceutical and agricultural industries.²²

Glutamic acid is also non-essential and biologically active. It can be synthesized from arginine, proline, and ornithine and is then converted to glutamine within the body.²¹ It's the only amino acid metabolized by the brain; therefore, it is found in a very high concentration within the brain. Glutamic acid helps to transport potassium through the blood-brain barrier by providing the necessary nutrients to metabolize fats and sugars. Additionally, glutamic acid is a major excitatory neurotransmitter that's involved in fast

synaptic neurotransmission. There are many complex physiological processes in which glutamic acid is involved, like memory, learning, neuronal cell death, and plasticity.²³ Moreover, glutamic acid has the largest world market among all of the amino acids with glutamic acid and its derivatives being incorporated into a variety of drugs used to treat epilepsy, ulcers, hypoglycemia, Parkinson's disease, and other neurological disorders.¹⁸

The majority of research already performed on these specific amino acids delved into each individually, so these will be discussed separately here as well. Aspartic acid and its primary derivatives have been studied via many methods. He, Fan, and Tang (2010) studied the gaseous conformers of aspartic acid using solely computational methodology, finding a total of 1296 possible structures with 122 being confirmed as stable.²⁰ In two separate studies, Goldberg *et al.* (2009, 2011) observed the polycondensation of L-aspartic acid as described in two stages. The first step forms polyaspartic acid and the second involves dehydration to form polysuccinimide. Both TGA and DSC measurements were performed with the ability to then calculate the pre-exponential factor and activation energy. This is the basis for the prior experimentation performed in Praveen Bandarupalli's thesis as well.^{24, 25, 26} Additionally, polyaspartic acid could be studied through heating it in vacuo or removing the water through an azeotropic distillation and then determining the possible reaction mechanism. A four step reaction for this process is considered in the literature by Kovacs *et al.* (1961).²⁷ Multiple other studies performed by Heaton and Armentrout (2008) involved observing aspartic acid complexed with sodium, lithium, and potassium cations using a guided ion beam tandem mass spectrometer (GIBMS). This allowed for the discovery of their conformational binding properties, thermodynamics, and potential mechanisms of formation.²⁸ Sang-

aroon and Ruangpornvisuti (2006) used a DFT approach to look at aspartic acid species as well.²⁹

Similarly, glutamic acid and its various derivatives have been extensively studied as well. A neutron diffraction study was performed by Lehmann, Koetzle, and Hamilton (1972) on β -L-glutamic acid to determine its crystal and molecular structures. In its natural state, its structure is orthorhombic and zwitterionic molecularly with no intramolecular hydrogen bonds observed. This specific method is useful for finding atomic positions and thermal motions of hydrogen atoms; in this situation, the carboxyl group was found to be protonated.³⁰ A few other research projects executed by Wu *et al.* (2010) were the basis of Praveen Bandrupalli's thesis. They will be mentioned here and discussed further upon discussion of the observed results from all approaches. One article looked at the phase transformations of glutamic acid and its products upon decomposition using the complementary techniques of XRD, TGA, DSC, MS and gel permeation chromatography (GPC).²³ Their other project discussed L-pyroglutamic acid's polymorphism, phase transition, and thermal stability properties, which was also observed using multiple methodologies, like FT-IR, TGA, DSC, XRD, Raman spectroscopy, and optical microscopy.³¹ Therefore, the wide variety of methods used in the aforementioned studies will be applied to the work presented in this thesis. Hopefully this will allow for a deduction of more accurate results and give insight into possible potassium ion complexes within the amino acid molecules, especially when heated to critical temperatures of decomposition.

There were a few studies that observed both aspartic acid and asparagine (Asx) along with glutamic acid and glutamine (Glx) and compared these to one another.

Heaton, Moision, and Armentrout (2008) studied the binding of sodium ions to these compounds in order to understand the energetics of their individual structures along with steric influences caused by chain length and the action of cation binding. The experimental methods included use of an ion beam tandem mass spectrometer with an electrospray ionization source and a computational study at both the Hartree Fock 3-21G level of theory and the B3LYP/6-311⁺G(d,p) level. They found many possible chelation structures which were dependent upon the chain length and substituents.³² For example, longer chain Glx amino acids had less strain than shorter chain Asx ones, since the long chain caused the minimization of unfavorable steric influences. All experimentation involved the use of a guided ion beam tandem mass spectrometer (GIBMS), as used in prior approaches. In general, it was determined that carbonyl group binding was favorable, however there was a reduction in energy caused by the carboxylic acid group when it is present. For all sodium ion complexes, the tridentate structure appeared to be energetically superior to the others by having carbonyl oxygens and the amino nitrogen on the backbone of the main structure. Furthermore, the sodium ion complex with the amide derivatives were more strongly bounded than their acidic amino acid counterparts. This is possibly caused from electron withdrawing effects of the hydroxyl group on the carboxylic acid.³²

A follow-up study performed by Heaton, Ye, and Armentrout (2008) looked at these same kinds of complexes and focused on their products formed through dehydration and deamidation using the same type of procedural methods as the prior study. Use of collision-induced dissociation (CID) cross-sections with GIBMS allowed for the potential ligand products to be determined for each sodium ion ligand reactant. Ring structures

played an important role in the total energy considerations for each possible configuration. As a whole, the decomposition products didn't allow as much mobility for sodium ion solvation since they only have monodentate and bidentate cation configurations.³³ Both of these research projects provide a good basis for determination of prospective structural configurations that can be used regarding the approach in this thesis.

Finally, Van Holst, Kersten, and Hogendoorn (2008) studied various potassium amino acid salts, and this included research on both aspartic and glutamic acids. However, this project dissolved the amino acids in water so that they appeared as zwitterions having a protonated amino group. Then, potassium hydroxide was added to deprotonate the zwitterion, which differs from the research in this thesis. Densities, viscosities, and solubilities of aqueous potassium amino acid salt solutions were determined. Therefore, even though the approach of this project is much different than what is presented in this thesis, they both involve use of a potassium ion to better understand its physical properties resulting from its combination with amino acids.³⁴

Multiple other projects have been performed specifically on metal cations interacting with compounds like the PhePhe ligand, histidine, and both the pyrrole and pyridine carboxylate molecules. For example, Dunbar, Steill, and Oomens (2011) used FT-ICR mass spectrometry, infrared multiple photon dissociation (IRMPD), and the FELIX laser along with thermochemical and IR spectral theoretical calculations of DFT methodology to create and analyze complexes of PhePhe with six different cations. This kind of cation- π interaction is regularly found in biological systems along with a double cation- π structure, which allows for encapsulating a metal ion. Chelating complexes that

contain charge-solvated binding forms can have a zwitterionic salt bridge that is less stable. An amide oxygen is always bound to the metal ion, while the other chelation site is bound to either the amino nitrogen or carboxy carbonyl oxygen.³⁵ Citir *et al.* (2012) studied histidine in the gas phase being chelated to various mono-cations through IRMPD spectroscopy. This method helps determine ion-protein interactions and was compared to theoretical studies.³⁶ Research performed by Swiderski *et al.* (2011) utilized IR, Raman, and NMR spectroscopy while using a theoretical approach to compare pyrrole-2-carboxylate and pyridine-2-carboxylate interacting with alkali metal ions. It was confirmed that bands shifted to lower wavenumbers in IR and Raman spectra from lithium down to cesium and all alkali metals in between meaning that a higher frequency is occurring with this trend. There was also an increase in perturbation of electronic charge distribution in this manner due to a greater dipole moment in the entire molecule.³⁷ Although all of these studies involve compounds containing carboxylic acid groups being chelated to an alkali metal, none have looked at such similar amino acids in structure and compared them in the way that will be performed here.

Prior research on this topic through thermal studies utilized thermogravimetric analysis (TGA) and differential scanning calorimetry (DSC) and brought about some very interesting results. Other studies used gas chromatography-mass spectrometry (GC-MS), neutron diffraction, gel permeation chromatography (GPC), infrared multiple photon dissociation (IRMPD) spectroscopy, and many other methods. Results from these studies were often compared to computational methods utilizing the Spartan or Gaussian computer modeling systems. Understanding the decomposition of these various amino

acids along with widely-used substances in general and how they affect a product's quality is important for the safety of consumers.¹⁸

Once again, being able to understand the hydrogen bonding energies associated with the metabolism of various chemicals used as pharmaceuticals can provide vast information as to the drug's potential design and action. Both aspartic and glutamic acid can possibly be chelated to the potassium ion in various ways, so knowing how this might occur will offer valuable data as to their potential functions within biological systems. Now that the general background has been discussed and understood in terms of the research problem, the next three sections of this chapter will delve into each individual research method employed in this project and explain the workings of each piece of instrumentation. The section immediately following those will discuss theoretical methodology in determining energies, bond angles, and bond lengths of the compounds of interest. Finally, the chapter will conclude with the specific experimental procedure, results, discussion, and future work.

3.2 Raman Spectroscopy

Raman spectroscopy is a type of molecular spectroscopy that produces a spectrum by observing the changes in energy resulting from electronic, rotational, and vibrational states. Essentially, the wavelength of scattered light is different from the incident light due to the varied vibrational energy of the molecule which dictates scattering.³⁸ The amplitude of vibration is referred to as nuclear displacement, meaning that monochromatic laser light having a certain frequency will excite and transform molecules into oscillating dipoles.³⁹ Often, molecular spectra can offer information on bond

strength, bond length, bond angles, and dipole moments. Specifically, Raman spectroscopy discovers changes in the molecular state by examining the frequencies that exist in the radiation through inelastic scattering of a photon by those molecules. Different types of scattering can be present, including Stokes and anti-Stokes Raman scattering. In anti-Stokes, an incident photon is scattered from a molecule with an increase in frequency; therefore, radiation is collecting energy from the molecule, and the scattered light has more energy than the incident light. In Stokes, an incident photon is scattered from a molecule with a decrease in frequency, so the scattered light has less energy than the incident light. This corresponds to a loss in radiative energy to the molecule. These differ from Rayleigh scattering since that process involves scattering with a constant frequency, meaning that the final and initial states are at the same energy level, or elastic, and there is no energy loss. Figure 3.2 below is an illustrative diagram of all processes.^{38, 40}

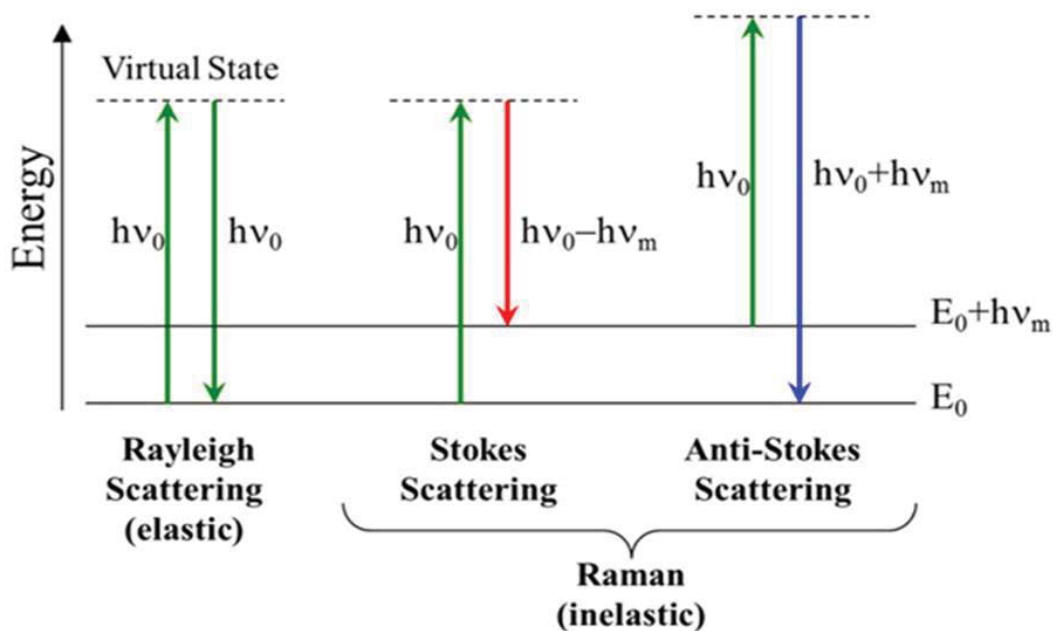


Figure 3.2 Illustration of Quantum Energy Transitions for Rayleigh and Raman Scattering⁴¹

A linear relationship occurs between the power of scattered light and the intensity of the response measured by the incident light. There is also a direct relationship between the power of scattered light and inverse of the wavelength to the fourth power. Based on these relationships and theory, it could be suggested that use of a shorter wavelength and higher power is advantageous to obtain spectra having the best results.⁴¹

A basic Raman spectrometer has the following main components: an excitation source, a sampling device, a wavelength selector, and a detector.³⁸ The excitation source in all Raman systems is a laser, since this source provides intense monochromatic radiation allowing photons to stimulate other photons having the same frequency. Additionally, lasers are unidirectional, due to photons being lost that don't travel along the cavity's axis, and are coherent, since this refers to the uniformity of phases in the electric field of photons. Most lasers used in Raman spectroscopy are continuous waves, meaning they produce an endless stream of light.⁴² Laser is an acronym for light amplification by stimulated emission of radiation; therefore, when energy is added to a system having a photon at a higher energy state, this photon will fall to the lower level giving off energy in the form of light. Stimulated emission indicates that there will be two photons instead of just one. Usually, the excited state of an atom has a lifetime of 10^{-8} seconds. By having a metastable state in which electrons aren't likely to decay as quickly, electrons will have lifetimes of 10^{-3} seconds or longer. This process, called population inversion, will allow for more atoms to be in the upper state. The employed laser must be extremely stable with a narrow bandwidth to ensure sharpness.⁴³

The optical Raman probe has to be able to focus the laser to the sample. There is a direct relationship between the photon density at the sample and the Raman signal. A

good focusing lens will allow for both to be at their ultimate potential.⁴² The sampling device is considered to be the illumination system and light collection optics, while the wavelength selector can be a filter or spectrophotometer. Scattered light can then be collected and filtered into the spectrometer.³⁸ The exit portion of the monochromator will create an image of very faint lines. Finally, the detector records the results.⁴² This device varies depending on the instrument but is either a photodiode array, charge coupled detector, or photomultiplier tube.³⁹

3.3 Fourier Transform Infrared Spectroscopy

Fourier Transform Infrared Spectroscopy (FT-IR) is a widely used spectroscopic method in which infrared radiation passes through a sample; some of this radiation is absorbed and some is transmitted. The actual absorption peaks that are present in the final spectra are directly related to the frequency of vibration of the bonds of atoms within the compound of interest. Since two different compounds will not produce the same spectra, this kind of spectroscopy can be used as a qualitative analytical method by providing information rich spectra. Furthermore, FT-IR is favored over other dispersive or filter methods for various reasons, including that it's non-destructive, quick, sensitive, universal, mechanically simple, internally calibrated, and has a high optical throughput.⁴⁴ FT-IRs have exceptionally great signal-to-noise ratios (SNRs) of 100 or higher giving it a throughput and multiplex advantage. This method gives a high resolution for the measurements allowing for a more precise set of data overall.⁴⁵

FT-IR instruments need the following vital parts to properly analyze compounds: a source, an interferometer, the sample of interest, a detector, and a computer. The black-

body source is where the infrared energy is given off by using a beam to allow only a certain amount of energy to contact the sample and detector. Each FT-IR uses an interferometer to create an exclusive signal that has all infrared frequencies programmed into it. Additionally, interferometers have a beamsplitter which transmits some light and reflects the rest. Essentially, it divides the infrared beam into two optical beams; one reflects off a mirror that is fixed into place, while the other reflects off of a mirror that is moving away from the beamsplitter. These two beams will recombine and interfere with one another either constructively or destructively via the interferometer. This results in the formation of an interferogram of the information that enters the interferometer and is unique for every sample. Therefore, all frequencies can be measured at once which expedites the entire process. Since no monochromators are involved, any frequency that is not absorbed will reach the detector. The detector will then find the final measurement of the interferogram before it is sent to the computer where Fourier transformation occurs. An illustration of this process is provided below along with an FT-IR spectrometer visualization.^{43, 44}

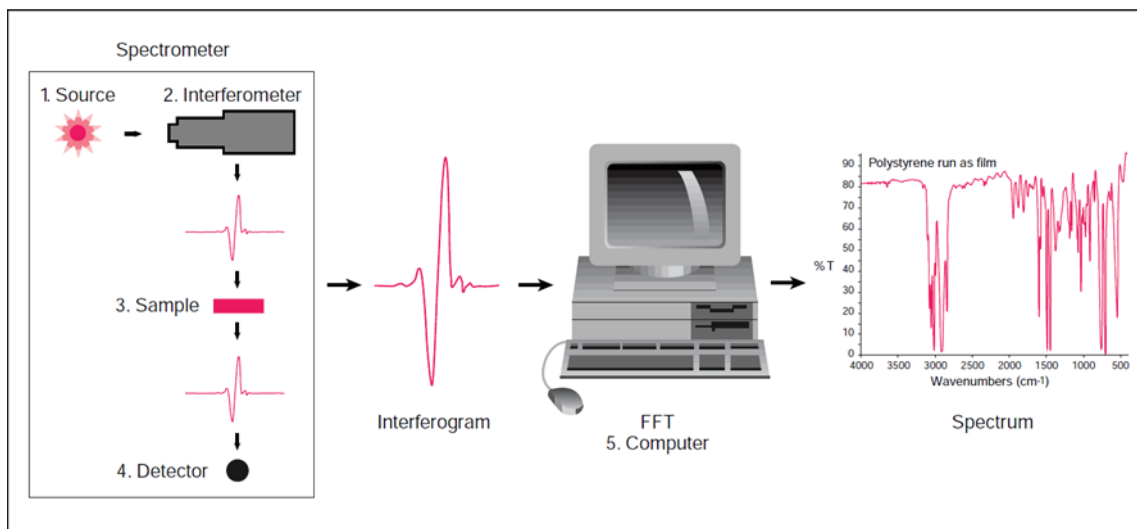


Figure 3.3 Illustrative Process of FT-IR Sample Analysis⁴⁴

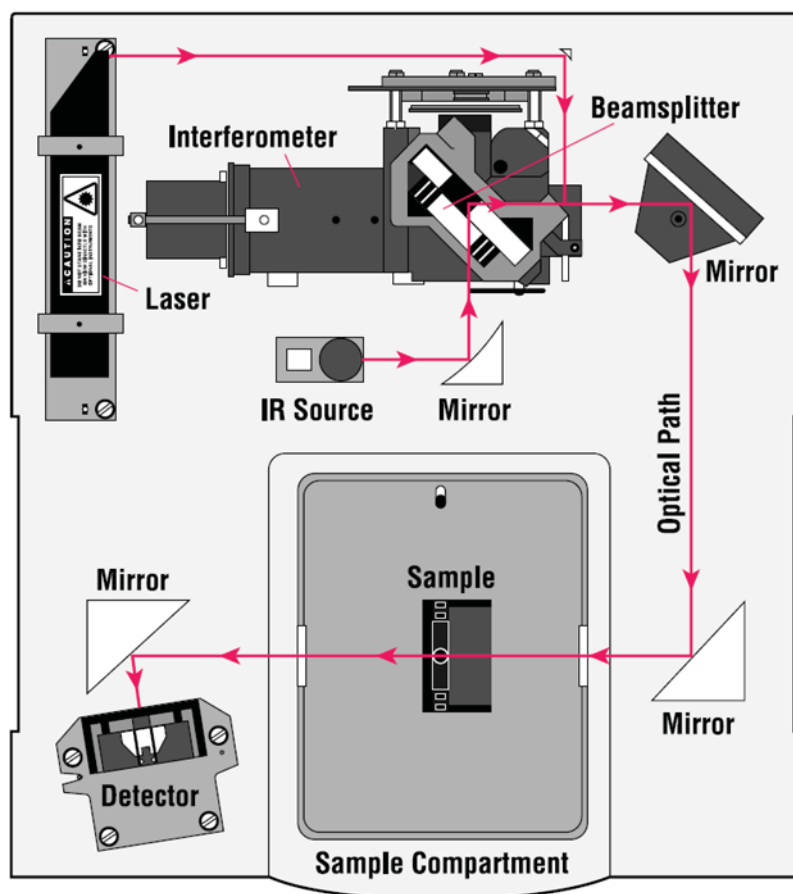


Figure 3.4 Layout of a Typical FT-IR Spectrometer⁴⁴

It's important to note that a background spectrum must always be taken to ensure that there is a comparative measure for the strength of absorption. This is performed without a sample in the device and is then automatically subtracted to obtain the sample's spectrum.⁴⁴ Specifically, spectral subtraction is the process that is used to eliminate undesirable influences from potential spectra, such as carbon dioxide, water vapor, solvents, impurities, and remaining residues from prior samples. Removal of these unwanted materials allow for a sample's spectrum to be more easily measured and can also help improve spectral SNRs. Other factors that could improve this ratio are increasing the number of scans, having the proper method of making and purifying samples, and smoothing of the spectra to lower the spectral noise.⁴⁵

As with any analytical method, there are a few general disadvantages to infrared spectroscopy, including that it's unable to detect some molecules, has issues with determining spectra of mixtures of compounds, and is water sensitive. For example, individual atoms that aren't bonded to any other atoms will not appear within spectra, since they aren't able to vibrate. Homonuclear diatomic molecules have the same problem because they only possess a symmetrical stretch vibration. Mixtures cause concern due to the inability to correctly label the peaks within their spectra. The only remedy to this predicament is to measure each compound within the mixture separately to confirm the positioning of their individual peaks. Also, water becomes concerning in hygroscopic compounds, so care should be taken in sample preparation. Finally, although FT-IRs are an extremely useful tool for analyzing compounds, they are even more successful if combined with other analytical methods; this will confirm the data and provide another approach to collecting information.⁴⁵

3.4 Powder X-ray Diffraction

Peter Debye and Paul Scherrer are credited with developing the technique known as powder x-ray diffraction (XRD).³⁸ It was also established as a useful method independently by Albert Hull around the same time. Powder XRD can identify solid samples, or unknown crystals within a sample, and can often give enlightenment toward unit cell dimensions and symmetry.⁴⁶ A Debye-Scherrer diffractometer is used in powder diffraction and has monochromatic radiation so that only one degree of freedom is present when the diffraction conditions are changed due to the 2Θ angle. This differs from single crystal diffraction due to three additional degrees of freedom being present with inclusion of monochromatic radiation.⁴⁷

The process of powder XRD is performed through measuring the intensity of peaks as a detector is rotated around the sample of interest while it's in the plane containing the ray of incident light. In general, constructive interference of monochromatic x-rays and a crystalline sample allow for this methodology to work.⁴⁶ Therefore, when an x-ray hits a crystal surface, some of the x-ray is scattered while the rest passes onto the next layer. Here, it can once again either pass through or be scattered. This continues and results in a diffraction pattern with peaks only occurring when the following equation, called Bragg's Law, is true:

$$\sin \Theta = n\lambda/2d$$

In this equation, Θ is the angle of incidence of the x-ray, n is an integer, λ is the wavelength, and d is the spacing between layers of atoms.⁴⁸ Coherent scattering allows for wave periodicity with both constructive and destructive interference occurring from scattered waves which are emitted by atoms of varying types and positions. Therefore,

the geometry is an important aspect determining how a diffraction pattern may look.⁴⁷ It's important to note that only crystalline solids will diffract due to the necessity of an extremely regular structure, so amorphous materials won't provide a diffraction spectrum.⁴⁸

There are three fundamental parts within an XRD machine: an x-ray source, a sample holder, and an x-ray detector. Additionally, it's necessary to have a piece that mechanically varies the angle Θ where the x-ray can be focused and the sample can be rotated. This is called a goniometer, and its movements occur with respect to the monochromatic x-rays. Also, an electronic device used to count detector pulses must be in synchronization with the goniometer at all positions. The x-ray source is usually a sealed x-ray tube; modern forms of this tube include a thin anode with a cool water flow behind it. A few figures of merit are used to determine if an x-ray source will give useful photons to measure. The intensity per area of emitter is measured in photon(s) per cm^2 and is the most useful figure of merit regarding the brightness of the x-ray. A large intensity and well-defined diffraction angles are present when a line source is used, referring to a slit that collimates the incident and diffracted beams controlling the equatorial divergence between the sample and detector. Axial divergence is regulated by soller slits. As a sample rotates in the path of a collimated x-ray beam at the angle Θ , the actual detector collects the diffracted rays at an angle 2Θ away from the path of the source.^{46, 47, 48}

The directions and intensities of the diffracted waves are then recorded and presented in the diffractogram, providing real space periodicities in the compound of interest. For example, atomic periodicities having longer repeating distances allow for

diffraction at small angles. Conversely, when shorter repeating distances are observed due to small interplanar spacings, diffraction occurs at larger angles.⁴⁷ Ideally, a detector needs to possess the following four characteristics: an output pulse for every incident x-ray, a pulse of current with a proportional net charge to the energy of the x-ray photon, a consistent amplitude of the detector pulse, and a large angle extending from the detector to the specimen. Maximizing all of these basic parts of a powder XRD instrument can provide a high quantum efficiency and the best possible results. In fact, lattice parameters have the potential of being measured accurately to better than 1 part in 10,000.⁴⁷

A cathode ray tube produces the x-ray that creates monochromatic radiation and directs it toward the sample. The resulting powder XRD diffractogram can then be compared to known ones stored in a database so that samples can be compared and identified. The patterns produced are plots of intensity versus the angle of the detector, which is set at 2θ . Each material has a specific spectrum it produces caused by its exclusive set of interplanar d-spacings.⁴⁶ Matching the positions and intensities of peaks within a diffractogram to known patterns determined from another sample or from a calculation give a great idea as to a sample's composition. However, this is often difficult if a sample contains multiple phases or if there is an overlap of peaks. Furthermore, peak size and shape can be impacted by a variety of factors, including internal strains and the number of crystallographic planes to the diffraction.⁴⁷

As with many important chemical instrumentation processes, momentum and energy are tremendous factors whose contributions need to be considered. Crystals that do diffract need to gain an equal but opposite momentum so that this factor is conserved. If energy transfer is occurring, the x-ray that is scattered will have less energy than the

incident energy providing inaccuracies in the diffraction results. Kinetic energy may follow the transfer of momentum so recoil is accounted for by the crystal's motion. Additionally, energy transfer to a single atom is possible through moving the nucleus causing atomic vibrations. This can also happen if ionization occurs due to an electron escaping from an atom.⁴⁷

There are multiple strengths associated with this method, including having a relatively quick time needed for unknown identification, using a small amount of sample for the measurement, and being an easy method for data interpretation.⁴⁶ Sample preparation time is short and the procedures are relatively easy making it a good technique to use; however single crystal XRD is a much more powerful technique to determine the actual structures of compounds. A powdered sample can be used, as sometimes crystals are unable to be created, and diffraction can still occur. Therefore, single crystal XRD is often not a feasible method to determine the desired features.³⁸ However, a few limitations exist as well, mainly regarding its use in analyzing mixed samples. For these, it has a detection limit of about 2% of the sample and peak overlay might provide inaccuracies in determining its correspondence to a certain compound within a mixture. Even worse, the EVA database where all known spectra are stored may not be able to identify these mixtures.⁴⁶ Additionally, if only Bragg's law is applied, there can be problems with not having the center of diffraction at the center of the goniometer due to bad sample positioning, different samples having varied x-ray dispersion depth, and samples having irregular surfaces.⁴⁷

3.5 Theoretical Calculations

Dimer coupling in molecules containing carboxylic acids can reorganize vibrational frequencies giving different fluorescence spectra, while the hydrogen bonding involved in dimerization leads to pertinent biological electron transfers. Specifically, when observing benzoic acid dimers, the carboxyl group and the aromatic ring have the most change in shifts in the spectra when compared to their monomeric components. Therefore, systems of dimers have been shown to have vibrations of low-energy hydrogen bonds mixed with those of the ring, which is in an excited mode. Additionally, six extra intermolecular vibrations occur from forming dimers; usually, both constituents have degeneracy but when dimers form no degeneracy occurs.¹⁷

In order to model biological systems and compare experimental results such as those stated above, it's often very useful to use computer programs that are able to perform theoretical calculations, like Spartan and Gaussian. This will predict how the experiment might transpire and will investigate the research at the molecular level in the gas phase. There are different levels of theory that vary in their mathematical convergence procedures. The density-functional level of theory at the ground state is normally extremely accurate regarding these types of calculations with full optimization using the MP2 model system at 6-31G*. These suites of programs are able to easily expose a system to differing environments, along with modeling reactions and dissociations. Outputs from these calculations give information inherent to compounds such as heats of formation, bonding energies, vibrational modes, structural geometries, and heat capacities as a few examples.¹⁷

Comparing results that have already been performed on dimers, the hydrogen bond alone has the most influence on the overall energy of the coupled dimer; however, this specific amount of energy is modified among different systems. For example, a benzoic acid dimer has a transition state energy and a shift in bands that are unlike that of a formic and benzoic acid mixed dimer. The homodimer appears to be slightly bent with hydrogen bond lengths that aren't the same within the dimer. However, the specific vibrations within each dimer system are very similar, as evidenced by both the theoretical calculations and experimental spectra. Therefore, computational calculations can provide a valuable comparison to actual results as can be seen here, which is useful within the research that is being performed in this thesis.¹⁷

Therefore, this research project will make use of the molecular mechanics and quantum chemical calculations starting from all that's been derived from the Schrödinger equation. The solution to the Schrödinger equation is in terms of the motion of electrons which gives important information regarding molecular structure, bonding, and energy. The problem with this equation is that it can only exactly solve one-electron systems; hence, quantum chemical models can be used to approximate the energies. For example, the Born-Oppenheimer approximation assumes that the nuclei of a molecular system do not move compared to the movement of its corresponding electrons. From this type of general theory, many levels of computational modeling have been developed using different ways of determining the total energy present in a molecule, bond angles, and bond lengths.⁴⁹ The two specific models utilized in this research, Hartree-Fock and Density Functional, will be discussed here to differentiate between them.

The Hartree-Fock approximation uses a set of coupled differential equations containing coordinates for a single electron. Even though this can be solved, it's more accurate to include another approximation allowing for conversion of the Hartree-Fock equations into a set of algebraic equations. Therefore, linear combinations of atomic orbitals (LCAO) can be taken into account by making linear combinations of a finite set, or basis functions. Molecular orbitals are utilized, as these account for electrons being assigned in pairs to functions. Use of the electronic Schrödinger equation, Hartree-Fock approximation, and LCAO approximation, result in Roothaan-Hall equations, whose solution is termed a Hartree-Fock model. This kind of model separates each electron's motion in many-electron systems resulting in a product of the motions of individual electrons; however, this causes an overestimation of the total energy, since it accounts for a higher electron-electron repulsion energy. The main Hartree-Fock basis set used in this research is 6-31G*. This is a polarization basis set having functions of higher angular quantum numbers than the ground state. In general, this type of basis set is available for the elements hydrogen through krypton with good accuracy.⁴⁹

Density functional model systems work in a different way by introducing an “approximate” correlation term using very clear methodology. This system utilizes the electron density instead of the many-electron wavefunction while being well-defined as neither size consistent nor variational. Therefore, it employs use of Hamiltonian terms using an exact solution of an ideal many-electron system. This method uses the same analytical procedures as Hartree-Fock by using its exchange terms but also adds a calculation to handle the exchange/correlation function. This makes hybrid density functional models very popular as well with one such model being used in this research.

This is called the B3LYP model, and it specifically accounts for the exchange energy from Hartree-Fock by using the Hartree-Fock 3-21G calculation for geometry then calculating the B3LYP 6-31G* density functional. The density functional model involves three changeable parameters that better elucidate non-uniformity in electron distributions.⁴⁹

3.6 Experimental Methods

A variety of experimental methods were performed in this research project to provide a diverse approach to studying aspartic and glutamic acids in a potassium chloride matrix. Therefore, the explanation of each technique will be provided below with an initial explanation of the sample preparation followed by procedures for the various analytical techniques used to examine these mixtures. Each method is meant to complement the others that have been performed to give a more complete picture of what may be occurring.

3.6.1 Mixture Preparation

In order to make these mixtures and provide data that would complement prior studies in this laboratory, 10% (w/w) ratios of each single amino acid with potassium chloride were weighed. Therefore, the blends of amino acid:KCl were the following; 100:0, 90:10, 80:20, 70:30, 60:40, 50:50, 40:60, 30:70, 20:80, 10:90, 0:100. All chemicals were stored at room temperature and used without additional purification. The mixtures were then ground into a powder using a mortar and pestle, were stored in 15 x

45 mm labeled vials, and were placed in a desiccator until further experimentation was performed.

Once all experiments for Raman, FT-IR, and powder XRD were executed on every unheated mixture, these samples at each ratio could then be distributed into two 1 gram portions, placed in separate crucibles, and heated to their two decomposition temperatures based on the prior findings from thermogravimetric analysis and differential scanning calorimetry research. The graphs from which these temperatures were determined are shown in Appendix A on page 173. For the aspartic acid mixtures, the decomposition temperatures were determined to be at 237 °C and 277 °C, while the glutamic acid mixtures decomposed at 200 °C and 209 °C based on the previous experimentation. A CF1400 Muffle Furnace (Across International, 200V) was used to accomplish heating these samples. The samples were positioned in the furnace two at a time with an aluminum foil covering placed firmly on top of each. At a ramp rate of 20°C per minute, each sample was raised from room temperature to its corresponding decomposition temperature. Then, a dwell time of one minute occurred at this peak temperature before the samples were ramped back down to room temperature at the same rate. Samples could then be removed from the furnace, cooled down in a desiccator, and placed in labeled 15 x 45 mm vials. These vials were then stored in a desiccator until further experimentation was performed using the Raman, FT-IR, and powder XRD instrumentation.

3.6.2 Raman Spectroscopy

The Horiba Scientific iHR320 fully automated imaging spectrometer (Part No. J81092 rev. G, Model No. 356399) was employed in all Raman experimentation. Additionally, a fiber optic Raman sampling probe (Model RPSXXX/FF-YY) was used. Upon focusing the 531.43 nm laser beam, one gram of each mixture in all ratios was evenly poured onto a piece of weigh paper and placed on the stage. The laser was switched from image mode to Raman mode and the spectra was then recorded. This same procedure was executed for both unheated and heated samples. All data was collected using the NGS LabSpec software program over a wavelength range of 0 to 3000 nanometers.

3.6.3 Fourier Transform Infrared Spectroscopy

The Nicolet Nexus 670 FT-IR (Thermo Electron Corporation) was used to measure all FT-IR spectra along with the Foundation Series: Thermo Spectra Tech interior auxiliary stage attachment. Spectra were collected using 128 scans and a resolution of four while obtaining a background measurement before every sample. A gram of each sample was placed in the germanium windowed sample holder upon the completion of the background measurement. After each sample's measurement, the sample was removed, poured back into its corresponding vial, and returned to the desiccator. The window and cover plate were then rinsed with methanol, cleaned with a KimWipe, and put back on the stage to obtain another background measurement for the next sample. The OMNIC computer software collected all data while measuring the

percent transmittance obtained at each corresponding wavenumber. All of the spectra were acquired from 650-4000 wavenumbers.

3.6.4 Powder X-Ray Diffraction

Initially, a sample holder was obtained with the appropriate sample of interest and the holder was placed on a piece of weighing paper. The sample was then poured carefully onto the holder, and a microscope slide was used to press the sample evenly across the holder. Excess sample could be carefully scraped from the edges of the sample holder while ensuring it was completely level. The data collection software could then be used to initiate the following appropriate experimental set-up: start at a 5° angle and proceed to 90° at a 0.5° tilt per minute. Therefore, each sample required approximately a three hour completion time.

Every sample measurement was executed on the Rigaku MiniFlex II Desktop X-ray Diffractometer (Cat No. 2005H302, Ser. No. ED435511, Date 8/2008). The Diffraction EVA database could then be used to compare the experimentally observed spectra to those already in a known database.

3.6.5 Theoretical Calculations

An extremely important aspect of many experimental studies involves the comparison of applicable theoretical values to which results from the computational approach can be compared to one another. The molecules observed using this method are those that were determined to be potentially formed via Praveen Bandarupalli's thermal decomposition analysis. These structures are presented in Appendix A for aspartic and

glutamic acids on pages 173 and 175, respectively. Each possible molecule being formed was drawn into the Spartan '09 computer program with HF and DFT levels both performed on each. Therefore, the results from each of these can be compared with one another as well. According to theory, the DFT method should give the best results, since this level of theory supposedly has a better convergence to the “true” value compared to levels of theory beneath it.

3.7 Results

3.7.1 Spectral Data

One sample spectrum from each method for Raman spectroscopy, FT-IR, and powder XRD will be provided on the next three pages, respectively. However, the actual results from these methods will be discussed further in section 3.8 where comparisons to the literature will be made as well. The naming of each individual compound follows the following format: temperature, compound, compound's weight in ratio. For example, an Asp 10: KCl 90 mixture heated to 277 °C would be named “277 Asp 10.”

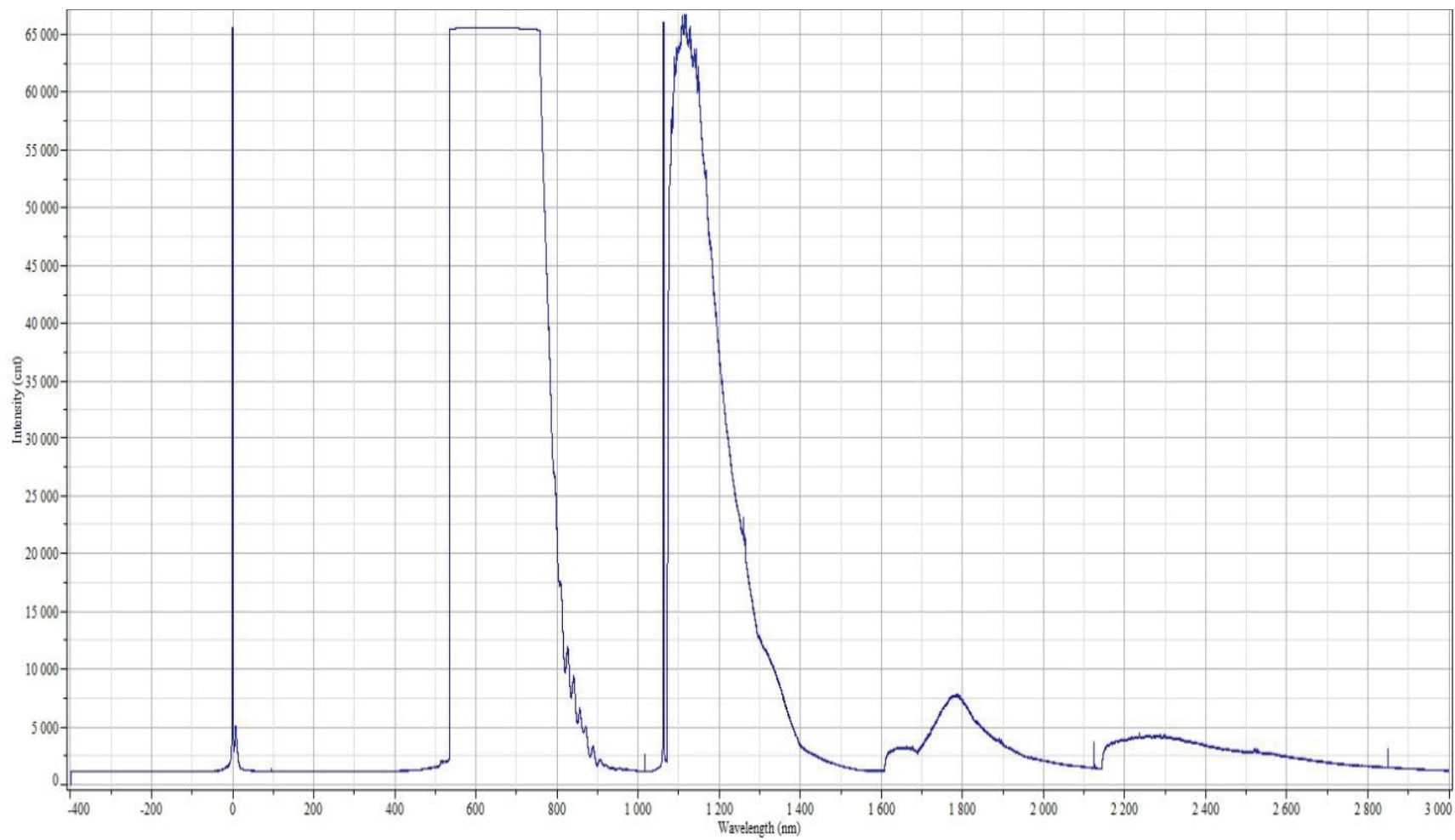


Figure 3.5 Sample Raman Spectrum for the 237 Asp 50 Mixture

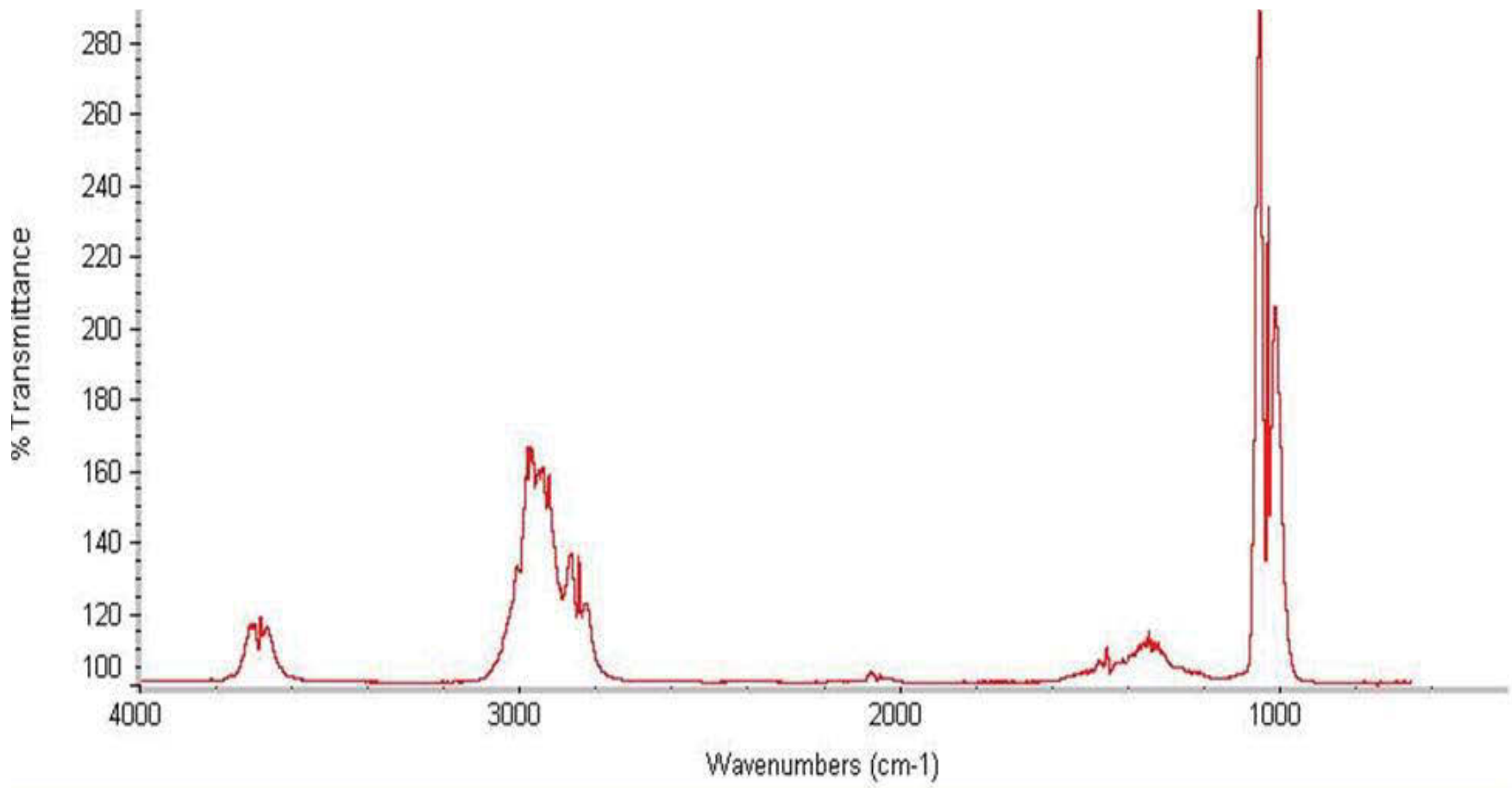


Figure 3.6 Sample FT-IR Spectrum for the 237 Asp 50 Mixture

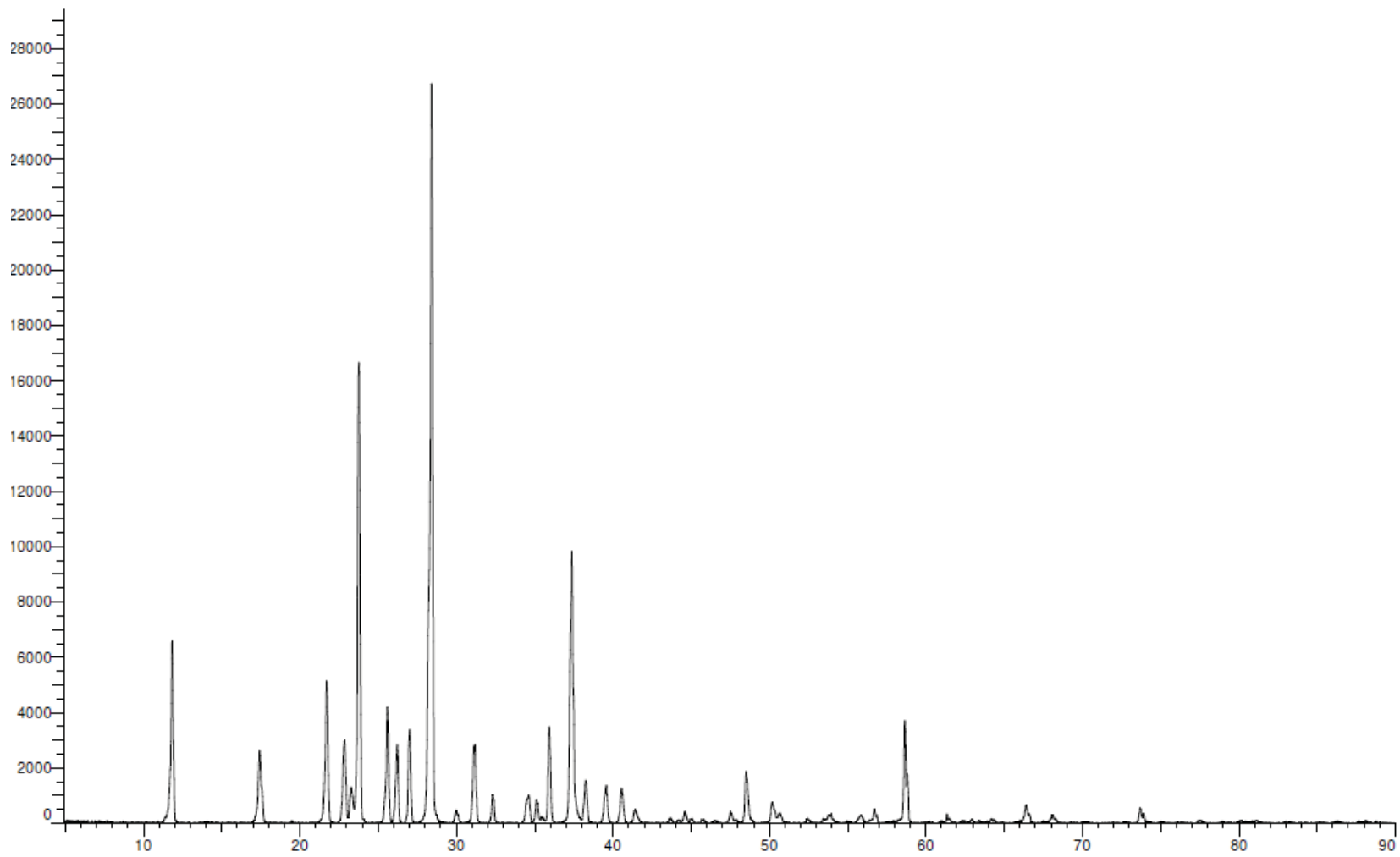


Figure 3.7 Sample Powder XRD Spectrum for the 237 Asp 50 Mixture (x-axis is 2θ and y-axis is intensity)

3.7.2 Spartan Exploration

Theoretical calculations were performed on all projected compounds that could form through heating of the samples both with and without the possibility of a potassium chelated complex. These were based on previous research and work from the Balendiran laboratory group.²⁶ Appendix A on page 173 shows the structural features of each option including its naming scheme and structure. The results in this section include a comparison between Hartree-Fock and density functional levels of theory in their bond lengths and Gibb's free energy values. The numbering of the bonds as well as images of each compound on Spartan before each run is provided in each figure directly before its corresponding table of bond length data. Appendix B on page 177 includes specific instructions on how to run the Spartan computer program.

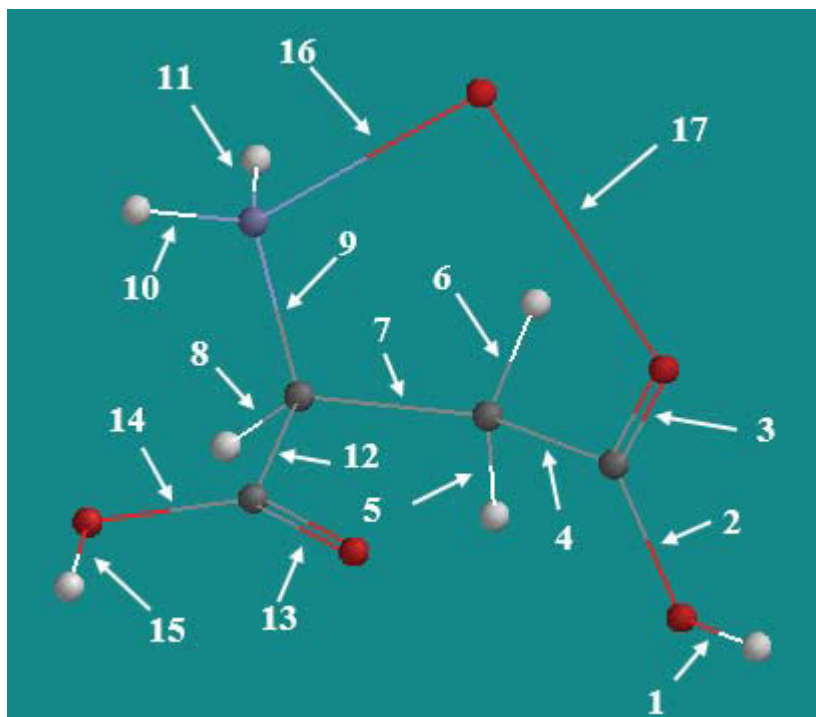


Figure 3.8 Asp (A) Complex with Minimized Energy before Calculation

Table 3.1 Asp (A) Complex Bond Lengths

Bond Number	Bond Type	Minimized Energy Before Run (Å)	Hartree-Fock After Run (Å)	Density Functional Theory After Run (Å)
1	H-O	0.981	0.955	0.977
2	O-C	1.351	1.306	1.329
3	C=O	1.299	1.202	1.225
4	C-C	1.531	1.508	1.515
5	C-H	1.096	1.083	1.095
6	C-H	1.100	1.085	1.097
7	C-C	1.554	1.530	1.537
8	C-H	1.099	1.088	1.101
9	C-N	1.448	1.462	1.477
10	N-H	1.022	1.004	1.021
11	N-H	1.021	1.004	1.021
12	C-C	1.529	1.522	1.530
13	C=O	1.223	1.180	1.202
14	C-O	1.341	1.340	1.372
15	O-H	0.981	0.956	0.979
16	N-K	2.665	2.881	2.800
17	K-O	2.647	2.608	2.564

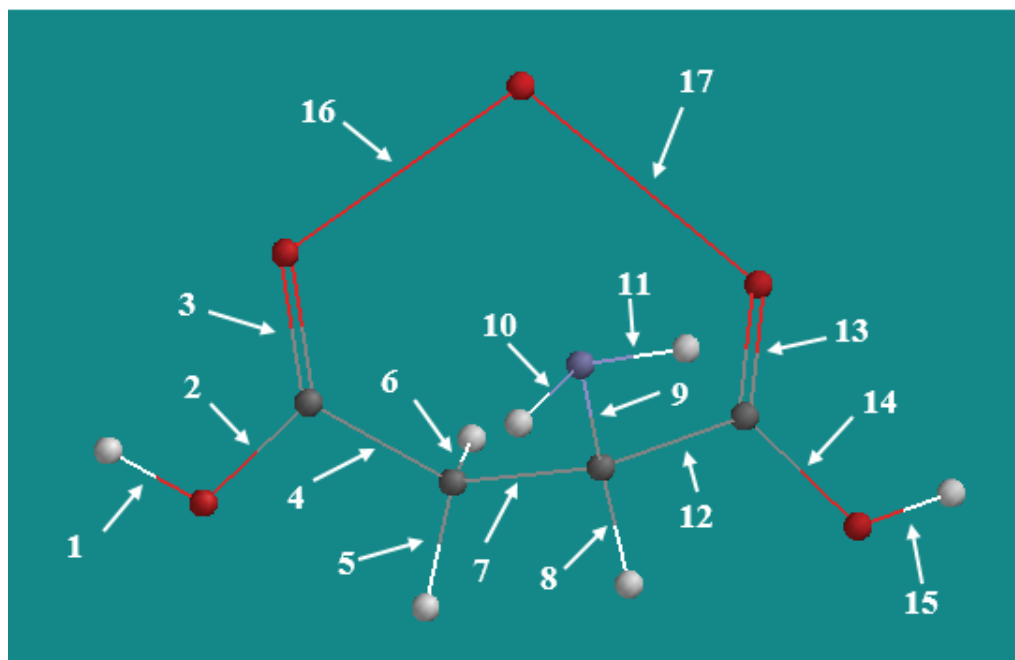


Figure 3.10 Asp (C) Complex with Minimized Energy before Calculation

Table 3.3 Asp (C) Complex Bond Lengths

Bond Number	Bond Type	Minimized Energy Before Run (Å)	Hartree-Fock After Run (Å)	Density Functional Theory After Run (Å)
1	H-O	0.985	0.955	0.978
2	O-C	1.344	1.308	1.331
3	C=O	1.289	1.200	1.223
4	C-C	1.509	1.509	1.516
5	C-H	1.098	1.085	1.097
6	C-H	1.095	1.084	1.096
7	C-C	1.539	1.533	1.538
8	C-H	1.098	1.088	1.101
9	C-N	1.479	1.457	1.473
10	N-H	1.034	1.003	1.020
11	N-H	1.035	1.004	1.021
12	C-C	1.551	1.521	1.530
13	C=O	1.290	1.195	1.219
14	C-O	1.346	1.311	1.334
15	O-H	0.985	0.955	0.978
16	O-K	2.647	2.651	2.591
17	K-O	2.647	2.663	2.613

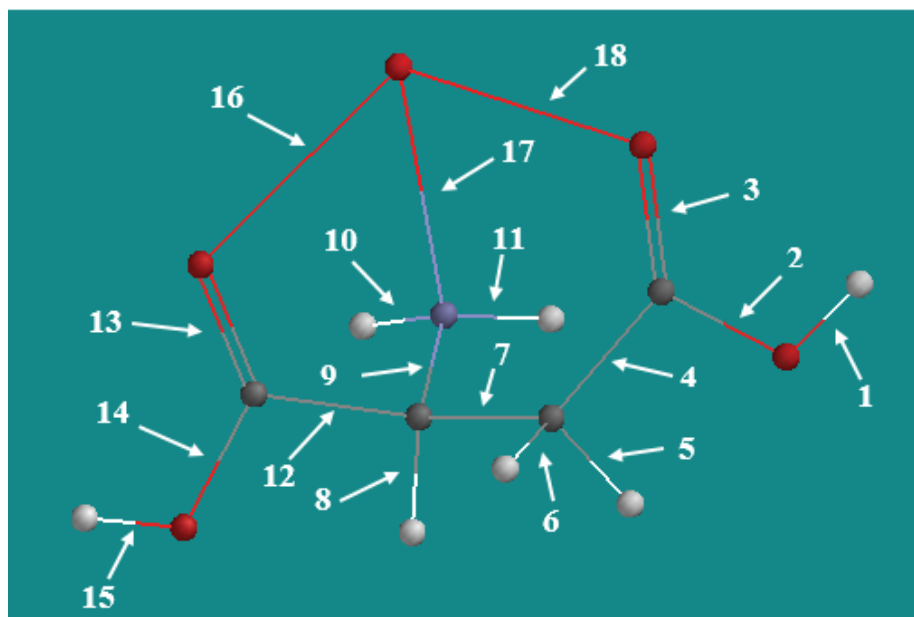


Figure 3.11 Asp (D) Complex with Minimized Energy before Calculation

Table 3.4 Asp (D) Complex Bond Lengths

Bond Number	Bond Type	Minimized Energy Before Run (Å)	Hartree-Fock After Run (Å)	Density Functional Theory After Run (Å)
1	H-O	0.985	0.955	0.978
2	O-C	1.354	1.308	1.331
3	C=O	1.303	1.199	1.223
4	C-C	1.574	1.509	1.516
5	C-H	1.102	1.085	1.097
6	C-H	1.100	1.084	1.096
7	C-C	1.578	1.533	1.539
8	C-H	1.101	1.088	1.101
9	C-N	1.470	1.457	1.473
10	N-H	1.022	1.004	1.021
11	N-H	1.019	1.003	1.020
12	C-C	1.670	1.521	1.531
13	C=O	1.321	1.195	1.219
14	C-O	1.347	1.311	1.334
15	O-H	0.985	0.955	0.978
16	O-K	2.649	2.662	2.617
17	K-N	2.657	2.956	2.840
18	K-O	2.644	2.654	2.599

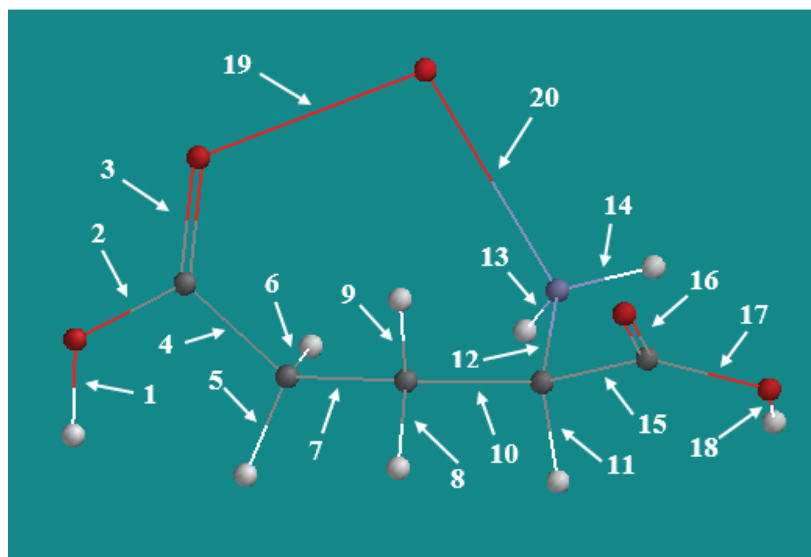


Figure 3.12 Glu 1 Complex with Minimized Energy before Calculation

Table 3.5 Glu 1 Bond Lengths

Bond Number	Bond Type	Minimized Energy Before Run (Å)	Hartree-Fock After Run (Å)	Density Functional Theory After Run (Å)
1	H-O	0.980	0.950	0.973
2	O-C	1.346	1.315	1.338
3	C=O	1.292	1.192	1.216
4	C-C	1.511	1.519	1.529
5	C-H	1.092	1.087	1.098
6	C-H	1.096	1.087	1.100
7	C-C	1.531	1.531	1.536
8	C-H	1.099	1.084	1.095
9	C-H	1.097	1.082	1.094
10	C-C	1.550	1.553	1.558
11	C-H	1.099	1.089	1.103
12	C-N	1.437	1.457	1.472
13	N-H	1.021	1.002	1.019
14	N-H	1.022	1.002	1.019
15	C-C	1.544	1.528	1.540
16	C=O	1.222	1.192	1.215
17	C-O	1.351	1.312	1.334
18	O-H	0.976	0.949	0.973
19	O-K	2.647	2.637	2.602
20	K-N	2.668	2.976	2.881

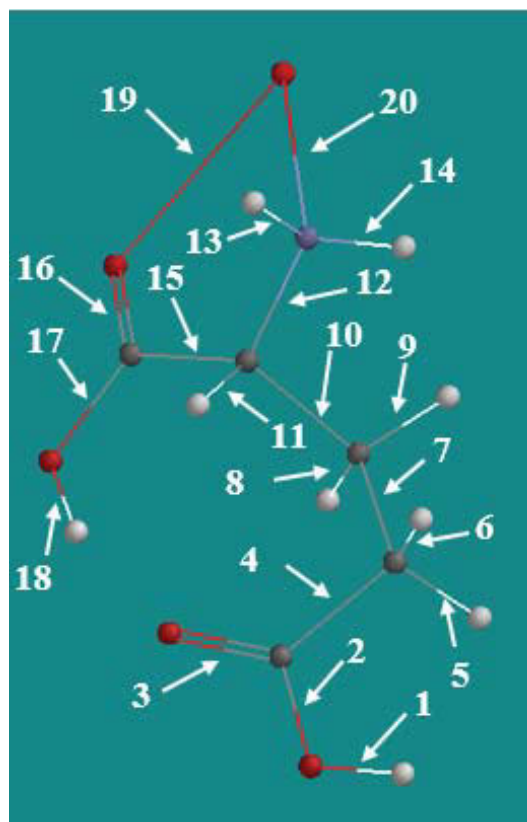


Figure 3.13 Glu 2 Complex with Minimized Energy before Calculation

Table 3.6 Glu 2 Bond Lengths

Bond Number	Bond Type	Minimized Energy Before Run (Å)	Hartree-Fock After Run (Å)	Density Functional Theory After Run (Å)
1	H-O	0.979	0.950	0.973
2	O-C	1.340	1.314	1.335
3	C=O	1.228	1.192	1.218
4	C-C	1.508	1.517	1.524
5	C-H	1.094	1.086	1.098
6	C-H	1.095	1.088	1.100
7	C-C	1.539	1.530	1.535
8	C-H	1.097	1.083	1.095
9	C-H	1.098	1.084	1.096
10	C-C	1.554	1.553	1.559
11	C-H	1.099	1.085	1.099
12	C-N	1.481	1.464	1.480
13	N-H	1.021	1.005	1.022
14	N-H	1.019	1.004	1.021
15	C-C	1.650	1.529	1.541
16	C=O	1.318	1.200	1.226
17	C-O	1.354	1.297	1.314
18	O-H	0.995	0.962	0.996
19	O-K	2.642	2.531	2.492
20	K-N	2.660	3.003	2.889

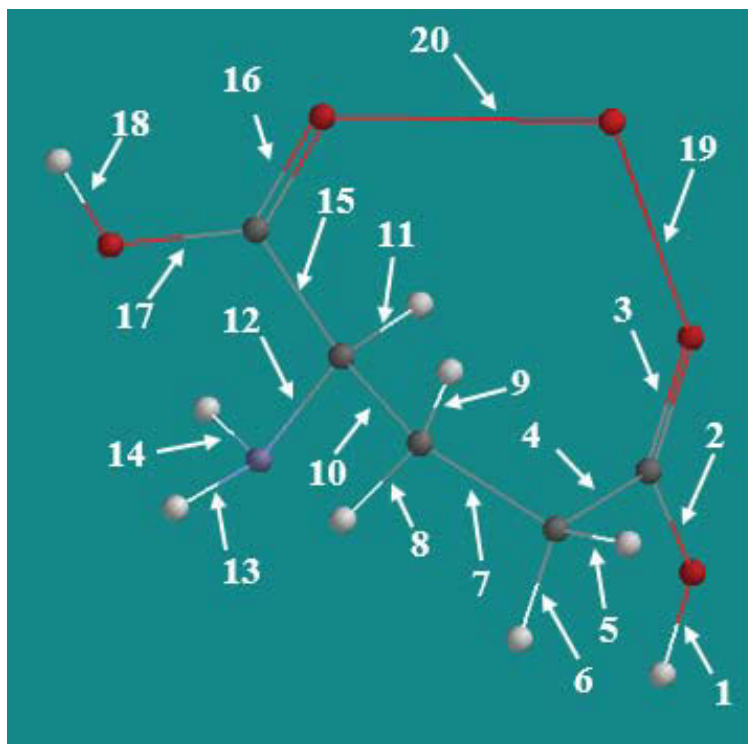


Figure 3.14 Glu 3 Complex with Minimized Energy before Calculation

Table 3.7 Glu 3 Bond Lengths

Bond Number	Bond Type	Minimized Energy Before Run (Å)	Hartree-Fock After Run (Å)	Density Functional Theory After Run (Å)
1	H-O	0.982	0.951	0.974
2	O-C	1.346	1.312	1.334
3	C=O	1.292	1.199	1.223
4	C-C	1.509	1.515	1.521
5	C-H	1.097	1.087	1.099
6	C-H	1.097	1.086	1.099
7	C-C	1.533	1.526	1.530
8	C-H	1.100	1.084	1.095
9	C-H	1.095	1.082	1.094
10	C-C	1.536	1.545	1.554
11	C-H	1.092	1.082	1.096
12	C-N	1.466	1.438	1.449
13	N-H	1.030	1.001	1.018
14	N-H	1.028	1.001	1.017
15	C-C	1.533	1.524	1.533
16	C=O	1.292	1.204	1.228
17	C-O	1.343	1.307	1.330
18	O-H	0.984	0.955	0.978
19	O-K	2.646	2.597	2.531
20	K-O	2.653	2.661	2.597

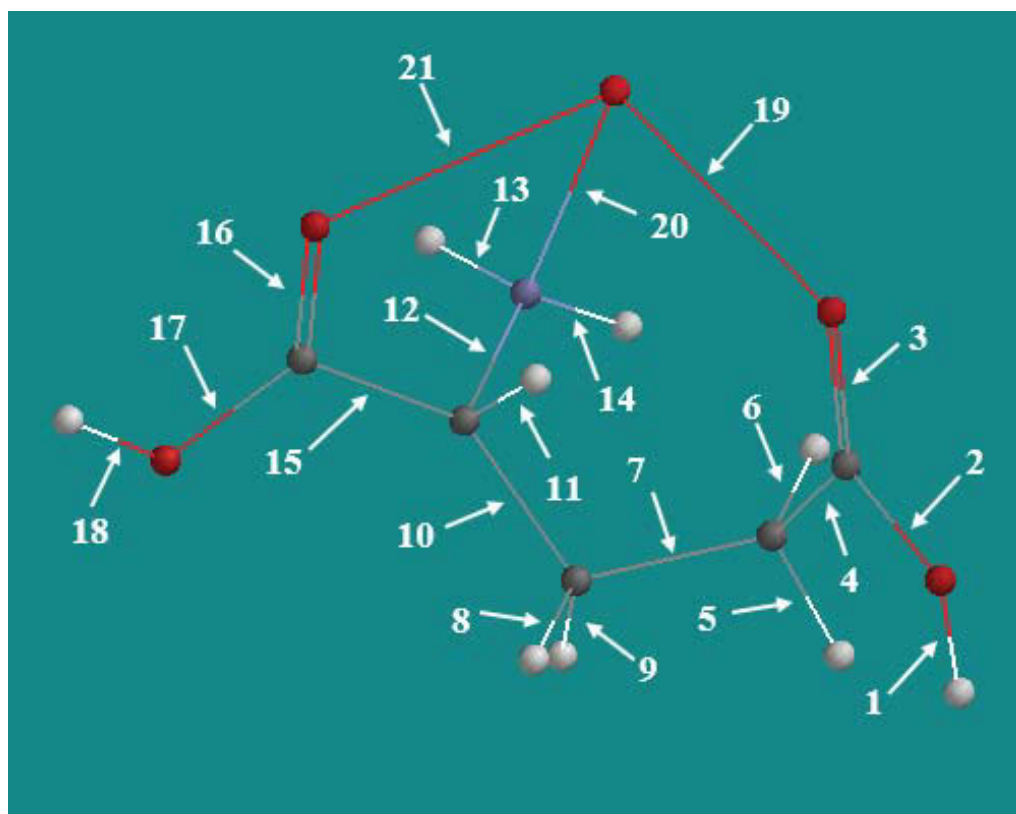


Figure 3.15 Glu 4 Complex with Minimized Energy before Calculation

Table 3.8 Glu 4 Bond Lengths

Bond Number	Bond Type	Minimized Energy Before Run (Å)	Hartree-Fock After Run (Å)	Density Functional Theory After Run (Å)
1	H-O	0.982	0.948	0.972
2	O-C	1.350	1.318	1.341
3	C=O	1.305	1.190	1.216
4	C-C	1.548	1.520	1.527
5	C-H	1.094	1.084	1.095
6	C-H	1.098	1.084	1.096
7	C-C	1.588	1.541	1.549
8	C-H	1.097	1.086	1.097
9	C-H	1.096	1.082	1.094
10	C-C	1.537	1.543	1.547
11	C-H	1.090	1.084	1.098
12	C-N	1.480	1.459	1.476
13	N-H	1.016	1.004	1.022
14	N-H	1.021	1.005	1.025
15	C-C	1.626	1.522	1.530
16	C=O	1.332	1.200	1.224
17	C-O	1.338	1.309	1.331
18	O-H	0.984	0.955	0.978
19	O-K	2.654	5.341	5.042
20	K-N	2.665	2.863	2.761
21	K-O	2.666	2.605	2.573

The following molecules' bond length data, which is provided below, were suggested as potentially forming upon degradation prior to what was proposed within Praveen's research. Appendix A provides the structures for all of the following molecules, and the Spartan '04 data is given here as well.

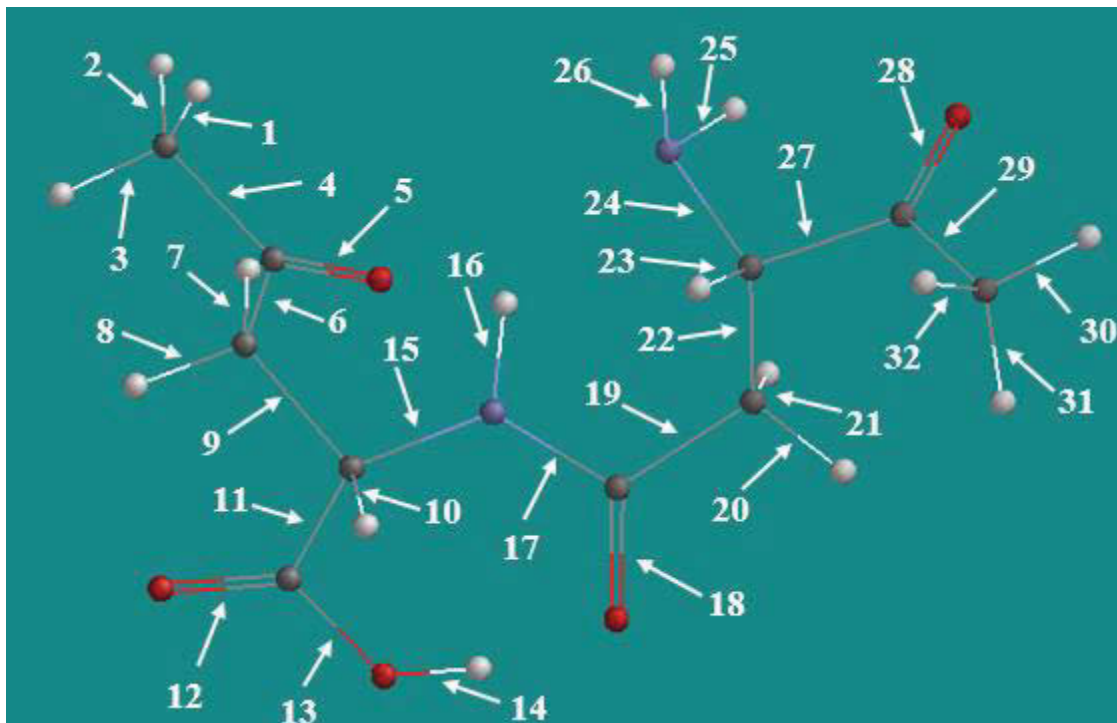


Figure 3.16 Polyaspartic Acid with Minimized Energy before Calculation

Table 3.9 Polyaspartic Acid Bond Lengths

Bond Number	Bond Type	Minimized Energy Before Run (Å)	Hartree-Fock After Run (Å)	Density Functional Theory After Run (Å)
1	C-H	1.094	1.081	1.092
2	C-H	1.093	1.086	1.097
3	C-H	1.093	1.086	1.097
4	C-C	1.507	1.513	1.518
5	C=O	1.231	1.195	1.219
6	C-C	1.516	1.518	1.523
7	C-H	1.096	1.087	1.099
8	C-H	1.096	1.087	1.099
9	C-C	1.533	1.523	1.526
10	C-H	1.098	1.084	1.100
11	C-C	1.543	1.534	1.550
12	C=O	1.225	1.187	1.211
13	C-O	1.352	1.317	1.334
14	O-H	0.998	0.960	0.997
15	C-N	1.470	1.457	1.468
16	N-H	1.023	1.000	1.026
17	N-C	1.367	1.342	1.350
18	C=O	1.229	1.212	1.242
19	C-C	1.511	1.518	1.526
20	C-H	1.096	1.081	1.093
21	C-H	1.097	1.086	1.098
22	C-C	1.529	1.544	1.554
23	C-H	1.096	1.085	1.096
24	C-N	1.490	1.454	1.469
25	N-H	1.030	1.004	1.022
26	N-H	1.025	1.002	1.019
27	C-C	1.533	1.532	1.541
28	C=O	1.233	1.193	1.217
29	C-C	1.507	1.510	1.513
30	C-H	1.094	1.081	1.092
31	C-H	1.092	1.084	1.096
32	C-H	1.093	1.087	1.099

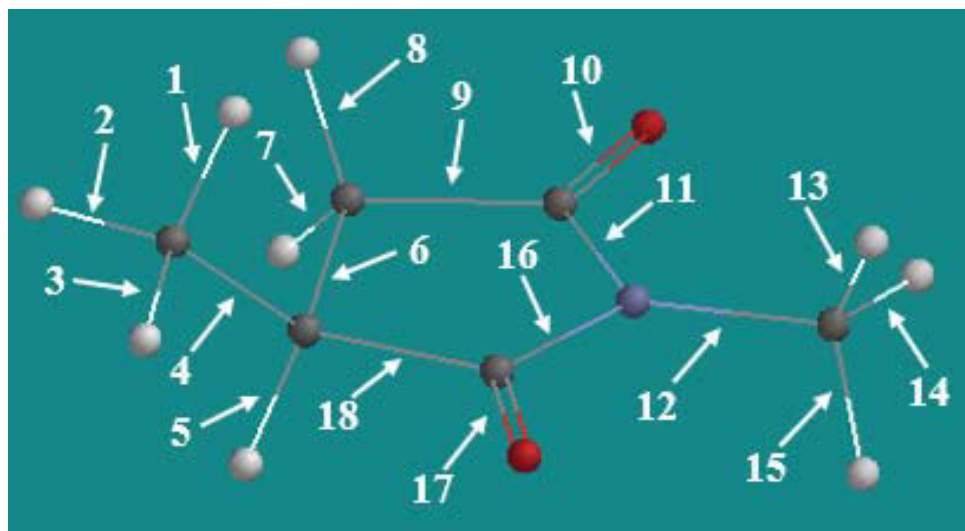


Figure 3.17 Polysuccinimide with Minimized Energy before Calculation

Table 3.10 Polysuccinimide Bond Lengths

Bond Number	Bond Type	Minimized Energy Before Run (Å)	Hartree-Fock After Run (Å)	Density Functional Theory After Run (Å)
1	C-H	1.096	1.086	1.096
2	C-H	1.095	1.085	1.095
3	C-H	1.095	1.082	1.094
4	C-C	1.519	1.527	1.532
5	C-H	1.096	1.086	1.098
6	C-C	1.524	1.535	1.541
7	C-H	1.094	1.082	1.094
8	C-H	1.095	1.085	1.097
9	C-C	1.501	1.516	1.526
10	C=O	1.222	1.190	1.213
11	C-N	1.363	1.378	1.396
12	N-C	1.443	1.451	1.454
13	C-H	1.094	1.081	1.094
14	C-H	1.093	1.078	1.091
15	C-H	1.094	1.082	1.093
16	N-C	1.365	1.375	1.392
17	C=O	1.222	1.190	1.214
18	C-C	1.508	1.521	1.532

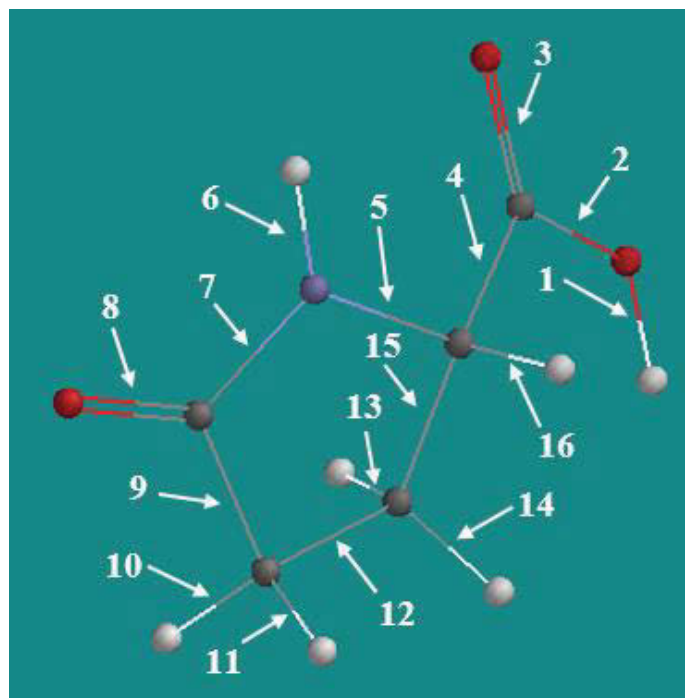


Figure 3.18 Pyroglutamic Acid with Minimized Energy before Calculation

Table 3.11 Pyroglutamic Acid Bond Lengths

Bond Number	Bond Type	Minimized Energy Before Run (Å)	Hartree-Fock After Run (Å)	Density Functional Theory After Run (Å)
1	H-O	0.975	0.949	0.973
2	O-C	1.353	1.333	1.360
3	C=O	1.224	1.181	1.205
4	C-C	1.531	1.520	1.529
5	C-N	1.441	1.434	1.445
6	N-H	1.016	0.997	1.013
7	N-C	1.375	1.355	1.372
8	C=O	1.217	1.195	1.219
9	C-C	1.505	1.520	1.533
10	C-H	1.092	1.081	1.093
11	C-H	1.094	1.086	1.098
12	C-C	1.527	1.533	1.539
13	C-H	1.098	1.085	1.096
14	C-H	1.094	1.084	1.095
15	C-C	1.523	1.549	1.560
16	C-H	1.095	1.091	1.105

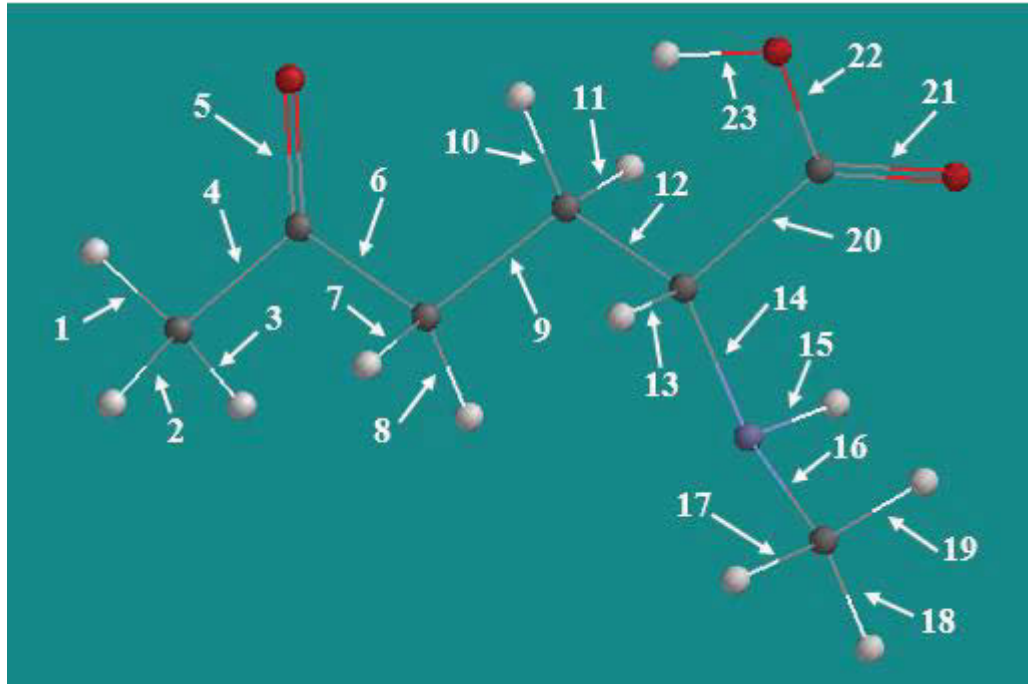


Figure B.19 Polyglutamic Acid with Minimized Energy before Calculation

Table 3.12 Polyglutamic Acid Bond Lengths

Bond Number	Bond Type	Minimized Energy Before Run (Å)	Hartree-Fock After Run (Å)	Density Functional Theory After Run (Å)
1	C-H	1.094	1.080	1.092
2	C-H	1.093	1.085	1.097
3	C-H	1.093	1.086	1.098
4	C-C	1.506	1.514	1.520
5	C=O	1.231	1.212	1.217
6	C-C	1.517	1.514	1.524
7	C-H	1.095	1.088	1.102
8	C-H	1.095	1.083	1.097
9	C-C	1.530	1.529	1.528
10	C-H	1.099	1.083	1.097
11	C-H	1.098	1.083	1.097
12	C-C	1.535	1.544	1.547
13	C-H	1.097	1.085	1.101
14	C-N	1.482	1.454	1.454
15	N-H	1.027	1.007	1.020
16	N-C	1.460	1.475	1.466
17	C-H	1.095	1.083	1.097
18	C-H	1.094	1.082	1.094
19	C-H	1.094	1.085	1.102
20	C-C	1.542	1.524	1.545
21	C=O	1.224	1.198	1.206
22	C-O	1.354	1.359	1.359
23	O-H	0.976	0.963	0.972

It should be noted here that polyglutamic acid would not run at the Hartree-Fock level of theory using 6-31G*, so the above data are from Hartree-Fock 3-21G*.

Tables 3.13 and 3.14 below use the following equation to calculate the percent difference between the Hartree Fock and Density Functional Theory's Free Energy values:

$$\text{Percent Difference} = \frac{N_1 - N_2}{((N_1 + N_2)/2)} \times 100$$

Table 3.13 Gibbs Free Energy for Hartree-Fock and Density Functional Theories with Percent Differences

Molecule	Hartree-Fock (kJ/mol)	Density Functional (kJ/mol)	Percent Difference
Aspartic Acid	262.8201	232.8895	12.076%
Asp A	307.7497	230.0971	28.88%
Asp B	202.7166	230.9535	13.02%
Asp C	188.7738	230.7310	20.00%
Asp D	226.2237	230.9835	2.08%
Glutamic Acid	337.3616	302.4471	10.91%
Glu 1	370.5886	297.3759	21.92%
Glu 2	299.7071	302.8250	1.035%
Glu 3	297.8646	298.5379	0.23%
Glu 4	313.4546	300.1413	4.34%
Potassium Chloride	-59.8664	-59.8217	0.08%

Table 3.14 Gibbs Free Energy for Prior Suggested Thermal Decomposition Intermediates Using Hartree-Fock and Density Functional Theories with Percent Differences

Molecule	Hartree-Fock (kJ/mol)	Density Functional (kJ/mol)	Percent Differences
Polyaspartic Acid	548.4167	573.9755	4.55%
Polysuccinimide	329.6422	301.0173	9.08%
Pyroglutamic Acid	228.3148	239.9881	4.99%
Polyglutamic Acid	461.8014	424.2731	8.47%

3.8 Discussion

Regarding the Raman data, each set of samples will be discussed individually and then compared to one another and to values in the literature. There were no major differences across unheated aspartic acid mixtures. A broad peak in the 550-800 nm region intensified with increasing aspartic acid, except for Asp 40, which could've been due to the run not being optimized completely. The peak from 1080-1300 nm intensified with increasing aspartic acid as well along with other subtle peaks becoming more prominent for the same reason. Asp 40 did not follow the general trend and might have had a poor run. When aspartic acid samples were heated to 237 °C, much more prominent peaks appeared than in the unheated aspartic acid mixtures. Although no new peaks appeared within these spectra at this temperature level, it was shown that increasing the aspartic acid within each mixture increased the intensity of the peaks generally which is expected. The only anomaly was within the 237 Asp 90 case, in which another poor data collection may have occurred. Finally, aspartic acid samples heated to 277 °C showed much more prominent peaks even compared to the 237 Asp spectra. In fact, the peaks appear to take up the majority of every spectra with not much background present. All of the spectra appear very similar except for Asp 40 and Asp 70 at this temperature. Both of these have two peaks merge into one from the 1600-3000 nm region, while all others have a slight indentation between them, indicating separation at roughly 2150 nm. Therefore, these two mixtures at this temperature may be important for complex formation.

Next, discussion of glutamic acid samples studied through Raman spectroscopy will be detailed. Unheated glutamic acid samples had really no major difference across

them with two major peaks appearing: one in the 550-800 nm range and the other at 1080-1300 nm. Both sets tend to encompass more area as the glutamic acid within each mixture increases. Additionally, Glu 20 mildly decreased in intensity. When samples of glutamic acid were heated to 200 °C, new peaks appeared as the glutamic acid within each sample increased. These were very prominent in the Glu 50, Glu 90, and Glu 100 mixtures starting at 1600 nm through 3000 nm. Both peak sets intensify with increasing glutamic acid; however, the peak at 1080-1300 nm grew slowly with increasing glutamic acid until Glu 60 and Glu 70. Then they increased again in intensity with a dip at Glu 100 as well. The glutamic acid samples heated to 209 °C had peaks located in the same locations as the unheated and 200 °C heated samples. Although the Glu 20, Glu 40, and Glu 60 all heated to 209 °C did not have optimized runs, the same conclusions can essentially be drawn as those from the 200 °C samples.

As a type of control, potassium chloride samples were analyzed as well through this method in their unheated form, as well as each degradation temperature that was determined in the prior study. Peaks appear in the same general locations with two major peaks appearing in the 550-800 nm and 1080-1400 nm ranges. In the first peak range area, the peak heights are all below an intensity of 20,000 except at temperatures of 237 and 277 °C. Also, in this second peak region, there is a negligible height intensity, except at the two high temperatures as well. Additionally, at both 237 and 277 °C, double peaks appeared in the 1600-1900 nm range along with a wide, low intensity peak from 2150-3000 nm.

Overall, there was a clear correlation between increasing temperature in aspartic acid samples and an increase in intensity with the potential for chelation behavior by

involvement of a potassium ion specifically from the 237 to 277 °C temperature change. For glutamic acid, the results are fairly inconclusive because all spectra generally look the same. This suggests that maybe a higher temperature was needed for greater interactions to occur and to be seen within the spectra and should be applied to future work. Although peak assignments to exact functional groups within both sets were unable to be performed, knowing the locations and changes in intensities of the peaks can be helpful in determining whether or not interactions are occurring.

Performing FT-IR spectroscopy on all samples showed that both aspartic and glutamic acid spectra have the following four designated peak portions: 1100-900 cm^{-1} , 1500-1200 cm^{-1} , 3100-2800 cm^{-1} , 3800-3600 cm^{-1} . There were very distinct peaks in the first portion and two distinct humps in the third peak portion as well. The fingerprint region, which is located between 1250 and 600 cm^{-1} , is not a very useful region to analyze. Many peaks in this area represent combinations of various vibrational modes which are sensitive to the overall molecular structure. Therefore, this region will not attempt to be analyzed. The peaks in the 3100-2800 cm^{-1} range are most likely caused by the carboxylic acid group stretching, part of which is a strongly bonded hydrogen. This could also be attributed to C-H stretching. Finally, the two distinct humps in the 3800-3600 cm^{-1} area are caused by the $-\text{NH}_2$ group, as this appears as two correlated peaks in most IR spectra.^{43,50} Additionally, a minor peak appears in the 2000-2100 cm^{-1} range and is especially noticeable in well-defined, smooth spectra. This region cannot be attributed to any other functional groups present within the molecule; therefore, some form of chelation may be occurring, or this could just be an impurity within all of the samples. The Glu 90 and Glu 100 samples have especially messy spectra from 1600-800 cm^{-1} .

Even though unheated KCl 100 plus all of the heated KCl samples are not resolved well, there are the same five distinct peaks in all of these spectra that were present in the aspartic and glutamic acid ones as well. Unfortunately, this means that all spectra appear to look the same, and there are no conclusions that can be made using this data.

The powder XRD results can be discussed next. Even though no true conclusions can be drawn from the x-ray diffraction studies, increasing the amount of aspartic acid or glutamic acid across all temperatures of their respective samples increased the complexity of the XRD spectra. Since nothing was able to be matched in the database aside from aspartic acid, glutamic acid, and potassium chloride by themselves, no useful information can be stated regarding what complexes may be forming. The only conclusion that can be made is that the starting materials of each were pure enough even though purification through crystallization or other methods didn't take place; this was confirmed through spectral comparison to the EVA database. For aspartic acid samples, some peaks became more prominent upon heating, while glutamic acid mixtures showed very similar spectra across the same ratio at differing temperatures. Additionally, potassium chloride was tested at all temperatures by itself as a control. Seven major peaks appeared in all KCl spectra; even though the placement of those peaks within the spectra were the same, their heights and therefore intensities varied.

The only XRD study that was found in the literature that possessed a similar approach to what is performed here was executed by Wu *et al.* (2010) Their study heated α L-Glu and β L-Glu to a variety of high temperatures and then quickly cooled them down to room temperature.²³ XRD could be performed to observe differences in spectra based on those temperatures and a comparison could even be made when the samples

were heated to those temperatures for certain allotted periods of time. An α to β transformation was shown through these spectra, however since no cations were present in these samples, there's no correlation that can be made between the spectra from Wu *et al.* (2010) and those found in this thesis. Therefore, further work will need to be performed using XRD to elucidate the locations of specific atoms within these spectra.

Finally, as an extra effort to confirm the presence of a potassium-bonded complex, solid state NMR (ssNMR) was performed on the 237 Asp 50, 277 Asp 50, 200 Glu 50, and 209 Glu 50 mixtures. A few interesting results arose from this set of experimentation. Similar to ^{13}C , the ^1H NMR spectrum of 277 Asp 50 gives a different spectrum when compared to 237 Asp 50, meaning a new interaction is occurring. This could be explained by exchange dynamics between the NH_2 protons and K^+ resulting in broadening of resonances for NH_2 peaks. Additionally, the 237 Asp 50 sample doesn't show any large changes compared to the 100% aspartic acid samples. Both the ^{13}C and ^1H spectra for 277 Asp 100 look similar to 277 Asp 50. For the glutamic acid samples, there were no changes in the spectra for ^1H and for ^{13}C with or without KCl. Finally, the ^{35}Cl NMR all look similar with or without aspartic and glutamic acids.

The Spartan computer analysis on all potential compounds showed an interesting set of results that will now be discussed. First, studies from the literature will be cited for a proper evaluation of their similarities and differences to what is observed here. Next, a comparison of bond lengths will be made among all potential complexes and prior research suggestions of compounds that could form in this process using both HF and DFT levels of theory. Finally, the Gibb's energies of all molecules at both theory levels will be discussed with their distinct variations to see which are more likely to form.

Many attempts have been made in the literature to elucidate the exact binding energies and bond lengths of varying amino acids complexed with different cations. Sang-aroon and Ruangpornivisuti found that a potassium ion complexation reaction requires the least amount of energy compared to the lithium and sodium ion counterparts, which is one reason why the potassium ion was observed in this study.⁵¹ Its complex with aspartic acid in their study gave values of 2.786, 2.517, and 2.543 Å for the potassium ion chelated to nitrogen, to the oxygen closest to nitrogen, and to the oxygen farthest away from nitrogen, respectively.⁵¹ They performed another study as well and found the values to be 2.670, 2.614, and 2.734 Å for the carbonyl oxygen closest to nitrogen, the other oxygen closest to nitrogen, and carbonyl oxygen farthest from the nitrogen, respectively, when all complexed with a potassium cation. Compared to the theoretical research of aspartic acid complexes in this thesis, the N-K interaction gave roughly a 2.6 Å bond length with energy minimization and around 2.8 Å at the highest level of theory after the run.²⁹ Therefore, the value found by Sang-aroon and Ruangpornivisuti for this comparison falls within the range of values determined in the research here. Regarding chelation of the potassium cation with the oxygen closest to the nitrogen for aspartic acid, O-K values of 2.64 Å before the run and about 2.62 Å after the run were calculated. These are slightly higher values than what was found in the first study but do encompass the value within their second study. Finally, the complexation with the oxygen located farthest away from the nitrogen gave values of 2.64 Å and 2.5 Å before and after the run, respectively. This does align with the value determined in the first study as well.

Heaton, Moision, and Armentrout (2008) performed a theoretical study on sodium ions complexed with aspartic acid, asparagine, glutamic acid, and glutamine in varied

conformations.³² An observation of their bond distances for aspartic and glutamic acid can be compared to the results found here. In these cases, the only difference between the studies are that the 2008 study used a sodium ion, while a potassium ion was used in this approach. In both cases, the bond lengths were on average 0.2 Å shorter with a nitrogen chelation and 0.4 Å shorter with an oxygen chelation when the sodium ion was used.³² Additionally, Heaton and Armentrout (2008) looked solely at a sodium ion in complex with asparagine using the DFT theory level in another study. The only difference between asparagine and aspartic acid is that the O-H group that's farthest away from the -NH₂ group in aspartic acid is substituted another -NH₂ group. Therefore, it will be a bit less electronegative than the oxygen that it's replacing.²⁸ A general trend shows that once again exchanging the potassium ion with a sodium ion and aspartic acid for asparagine results in the shortening of bond lengths for each cation in complex with oxygen and nitrogen. This could be caused by sodium being smaller than potassium or the electronegativity dispersion amongst each amino acid when in complex with the cations.

Dunbar, Steill, and Oomens (2011) observed the PhePhe ligand, which is larger than aspartic and glutamic acid; both studies involve a potassium ion interaction, so they can be loosely compared to one another in that respect. They found the bond length between the oxygen and potassium to have a value of 2.57 Å, while calculations within this thesis determined roughly a 2.64 Å bond length when energy was minimized for both aspartic and glutamic acid in the same type of conformation.³⁵ Since the difference is only 0.07 Å, this is not a significant variance. However, all of the ground state configurations in the Dunbar, Steill, and Oomens (2011) study were determined to be tri-dentate, while both bi- and tri-dentate complexes were examined in this thesis. Therefore,

although these studies are similar, they can only really be compared and appreciated for their contributions to this subject.

An assessment of all of the bond lengths for all potential complexes provides interesting results. There are minor differences between the HF and DFT calculations of bond lengths in almost all cases; this shows that the level of theory and the way that these methods converge upon an answer do differ and give varying data. Based on all results and conclusions in the literature, the DFT computational approach is better than HF and will be used for further comparison. In all aspartic acid complexes, the N-K bond lengthens while the O-K bond shortens upon comparison of lengths before and after each calculation. Glutamic acid complexes provide the same results, except in the case of Glu 4; bond number 25, which is a K-O bond jumps from 2.654 Å to 5.042 Å when observing results at the DFT level of theory. This could be caused by a strain in the tri-dentate version compared to the other three bi-dentate options, however aspartic acid doesn't show these results either. This anomaly needs to be researched further but is an interesting finding.

The bond lengths for all intermediates and products of aspartic and glutamic acid's thermal decomposition reactions that were suggested prior to other research performed in this laboratory were studied here as well. The values determined can be appreciated, however no data analysis will be performed on them. For aspartic acid, these molecules included polyaspartic acid and polysuccinimide, while pyroglutamic acid and polyglutamic acid were studied for the decomposition of glutamic acid.

The Gibb's Free energies are stated in the above tables with the percent difference between the HF and DFT levels provided. The DFT investigation performed by Sang-

aroon and Ruangpornvisuti determined that the most stable complex conformer was the bi-coordinated complexes of aspartate with the potassium ion.²⁹ The data here do reflect that with the DFT level of theory but not the HF level. The HF level showed that Asp A has the highest Gibb's energy of all the Asp complexes, referring to the least spontaneous option; the DFT values for these are all very close for these complexes, but Asp D does have the highest value here. Once again, this illustrates that the DFT level of theory may possibly provide better, more accurate data than the HF level. The largest percentage differences in Gibb's energy occur for Asp A and Glu 1 at 28.875% and 21.921%, respectively for each aspartic and glutamic acid chelation. In fact, chelations of potassium to three atoms have less percent differences associated with them compared to the ones with two chelated atoms to potassium. As a side note, it can be seen that potassium chloride has the smallest percent difference when comparing the HF and DFT levels of theory, but this is to be expected; it's the smallest compound and has the least amount of rotations, vibrations, and translations that need to be accounted for in this case.

3.9 Future Work

It was found through this research that the initial Glu-KCl information obtained through prior work²⁵ had incorrect temperature measurements. Both temperatures determined for decomposition were too low to show any type of interactions. Therefore, raising the temperature by 20 degrees was already attempted and showed formation of an amalgam. There was no time to study all of the heated compounds using the stated methods, so Raman spectroscopy, FT-IR, and powder XRD could all potentially be performed in the future to compare those results to what is seen here. Potentially even

completing Raman spectroscopy should be enough evidence needed to confirm a better interaction.

Further work on this topic may include studying other types of compounds and their potential chelation behaviors. These should include different amino acids and other compounds that contain both amine and carboxylic acid groups to draw conclusions on their specific chelating and bonding characteristics. Therefore, initial studies would need to be performed using TGA and DSC analysis to confirm degradation temperatures, and then the four methods utilized in this project could be performed for further investigation. Other methods of analysis should be considered as well, such as mass spectrometry and infrared multiple photon dissociation (IRMPD) spectroscopy. This latter method was used in many similar studies within the literature and gives information on a compound's structure in the gas phase to better understand ion-protein relations.³⁶ Knowledge here could provide useful information as to which structures occur in the solid state as well.

Additionally, potentially changing the ramp rate on the furnace or having a longer dwell time at the peak temperature when heating could vary the results and might be interesting to consider. Even heating the amino acids in the current study to different higher temperatures could possibly change their spectral properties as well.

Determination of the exact peak locations for various functional groups within Raman spectra would be useful knowledge as well and should be looked at in the future. Since the compounds in this research project weren't purified, additional work may need to compare the results found here with those of completely purified samples. Furthermore, work should be attempted on obtaining crystal structures of samples at all temperatures through single crystal XRD methodology to obtain exact configurations of all species.

Chapter 4: NMR Dimerization and Dissociation Studies of Fibrates

4.1 Background Information

The ability to understand how hydrogen bonding occurs in fibrates is of great importance in the realm of treating diabetes and its potential complications. Dimerization of these compounds is of great interest as well due to their functionality and stability. Hydrogen bond energies occurring in this fashion vary based on the environment in which they are present. For example, enzyme interiors, grooves of nucleic acids, and synthetic receptors all are affected by these interactions. In general, hydrogen bonding interactions are weak and occur very quickly in a bulk solution. However, when in a confined solution phase, some molecules form complexes in which the formation of carboxylic acid and primary amide homodimers and heterodimers are all stable in specialized forms.⁵² Therefore, understanding these kinds of interactions is of great importance at the molecular level as it can greatly affect bulk properties.

Use of variable temperature nuclear magnetic resonance (VT-NMR) technology gives an interesting approach to studying these carboxylic acid containing compounds. However, with use of NMR, solvent often is a factor in determining interactions. A theoretical study performed by Efimov and Brazhnikov (2003) related intramolecular hydrogen bonding to solvent interactions with side-chain groups looking at the effect of water on protein folding. Proteins having more hydrogen bonds have less solvent available for interaction with their donor and acceptor side groups. This shows that there is a direct competition between water causing hydrogen bonding and intramolecular hydrogen bonding by about 40-50 %. The study showed that it's highly likely that hydrogen bonds form in these situations due to excessive protein folding.⁵³ Furthermore,

Wuthrich, Shulman, and Peisach (1968) attempted to understand structures of heme protein compounds in solution phase, which is of high importance in comprehending its interactions in the body. Specifically, sperm whale cyanometmyoglobin was studied with a high resolution VT-NMR approach. Findings showed hyperfine relations of the paramagnetic heme groups and localized magnetic fields from ring currents with estimations of electron spin density distributions caused by the heme group itself.⁵⁴ Overall, these studies illustrate the use of VT-NMR to study very large protein compounds. Therefore, being able to observe much smaller carboxylic acid moieties should prove not to be very difficult.

Additionally, hydrogen bonding is very important in molecular recognition due to its great directionality and promotion of other favorable interactions. Observing the vibrational properties of carboxylic acids using IR spectroscopy, especially in gases and solutions, can provide information on the excitation energies and timescales of hydroxyl bond stretching, ring-opening, and dissociation for example. Structural rearrangement is only seen in the gas phase; an increase in temperature here causes a decrease in the intensity of bound O-H and an increase in the unbound form based on their spectra. Also, dimerization is found to occur at lower temperatures along with lower monomer contributions. Furthermore, in both phases that were studied, hydrogen bonds break and re-form on very short timescales due to quick redistribution of O-H stretching modes and other modes. However, these phases act differently at longer timescales because more structural changes appear to occur in the gas phase than the solution one.⁵⁵ This research project by Shipman *et al.* (2007) is very similar to what's performed in this thesis by

using a single piece of instrumentation and utilizing solution phases to study hydrogen bonding.

4.2 Fibrate Derivatives

Fibrates and their corresponding acids have been found to have certain properties making them useful as aldose reductase inhibitors (ARIs) and have been used to manage dyslipidemias. Their main action is to aid in lipoprotein disorders, since diabetes is usually indicative of increased low density lipoprotein (LDL) levels and lowered high density lipoprotein (HDL) intensities.⁵⁶ Those with type 2 diabetes also have at least a three-fold higher chance of developing coronary heart disease leading to an earlier risk of death. Therefore, ARIs can help to control the LDL and HDL fluctuating factors.⁵⁷ These types of drugs are absorbed in the gastrointestinal tract and excreted renally. The fibrates that are most widely studied are clofibrate, gemfibrozil, fenofibrate, and bezafibrate; however, clofibrate isn't often considered anymore due to its potential carcinogenic properties. Clofibric acid will still be observed in this study though. Gemfibrozil isn't a fibrate derivative, but it does have similar properties to the others.⁵⁶ Gemfibrozil, or 5-(2,5-Dimethylphenoxy)-2,2-dimethyl pentanoic acid, is still used to treat hyperlipidemia and coronary heart disease.⁵⁸ Fenofibrate only has an oral bioavailability of 60 % but can be given in a long-acting form to give a 100 % bioavailability. All of the fibrates have a great degree of plasma protein binding but do vary in their half-lives and volumes of distribution.⁵⁶ Use of non-statin drugs like these for treatment are still a bit uncertain and many aren't prescribed due to potential toxicity.⁵⁹ Therefore, all fibrates listed above will be studied in order to determine their dissociation factors in these situations.

Fenofibrate, which is used to treat dyslipidemia, has a systematic name of 2-[4-(4-chlorobenzoyl)phenoxy]-2-methylpropanoic acid, 1-methylethyl ester. Administration of this drug orally allows for absorption in the gastrointestinal tract, which is then hydrolyzed by the CYP3A4 isozyme to form fenofibric acid. This is its active metabolite which has a systematic name of 2-[4-(4-chlorobenzoyl)phenoxy]-2-methylpropanoic acid and a formula of $C_{17}H_{15}ClO_4$. Fenofibric acid specifically causes a reduction in total cholesterol, LDL cholesterol, apolipoprotein B, total triglycerides, and triglyceride rich lipoprotein.⁵⁹ It consists of a carboxylic acid functional group and can hydrogen bond through acid-ketone interactions. Aside from treating hyperlipidemia, it can help combat heart disease and other problems caused by diabetes. When fenofibrate is administered orally, it's hydrolyzed to fenofibric acid through esterases, but the acid form can be prepared through an alkaline hydrolysis beforehand. Dimers of this can form that have strong hydrogen bonds between the carbonyl of one molecule and the hydroxyl of a second molecule. Binding affinities can differ due to the potential dimerization abilities as well, since the polar carbonyl and carboxyl groups of fenofibrate and fenofibric acid cause very specific interactions with target sites.⁶⁰

Reports have shown that administration of fenofibric acid relates to a 15 % drop in total and LDL cholesterol with the possibility of a 10-15 % increase in HDL levels.⁵⁷ Furthermore, out of 544 people with diabetes taking fenofibrate, there was an 11 % drop in the probability of them having a first heart attack or death from coronary heart disease. Additionally, there was a 24 % decrease in non-fatal heart attacks and another 11 % reduction in the total number of cardiovascular disease events caused from administration of fenofibrate.⁵⁷ This drug provided a significant reduction in microvascular-associated

problems as well. However, there was not a treatment-related benefit in administering fenofibrate to diabetics who already experienced cardiovascular disease and no benefit was found in patients over the age of sixty-five. The only three negative aspects of fenofibrate therapy are that patients have a slightly higher chance of developing pancreatitis, a pulmonary embolism, and deep venous thrombosis.⁵⁷

One specific study that was performed by Balendiran *et al.* (2012) on the isopropyl (iPr) ester form of fenofibric acid explains that fenofibrate is a stronger ARI than its acid while the opposite is true for clofibrate and its corresponding acid. Fenofibrate is rapidly hydrolyzed to its active metabolite, fenofibric acid, via hydrolases when administered orally. Looking at their conformations, both the iPr clofibrate and fenofibrate species have a puckered geometry in the solid state which is lower in energy and much more stable than any other conformation. Also, fenofibrate and iPr clofibrate are unable to hydrogen bond and form intermolecular dimers since neither of them have acidic protons. This not only affects how they pack and arrange themselves but how they interact biochemically as well. Additionally, there are different packing energies for each type of fenofibrate, causing varying rates of solubility and overall thermodynamic properties. The acid forms of fibrates and their main structures appear to have greater membrane permeability and a better ability of absorption than the iPr esters of the fibrates. This was determined through surface area calculations and showed that the prodrugs have a better efficacy when given orally. The affinity of these drugs with critical residues changes by changing the iPr group, however continued studies need to be performed on other functional groups to see how these factors will truly be effected overall.⁶¹

The research performed here will focus solely on clofibrac acid, as this is the simplest of the fibrates. Being able to understand this compound and its NMR spectra across varying temperatures will give vast information that can be utilized in the future on observing the others. Therefore, the methodology and sample preparation will be the main focus of this study.

4.3 Nuclear Magnetic Resonance

Nuclear Magnetic Resonance (NMR) technique is a very powerful tool in chemistry, as it provides information about the structure of a compound through use of magnetic fields. Since nuclei will interact with these fields due to magnetic moments caused by orbital and spin angular momenta, this method is greatly used.³⁸ Protons absorb within the radiofrequency region when a molecule is placed in a strong magnetic field. Transitions in NMR spectroscopy occur between spin states of an atom's nucleus.⁶¹ Therefore, when a magnetic field is applied to a molecule, degenerate energy levels will split; this is referred to as the Zeeman effect. In an applied magnetic field, both electrons and nuclei act like small bar magnetics with their energies dependent upon how they orient themselves.³⁸ The applied magnetic field will cause a change in the nucleus' spin and move to a higher energy state, which is referred to as resonance. Once the nuclei begin to relax and fall back to their normal energy state, they emit energy in the form of electromagnetic radiation which is measured by the NMR experiment. A plot of frequency versus intensity is then produced with the frequency being related to the difference in energy between the lower and upper states.⁶²

In general, there are a few characteristics which can aid in determining what a spectrum may look like before a sample is even run on the NMR. The nuclear spin quantum number, referred to as I , is a secure characteristic property of a nucleus and is either an integer or half-integer. Additionally, the spin, and therefore the magnetic moment, of the nucleus may be in $2I+1$ different orientations relative to the z-axis. Furthermore, the “spin” of a nucleus is determined by the number and pairing of the individual nuclear particles. Table 4.1 below gives the number of protons and neutrons and their effect on the value of I .³⁸ It’s very important to note that only situations of half integers can be studied by the NMR, while integers cannot. Therefore, it’s critical to know what the compound looks like or is expected to look like structurally before the NMR produces a spectrum.

Table 4.1. How the Number of Protons and Neutrons effects the Value of I

Number of Protons	Number of Neutrons	I
Even	Even	0
Even	Odd	Half-Integers
Odd	Even	Half Integers
Odd	Odd	Integers

Structurally, ^1H NMR spectra reflect the carbon-hydrogen skeletons of molecules. Another significant aspect of finding the number of NMR signals is understanding chemically equivalent protons. These are protons that are in the same chemical environment within a molecule.⁶² Additionally, protons located within an electron rich

environment are shielded, located upfield, and give signals having a lower frequency. Alternatively, those in an electron poor environment are deshielded, located downfield, and have higher frequency values. Proton deshielding can also occur when electronegative atoms like fluorine and oxygen are withdrawing electron density; this leads to their representation at a higher chemical shift value.⁶²

Pascal's triangle can be used to determine how line spectra may appear for any given compound. Peak multiplicity of signals can occur due to splitting of a signal into doublets and triplets or peaks may not be split at all.⁶² Coupled protons can occur when protons are in a close enough proximity to one another to affect each other's magnetic fields. The patterns that arise from these interactions indicate the number of nonequivalent neighbor hydrogens within three bonds.⁶² An illustration is shown below, where m refers to the spin. One spin is aligning with the magnetic field while the other is opposing it. The opposing spin, indicated by the negative sign, is found at a higher energy than the spin lining up with the field, which has a positive sign.

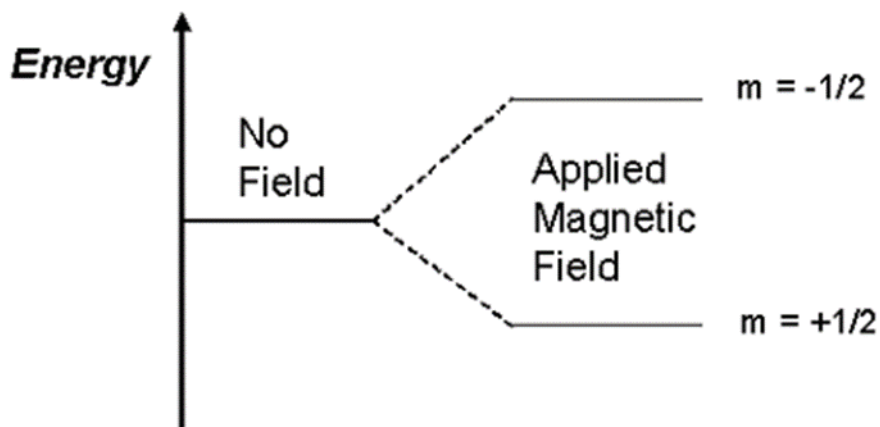


Figure 4.1 Energy Levels for a Nucleus Having a Spin Quantum Number of $\frac{1}{2}$ ⁶³

The actual NMR spectrometer consists of a magnet that allows for the production of a uniform, intense field and a source of radio frequency radiation. Samples are rotated rapidly to average any magnetic irregularities, but for larger molecules, sample rotation can lead to inaccuracies in data results. Different nuclei of the same element experience different total magnetic fields due to their chemical environment.⁶² This is referred to as the chemical shift and can be calculated as follows:

$$\delta = \frac{\nu - \nu_0}{\nu_0} \times 10^6 \text{ (ppm)}$$

In general, the chemical shift is defined as the position at which a proton appears in an NMR spectrum along the x-axis.⁶² Chemical shifts indicate the electron density around a proton as well, while peak integration gives the ratio between the different kinds of protons. This is determined by how far the signal is located from the reference point.⁶²

The standard reference material for proton spectra in NMR spectroscopy is tetramethylsilane (TMS) and its peak appears at 0 ppm in all spectra. In most cases, all deuterated solvents contain TMS within them so it's not necessary to add this solvent to the mixture. TMS is advantageous to use as an NMR solvent since it doesn't react with most other solvents, meaning that it's inert. The proton resonance of TMS helps determine the position of peaks for the other protons in the compound of interest.³⁸ For a proton NMR spectrum, the hydroxyl proton appears between 10 and 12 ppm downfield, while the carbonyl carbon signal is located around 180 ppm downfield in a carbon NMR spectrum. Additionally, when observing chemical shifts in NMR spectra, there is a concentration dependence especially when performing proton NMR.⁶⁴

Reaction rates can be determined through the use of NMR spectroscopy as well. The Bloch equations can be modified and used to describe the conversion of one species

usually between two magnetic states.⁶⁵ Both of these processes can relax independently from one another with their differing times being caused by nuclear electric quadrupole interactions. The rapid reversible molecular processes transfer a nucleus between two molecular environments with the nuclear magnetization being in phase with the rotating field, out of phase with the rotating field, or in the same direction as the large stationary field. Shorter relaxation times can occur with hyperfine interactions caused by unpaired electrons or a strong nuclear electric quadrupole relaxation.⁶⁵

Various effects can influence the placement of spectral lines. For example, electrons can interact with different species flipping their orientation causing different shielding effects. Additionally, if a hydrogen is lined up against the magnetic field, a higher field and higher energy is required for resonance. Therefore, the magnetic moment and spectral line will show more upfield compared to the signal with no field applied. The opposite is true for a species lined up with the magnetic field, as this needs a lower field and lower energy required for resonance compared to when there's no field. Furthermore, if a nucleus has a large chemical shift downfield, it's considered to be strongly deshielded.³⁸

In research projects such as what is described in this thesis, it's important to note the mathematics behind understanding the use of VT-NMR to determine hydrogen bonding behaviors. A monomer chemical shift of a self-associating system can be determined through extrapolation of the dilute chemical shifts to zero, however the slopes might not be linear and may give an imprecise measurement. The dilution shift data can be calculated based on relationships of monomer shifts, dimer shifts, dimerization constants, and total monomer concentration in a system having monomer-dimer

equilibrium. Rapid interconversion can be assumed in a system and can be represented as what's shown below⁶⁶:



This refers to A being the monomer type and A₂ being a dimer of each individual monomer put together. Furthermore, the following equation can find the δ_{obsd} , or weighted average of shifts of monomer and dimer⁶⁶:

$$\delta_{\text{obsd}} = f_m \delta_m + f_d \delta_d$$

In this calculation δ_m is the monomer shift, δ_d is the dimer shift, $[A]$ is the monomer concentration, $[A_2]$ is the dimer concentration, and $[A]_o$ is the total concentration. Additionally, f_m and f_d are mole fractions of A in their respective monomer and dimer forms, where $f_m + f_d = 1$. The mole fractions can be determined from knowing chemical shift parameters such as what's given below. Also, the dimerization constant, K can characterize the equilibrium by assuming there is only one type of dimer forming.⁶⁶

$$f_m = \frac{\delta_d - \delta_{\text{obsd}}}{\delta_d - \delta_m}$$

$$f_d = \frac{\delta_{\text{obsd}} - \delta_m}{\delta_d - \delta_m}$$

$$K = \frac{[A_2]}{[A]^2} = \frac{f_d}{2[A]_o f_m^2}$$

All of these equations will be utilized in this research by having different concentrations of each compound of interest to be studied. This will allow for different chemical shifts to be determined and then these can also be compared at different temperatures. The monomer-dimer equilibrium tends to dominate due to the geometric preferences of most compounds.⁶⁶

Dimerization effects will be studied, since fenofibric acid can form strong hydrogen bonds due to its carboxyl group. Specifically, it's expected to form through the

carbonyl of one molecule bonding with the hydroxyl group of another, which has already been described. This can be explained through the alignment of the atoms in the overall dimer; the hydroxyl tends to situate itself on the same side as the carbonyl and a better interaction can occur. This advantageous arrangement allows it to be a more potent ARI, which makes it advantageous as a possible drug option in controlling diabetes.⁵⁷ Not much research has actually been performed regarding temperature effects on dimerization and dissociation, however use of nuclear magnetic resonance (NMR), thermogravimetric analysis (TGA), and differential scanning calorimetry (DSC) will be researched here to explore these factors. Additionally, bonding conformations and strength of hydrogen bonding can be analyzed through use of infrared spectroscopy (IR), Raman spectroscopy, and mass spectrometry (MS).

A few important pieces of research have been performed using each of the stated methods separately on carboxylic acids, specifically looking at their structural changes with temperature and hydrogen bonding effects. The first study by Mora *et al.* (2005) on 4-piperidinecarboxylic acid utilized TGA and DSC analysis by exposing it to a range of temperatures and noting its changes in conformation and hydrogen bonding.⁶⁷ Results from this investigation provided evidence that there are three distinct phases of the acid: a monohydrate form from room temperature to 353 K, an endothermic transition anhydrous phase, and a high temperature anhydrous state. When water escapes from one state to the next due to heating, the compound needs to fix and reorder its structure leading to different torsional interactions. Similarly, increased temperature causes the hydrogen bonds to lengthen, even causing some of these bonds to break and new ones to form.⁶⁷ This gives highly important information, considering it can be applied in a similar fashion

to a study on fenofibrates' carboxylic acid groups, as the initial structure must remain intact in order for it to have a therapeutic effect.⁶⁸ Therefore, use of TGA and DSC are beneficial methods toward future research in this area of interest.

Another study by Zvereva *et al.* (2012) on the drug Xymedone, which stimulates the immune system creating an antibacterial environment, focuses on hydrogen bonding and use of vibrational spectroscopic methods.⁶⁹ Xymedone molecules are able to hydrogen bond intermolecularly by ketone groups interacting with protons on aromatic and methyl groups. As with fenofibric acid and its derivatives, this drug works well in aqueous media giving it great potential in biological molecules within the body. The main differences in IR spectra point to there being a few types of hydrogen bonds in the system and polymorphs as well; therefore, it's not surprising that this drug has the central ability to change its conformation depending on the conditions in which it's placed. Since the IR and Raman spectra along with theoretical calculations may be necessary to make exclusive conclusions, these methods can be utilized in studying how fenofibrates may interact with environmental changes, as in a physiological environment.⁶⁹

Finally, mass spectrometry (MS) can be a very useful method when studying molecules due to its high sensitivity and accuracy, while leading to information regarding interatomic distances and energies giving packing of the structure. The species studied have a hydroxyl group that's a more powerful donor than the N-H one on the amine since oxygen is more electronegative than nitrogen. Additionally, the use of deuterated solvents allows for the determination of potential dissociation pathways to be considered. There can also be a relationship between the length of the bonds in question and their collision energy, with the last broken bond being the one that is the shortest.¹² The method

employed through the use of MS analysis is extremely substantial and will help to find the exact dissociative properties of the fenofibrate derivatives that are being researched.

Various other experiments have been performed that attempt to understand hydrogen bonding through use of VT-NMR and DFT theoretical calculations. One NMR project by Chaudhari and Suryaprakash (2012) used DOSY, along with 1D and 2D NMR methods to study heterodimers of benzamide with benzoic acid, salicylic acid and phenyl acetic acid in a low polarity CDCl_3 solution.⁸ Measuring chemical shifts can give an indication as to the types of dimerization that are occurring. This specific study also utilized XRD to indicate structural properties and give further evidence on dimerization. Theoretical DFT calculations specifically aid in determining bond lengths and angles and do so relatively accurately for small molecules.⁸

Benzoic acid dimers were studied by Broughman *et al.* (1996) to see the influence of hydrogen bond tunneling on the dimers' structures.⁷⁰ Solid state studies of benzoic acid show that it forms centrosymmetric dimers connected by hydrogen bond pairs. Different tautomers have been shown to form as well with conversion occurring due to an increase in temperature. Studying atomic positions of the low temperature tautomer can indicate hydrogen bond compression patterns. Broughman *et al.* (1996) did find a correlation between the incoherent tunneling rate and hydrogen bond length of very closely related materials, however more studies need to be performed to see if other carboxylic acid derivatives have the same kinds of relationships with respect to this and other features.⁷⁰ A few other VT-NMR studies by Demsar *et al.* (2002) and Tensmeyer and Ainsworth (1966) observed shifts dependent upon concentration and can be used as a good comparison to the results obtained within this thesis.^{71, 72}

Denisov *et al.* (1995) studied chemical shifts along with nuclear magnetic relaxation times of hydrogen bonded pyridine complexes to see if a solvent's polarity effects these responses. For example, under certain solvents, a molecular complex can more quickly transform into an ionic pair through a shift of the proton equilibrium position or ultimately by a tautomeric equilibrium shift between both forms. It appears that there is less of a probability for complex formation and stronger intermolecular hydrogen bonds present in polar solvents. This is caused by a shortening of hydrogen bonds and lengthening of covalent bonds in these types of solvents.⁷³ Fenofibrate has previously been studied by Watterson *et al.* (2014) to determine its solubility in a variety of pure solvents over a vast range of temperatures.⁷⁴ Ethyl acetate, acetonitrile, and acetone all appeared to show a better solubility of the compound over alcohols; however, an increase in the aliphatic chain length causes alcohols to have better solubility. Furthermore, this approach observed crystallization of fenofibrate along with a solid-state characterization in which the samples were dissolved in deuterated chloroform and studied via FT-IR, NMR, DSC, and TGA.⁷⁴ Therefore, these studies show that solvent choice impacts the overall behavior of a system. Additionally, it may be useful in determining how some solvents may be better able to dissolve certain compounds, specifically fibrates.

A few other experiments will be discussed beforehand, as they use VT-NMR in order to better understand the structural and behavioral characteristics of certain molecules which can provide clinical approaches to their potential uses. Naito *et al.* (2014) looked at the synthesis, structure, and solution-state behavior of binuclear *trans*-bis(β -iminoaryloxy)palladium (II) complexes.⁷⁵ This is necessary to understand intra- and

intermolecular stacking behaviors of these clothespin-shaped molecules that are important in designing and forming supramolecular-type materials. The VT-NMR analysis on these large molecules studied both syn and anti forms, observing that both varieties had a downfield shift in signals at lower temperatures along with a fast flipping motion of the anti-conformer in the solution state at higher temperatures. Furthermore, monomer-dimer equilibrium constants were able to be established for the ultimate comparison between the forms using heavy calculations.⁷⁵

Castilla, Conn, and Ballester (2010) observed the general design, synthesis and analysis of macrocyclic receptors for peptide ligand stereoselective recognition. Specifically, hydrogen bonding patterns in protein β -sheets were studied to understand the size and shape specificities and enantioselectivities of biological protein-protein recognition processes. Dilution of the compound in CDCl_3 studied at room temperature provided evidence of varying chemical shifts that aligned well with theoretical dimerization calculations. NMR titrations and VT-NMR experiments were performed as well. Proton signals sharpened as the temperature increased, which eluded to chemical exchange occurring from increasing conformational equilibrium. This was further confirmed by cooling down the samples; new signals appeared and there was a slowed chemical exchange rate. Use of the HypNMR software program allowed for a full mathematical analysis of the chemical shifts, including calculation of dimerization constants.⁷⁶

Another set of studies focused specifically on carboxylic acid functional groups to determine temperature effects on NMR spectra. For example, one study by Kimtys and Balevicius (1979) used different concentrations of the same carboxylic acid at several

fixed temperatures observing the chemical shift in proton NMR spectra.⁷⁷ There was a determined dependence based on structure and volume of radicals within the carboxylic acid groups with dimerization occurring as well. By observing the monomer and dimer shifts of carboxylic acids like benzoic, acetic and trimethylacetic acid, temperature dependence could be calculated at the different concentrations and a temperature coefficient could be determined. Plots of the chemical shift at different concentrations and the shift at different temperatures were highly useful in illustrating the concepts of concentration and temperature dependence of compounds containing carboxylic acid groups. This study established that there was a form of contact between cyclic dimers, polymerization, and the presence of both *cis*- and *trans*- monomers that could influence chemical shifts.⁷⁷ A second very similar study by Kimtys and Mikulskis (1975) used trimethylacetic acid in cyclohexane and carbon tetrachloride to also study the carboxylic acid proton chemical shifts in various concentrations at five different fixed temperatures.⁷⁸ These chemical shifts for carboxyl protons were measured relative to internal methyl groups to determine monomer and dimer shifts. Assumptions were made on these calculations based on a Minsk-32 computer program with considerations of monomer-cyclic dimer-polymer-open dimer, monomer-cyclic dimer-open dimer, monomer-cyclic dimer-trimer-polymer, and a few other configurations.⁷⁸

Two other research groups observed encapsulated hydrogen bonds using NMR spectroscopy and dimerization effects. These types of encapsulation complexes occur frequently in confined spaces and are considered to be prearranged and prolonged.⁵² Ajami *et al.* (2011) found results showing that confinement of carboxylic acid dimers in capsular form causes a slow rate of exchange of hydrogen bonds and protons. Also, the

dimers acted as if they were experiencing outside pressure from the inside walls of the capsule when it was closed. Further, it was found that if a guest species was introduced into the main molecule and fit inside of it well, attractive van der Waals forces were at work and could be increased by constricting the guest. The study concluded that any kind of reversible encapsulation provides useful information on the molecular behaviors of compounds in extreme environments.⁷⁹ Jiang *et al.* (2012) considered the combination of a primary amide with a carboxylic acid to produce homodimers and heterodimers within capsules due to a disproportionation equilibrium. Since guest exchanges are relatively slow on the NMR timescale, this is a good method to measure these processes. Heterodimer formation is favored due to it having a dipole and being presented in a polar environment. Therefore, this study showed preferences in bonding depending upon the surrounding environment and structures as can be expected.⁵² The projects discussed in this section can be used as a basis for understanding the experimentation performed in the current work and investigative evaluations can be made more accurately due to this extensive literature search.

The most important working parts of the NMR will now be discussed. One important NMR feature is the free induction decay (FID) data set. This is a function of a complex number representing the intensity versus the time frame. A Fourier transform occurs allowing the function to represent intensity versus frequency with the displayed spectrum being the real or absorptive area of the function. Another important NMR feature involves the radio-frequency (RF) radiation exciting a sample's nuclear spins along the axis of the external magnetic field. This is caused from a closed electric current in a coil which is within the probe. Formatting it this way will give the strongest signal

from weak fluctuating currents due to the nuclear spins. Optimizing this aspect of the NMR is called tuning, which will provide the best NMR data.⁸⁰

Also, due to the air sensitivity of these compounds, many important experimental techniques were taken from prior studies within the literature. For example, distilling the solvent will remove the majority of impurities that are present within it. Since access to a glove box was not feasible, glove bags were employed to make sure samples were under argon and not exposed to air. Glove bags, however, do have their own advantages compared to their box counterparts. For instance, they are much less expensive to maintain and allow for an inert gas like argon to be presented and then purged much more quickly than a glove box. Additionally, glove bags are more mobile, yet have enough room to fit beakers, vials holding samples, and other necessary experimental equipment. Glove bags can be easily discarded if they become contaminated, while also having the ability to be used multiple times if necessary.^{81, 82} Finally, by permanently sealing the NMR tubes, this ensures that no solvent evaporates from the tubes and that no air is introduced to the sample. Flame sealing works well, since the sample is cooled to the temperature of liquid nitrogen causing a reduced pressure and ultimately allowing the walls of the tube to collapse upon sealing with an oxygen/methane torch.⁸³

4.4 Experimental Methods

Since the main goal of these VT-NMR studies is to find dimerization constants using shifts in peaks representing carboxylic acids, it's of great importance that as little air and water as possible are introduced into the samples. This assures the presence of clean spectra and provides the ability to analyze them without introducing unwanted

materials. Therefore, one measure to ensure purity was to distill the CDCl_3 (Aldrich, Lot # MKBQ7924V, CAS: 865-49-6) solvent before use. This was performed under argon, and once all solvent needed was distilled, it was stored under a syringed argon balloon through use of a septum. Since a glove box was unable to be used, glove bags having a “handy-glide closure” (Glas-Col, 108D S-30-20H-3) were purchased and utilized in the same manner. The following materials were placed into the glove bag before every use: the solid sample of interest already pre-weighed in corresponding vials, 8 mm NMR tubes (Wilmad Economy, WG-1228-8, 5 mm OD, 0.43 mm wall), pipettes, bulbs, syringes, and distilled solvent in a round bottom flask. Once the bag was sealed and the argon was allowed to inflate the glove bag, it was purged three times to guarantee that all air was removed from the bag and further prevent any reactions with air or water.

All solutions were made in vials, pipetted into a pre-labeled NMR tube, and capped all within the glove bag. Approximately 0.6 mL of the solution for each compound was pipetted into its designated NMR tube. These could then be removed for sealing, which is done in order to ensure that the concentrations within the tubes remain the same even while heating. Also, the method used here further confirms that no air or water is in the samples as introduction of these can cause further reactions and inaccurate results. This process requires that the NMR tube be placed under a strong vacuum, then the process of freezing in liquid nitrogen, pumping for air removal, and thawing of the sample can be initiated. Once all air appears to be removed from the samples through the observation of bubbling subsiding upon thawing, the vacuumed tube is frozen in liquid nitrogen for a final time. Next, an oxygen/methane torch is used to seal the tube using

180° sweeps around the same part of the tube. Gravity can then be used to slowly pull down the tube and the tip can be annealed with the flame once it's removed completely.

Each compound's spectra were recorded at their varying concentrations and temperatures using a Bruker Avance III 400 MHz NMR with broadband probe. ¹H NMR spectra were recorded using 128 scans from 25 to 55°C in increments of 3°C. This was done at each concentration for every compound of interest. There was a 20 minute equilibration time between each experimental run to allow for an accurate attaining of the temperature. Additionally there was a 30 millisecond wait between each scan, a dwell time of 60.800 microseconds, an oversampling dwell time of 0.025 microseconds, and the instrument was shimmed upon every experiment. The pulse program used was zg30 with a digital quad detection (DQD) acquisition mode. Additionally, a 0.30 Hz line broadening was used, and the size of the free induction decay (fid) was 65,536 TD. Through use of the Topspin NMR settings, the probe temperature was able to be raised by a thermocouple placed near the NMR tube.

The solvent selected for this procedure was deuterated chloroform, or CDCl₃, for a few reasons. This solvent has a melting point of -64.1°C and a boiling point of 60.9°C, which allows for a great range in which data can be collected. Additionally, a proton NMR spectrum of this solvent alone only shows one peak present at 7.24 ppm; therefore, it can be easily spotted within the spectra and did not appear to interfere with the results from each compound tested. Furthermore, it readily dissolves our compounds of interest, is inexpensive, and is easily able to be obtained. A few other solvents were tested to be used, but there were faults found with each. Deuterium oxide, or D₂O, was one initial solvent of interest, as it also has a wide range of potential temperatures to obtain spectra

along with only one peak in a proton scan. However, this solvent showed procedural issues. In order to properly ensure that the tubes have minimal air within them upon sealing, they must be frozen in liquid nitrogen, pumped for air removal, and thawed slowly. Unfortunately, D₂O's physical properties caused expansion of the solvent when placed in liquid nitrogen. This action made the tubes break; therefore, D₂O was discounted for use in this research. Another solvent, deuterated mesitylene, was attempted to be used as well, since it was found to be used in the literature for similar studies.⁵² However due to its high expense, it was not feasible for use in this research.

Additionally, many of the subtle NMR methods used in this study were taken from prior findings in the literature. One user guide suggests that a stable temperature is obtained in these studies through suitable heating and cooling where the thermocouple measures the temperature. A typical Bruker NMR can be used from the -150°C to 180°C temperature range, however the general plastic spinners that hold each sample are only usable up to 80°C. Any samples that need to be heated to temperatures exceeding that point have to be placed in a ceramic spinner.⁸³ This study only required plastic spinners, since the highest temperature of interest was 55°C. Another recommendation within the literature suggests that each sample needs to be re-shimmed at every new temperature, and this shimming increases the length of time of each run as this process occurs gradually.⁸² A third major suggestion is that each NMR tube should hold about 5 centimeters or what amounts to 0.6 mL of the mixed compound and solvent solution. Anything less than this quantity will make it difficult to achieve proper shimming of the magnet. Most of the time, anything more than this amount is sufficient, however VT-NMR experiments may present a distorted spectrum if subjected to this.^{83, 84} Finally,

temperature changes should occur in small increments, like 3 to 5°C, in order to achieve the desired temperature which will provide good data. Therefore, at least a 10 minute equilibration time should be used along with re-shimming and re-tuning.⁸⁰

4.5 Results

An overlay of all NMR spectra are shown on the next four pages for clofibric acid and the 1:1 clofibric acid:potassium chloride mixture. A full spectrum is given for each followed by a close-up of the shifting peaks of interest. Below is the structure of clofibric acid along with its predicted ¹H NMR peak values based on the ACD labs software system.

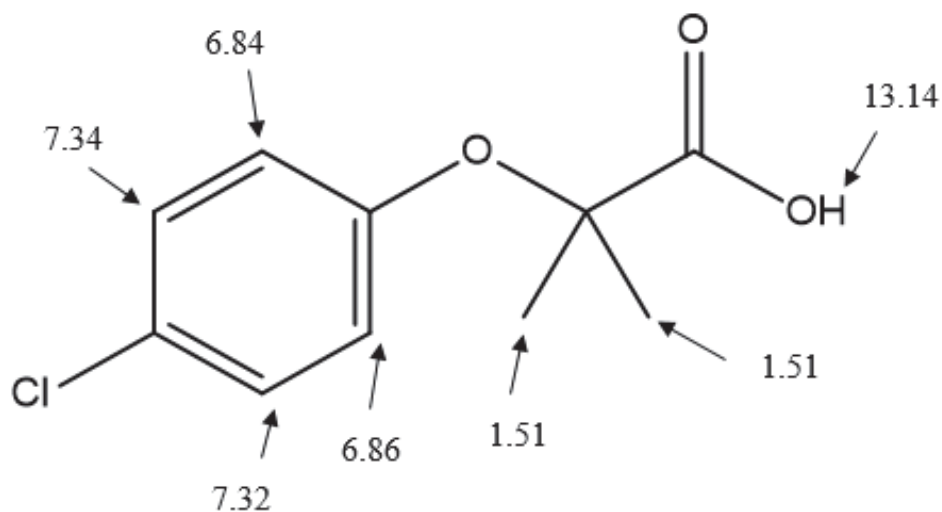


Figure 4.2 Structure of Clofibric Acid with Peak Assignments (in ppm)



Figure 4.3 ^1H NMR Entire Spectrum of 20 mg Clofibric Acid Sample

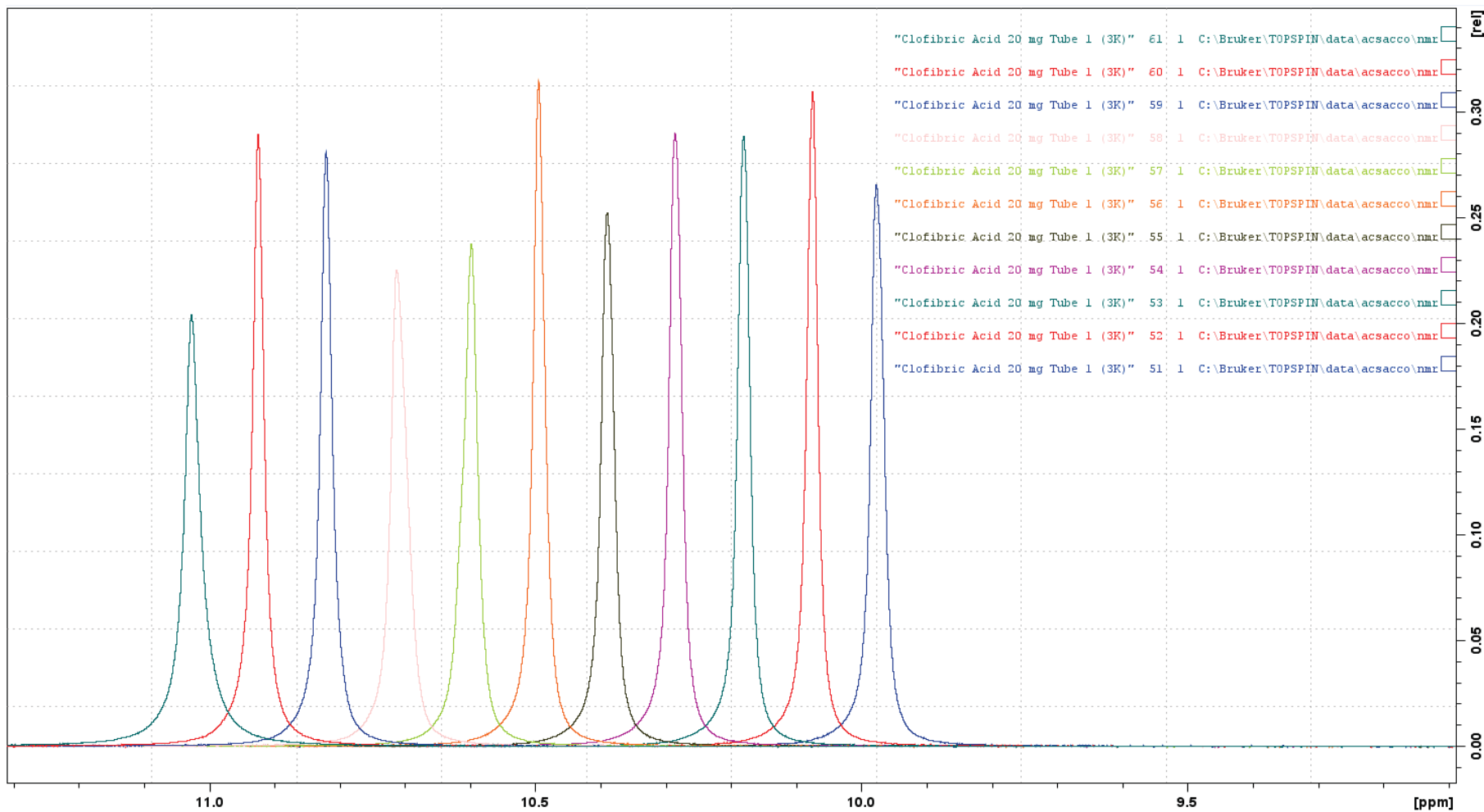


Figure 4.4 ¹H NMR Close-Up of Shifting Peaks of 20 mg Clofibric Acid Sample

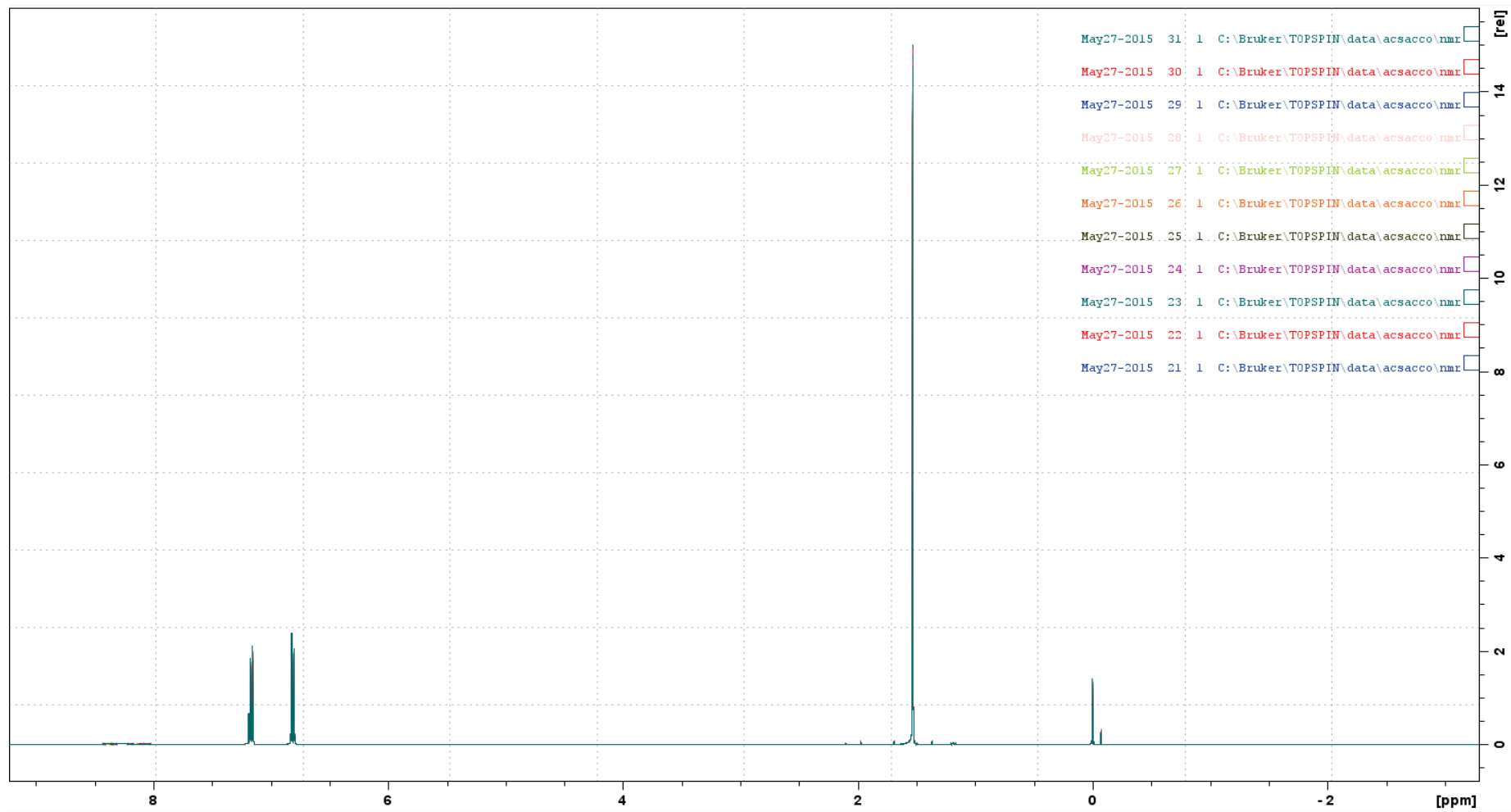


Figure 4.5 ¹H NMR Entire Spectrum of 1:1 Clofibric Acid: Potassium Chloride Sample

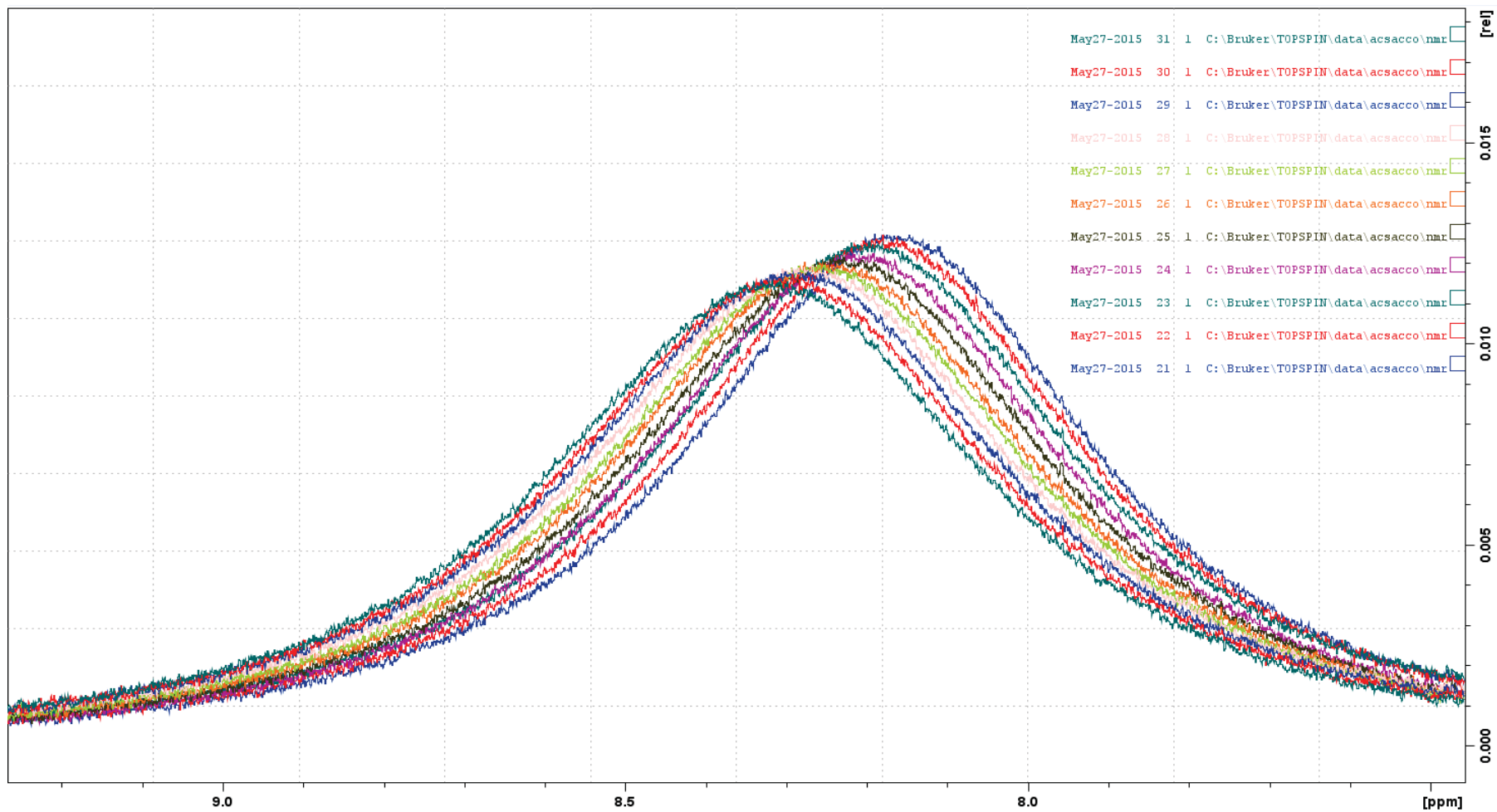


Figure 4.6 ¹H NMR Close-Up of Shifting Peaks of 1:1 Clofibric Acid:Potassium Chloride Sample

4.6 Discussion

All of the ^1H NMR spectra contain the correct peaks consistent with what would be expected for clofibric acid. There is a large signal present around 1.51 ppm corresponding to six hydrogens with all of them being the most shielded ones in this compound. The sets of doublets are present before and after 7 ppm, as computationally expected. Finally, heating the sample is consistent with the shifting peaks moving more upfield and becoming more shielded. When looking at the 20 mg clofibric acid sample, there is a spread of peaks from 9.95 ppm to 11.05 ppm and roughly even spacing of all peaks within that range. The signal at 9.95 ppm was run at 328 K, while that at 11.05 had an experimental temperature of 298 K. Therefore, it can be stated that as the temperature is increased, the peak for the proton corresponding to the carboxylic acid shifts upfield.

An overlay of the spectra showing a 1:1 mixture of clofibric acid:potassium chloride across the 298-328 K temperature range is provided as well. The same general peaks are present in the expected locations, however the carboxylic acid group's proton has shifted even further downfield with all peaks appearing within the 8.1 ppm to 8.3 ppm range. Therefore, the spaces between peaks aren't as large and tend to highly overlap with one another. These peaks are much broader than those in the 20 mg clofibric acid spectra and are also much less intense. The broadness of these peaks may correspond to the carboxylic acid's proton being involved in an exchange or interaction with the potassium chloride, since the samples were made the same exact way otherwise.

Unfortunately, there was an inability to differentiate between the monomeric and dimeric forms of clofibric acid. This could potentially be found through a shouldered

peak or one that appears to have two peaks within it. Without knowing this crucial information, no calculations could be performed to determine a dissociation constant. However, it is apparent that the addition of KCl completely changes the structure of the shifting peak of interest and this information could be critical in the future to calculating this value.

4.7 Future Work

Future studies on this topic will need to use the procedures followed in this research project to study all of the fibrates of interest. It may be helpful to study other smaller biological compounds that could be incorporated into potential drugs, not only for diabetes but for other purposes as well. Additionally, since the monomeric and dimeric forms of clofibric acid were unable to be determined based on the chemical shifts in these spectra, potentially studying these samples at low temperatures using the appropriate ceramic NMR sample holder will provide the differentiation between the species to be seen. This will allow for the appropriate calculations to be performed with the eventual construction of a van't Hoff plot and calculation of a dimerization constant. Furthermore, other studies should be done using a larger temperature range to incorporate all peak shifts that are occurring throughout a wide variety of temperatures. Finally, it should be noted that prior work was performed on this similar project using fibrates within the Balendiran lab.^{85, 86} The application of methods used there and within this thesis will be useful in the future.

Chapter 5: Use of Bomb Calorimetry to Probe Hydrogen Bond Energies and General Energy Comparisons within Fifty Compounds

5.1 Background

As discussed in the introduction to this thesis, knowledge on hydrogen bond energies of compounds is an essential component of drug design; understanding the influence of different parts of molecules on the specific energies of O-H bonds within carboxylic acid groups is of great importance. However, determination of these energy values is generally a compound-dependent issue, meaning that regardless of the number of compounds studied, there will always be anomalies to the general trend and variations in what is considered to be normal behavior. The approach taken in this research project is to group together compounds having similar characteristics into the same category and then to compare them within that individual collection and to the other sets of compounds. This will provide the most widespread generalizations to be made, while also noting specific details that may greatly impact bond energies and combustion energies overall.

Although this project observes many different kinds of compounds, including ones not containing carboxylic acid groups, this serves a fundamental purpose; many molecules have other functional groups, like amines, ketones, aldehydes, and aromatics. These can all be studied alone in compounds with and without carboxylic acid moieties in order to determine the affect each have in these situations. Furthermore, a few polymers and sugars will be considered in this project to bring about a diverse environment in which many functional groups are found. These types of compounds have very different properties that may be reflected in their energies of combustion. Therefore, this study is

meant to clarify bonding energies through use of a bomb calorimeter to calculate the internal energy and heat of formation of each compound of interest.

5.2 Calorimetry

The topic of thermochemistry involves studying the transfer of energy in the form of heat over the progression of a chemical reaction.³⁸ Knowledge of a compound's energy and molecular structure provide extremely important information as to how it can be characterized. Additionally, knowing the thermochemistry of a compound, like its enthalpy of formation, provides evidence on reaction pathway analysis and can point toward good synthetic strategies. Theoretically, studying and understanding specific energies can give knowledge on eliminating any competing reactions or formations of unwanted side products.⁸⁷ Additionally, being able to compare the properties of a compound's thermochemistry and its structure allows for trends to be established and better predict the compounds that haven't been studied.⁸⁸ Therefore, thermochemistry is the specific branch of chemistry utilized in the area of bomb calorimetry experimentation. In general, bomb calorimetry is a very useful technique in observing the transfer of energy in the form of heat during physical and chemical reactions.³⁸ The internal energy is one of the simplest measurements that can be performed on a compound and provides necessary information for the calculation of the enthalpy of formation; this can then potentially be utilized to find the Gibb's free energy of a compound if enough pertinent information is known. In fact, this exact method determines the amount of calories in food, while also having uses in the petroleum industry. The first description of a bomb calorimeter was in 1895; it was then revised in 1897 and fully published in 1903 as a

method of obtaining the heats of oxidation of food, by-products of animal metabolism, and other “feeding-stuffs.” The essential scheme of the apparatus has undergone only a few modifications since this time and still focuses on the main idea that the burning of a compound under a high oxygen pressure vessel submerged in water will raise the temperature of the water. Therefore, this will allow for a calculation of the heat of combustion of the substance.⁸⁹ In general, when combustion occurs from the hydrogen, carbon, and oxygen atoms and heat is released, carbon dioxide and water are the two major products formed. When other elements are present within the compounds of interest, other products and form and can be accounted for accordingly within the potential combustion reactions.⁹⁰

In order to determine calculations for unknown samples, an energy equivalent with a known energy of combustion must be used to calculate the heat capacity of the calorimeter itself. Included in this value are the heat capacities of the metal bomb, bucket, water, and other components of the system.⁹⁰ It is well known that benzoic acid can be used as a calibrator for the bomb calorimeter since this is an easily acquired pure compound, is cheap to make and buy, does not easily absorb moisture, is stable, and has a known heat of combustion. The temperature increase that occurs due to a certain amount of heat produced by the combustion allows for the calculation of the heat capacity of the calorimeter which in turn is essential for calculations of such parameters for unknown compounds.⁸⁹ Furthermore, benzoic acid is useful in igniting compounds that are more highly oxidized as these may have issues combusting on their own. For some compounds, partial combustion may occur or it may caramelize within the apparatus. These types of

compounds can be mixed in varying ratios with benzoic acid in order to ensure complete combustion and obtain a more accurate result.

The heat of formation, or enthalpy of formation, is a very important factor in many industrial and biochemical areas of analysis, as this refers to the change in enthalpy of a compound in terms of moles. One such study used the heat of formation idea to provide an estimate of the performance of high energy materials (HEMs) like explosive and propellant formulations and their individual components. By creating a computer code to perform this work, the heat of formation could be calculated theoretically, leading to the ability to calculate values such as the velocity of detonation for explosives, heat of explosion, temperature of explosion, and various other parameters. Therefore, knowing the heat of formation can really be a powerful tool in many scientific aspects.⁹¹

Since this process does involve use of a constant volume apparatus, ΔH and ΔU can easily be calculated. Initially, the heat capacity of the calorimeter must be determined, since this is accounted for in each compound's calculations. As temperatures are recorded, an average of the degrees per increment can be used to find the actual initial temperature in which combustion begins to occur. The change in temperature is found by subtracting the calculated value from the maximum temperature recorded upon total completion of the combustion. Therefore, C_{cal} for the heat capacity of the calorimeter, is found as follows⁹¹:

$$C_{cal} = \frac{[(\Delta U_{BA} * Mass_{BA}) + (\Delta U_{FE} * Mass_{FE})]}{\Delta T}$$

In that equation, each ΔU is a known value, where ΔU of benzoic acid is 26.410 kJ/g and ΔU of the iron wire is 6.68 kJ/g. The masses and change in temperature are known as

well. Next, for actual samples of interest, q_v for constant volume and ΔU for internal energy can be calculated with the following equations⁹²:

$q_v = C_{\text{cal}}(\Delta T)$, where C_{cal} is the calculated heat capacity of the calorimeter and

$$\Delta T = T_{\text{max}} - T_{\text{initial}}$$

$$\Delta U = \frac{q_v - (\Delta U_{\text{Fe}} * \text{Mass}_{\text{Fe}})}{\text{Mass}_{\text{Compound}}}$$

Finally, the heat of formation, correlating to the energy of combustion expressed in kJ/mol can be found through use of the following equation⁹²:

$$\Delta H = \Delta U + \Delta(pV)_{\text{gas}}$$

Since this process involves the use of a gas, there is a small contribution from the final term in the above equation and the ideal gas law can be used here^{92, 93}:

$$\Delta H = \Delta U + \Delta n_{\text{gas}}(RT), \text{ where } \Delta n_{\text{gas}} = (n_{\text{products}} - n_{\text{reactants}})_{\text{gas}}$$

The change in temperature, or ΔT , between the baseline temperature and final temperature is directly proportional to the energy of the reaction, referring to whether it is exothermic or endothermic.³⁸ An example of a graph generated through the use of bomb calorimetry is shown in Figure 5.1 on the next page.

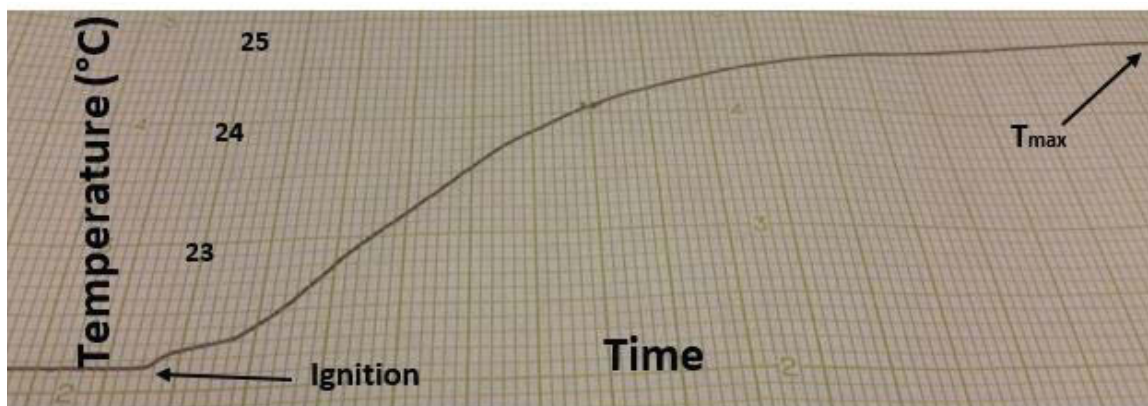


Figure 5.1 Sample of a Bomb Calorimetry Data Graph

There are eleven classes of compounds used in this research project with fifty compounds studied in total. They are separated into their specific sets based on structural similarities and functionalities for the most part. The rest of this calorimetry introduction will focus on general information and prior studies performed on all of the major compounds and their classes observed in this project.

Amino acids are the building blocks of all biological systems. In general, these contain a carbon atom attached to a primary amine group, a carboxylic acid moiety, a side chain, and a hydrogen atom.²¹ Therefore, knowing how these compounds decompose is of high importance. One study focused at the high temperature pyrolysis of aspartic acid, glutamic acid, and glutamine in a two-zone reactor. Prior studies using thermogravimetric analysis and differential scanning calorimetry (TGA and DSC) found that aspartic acid has two decomposition steps and three endotherms while glutamic acid has the same number of decomposition steps but one endotherm. Results showed that ammonia was produced in great amounts as a secondary reaction product with

deamination significant at these high temperatures. Also, decarboxylation reactions seemed to dominate glutamic acid at lower temperatures compared to aspartic acid.⁹⁴

Studies using gas chromatography coupled to mass spectrometry have also been performed on amino acids to try to identify potential fragmentation mechanisms. The mass spectra of the pyrolyzed amino acids showed the specific fragments so that a pathway could be suggested. For compounds containing amines, a nitrile may form from a loss of two hydrogen atoms, then the amine can further decompose via imine formation, dehydration, hydrocarbon formation, and loss of ammonia leading to formation of a cyclic product.⁹⁵ Furthermore, use of IR spectroscopy on carboxylic acid's crystalline salts have been performed to determine hydrogen bond energies as they relate to bands in spectra. The energy of combustion can be calculated in this study, since it accounts for increasing vibrations caused by bonded and free molecules. It also observes the decreasing frequency of valence vibrations and increasing frequency of proton vibrations that are out of the plane of symmetry. This approach showed very good correlations between different salt compounds.⁹⁶ However, neither of these methods give absolutely quantitative data and are not practical analytical techniques for the purposes of this research project.

Yang *et al.* (1999) captured combustion energies for thirteen amino acids through use of a precision rotating-bomb calorimeter. This type of calorimeter gives higher heat values than a static-bomb calorimeter since the combustion and reaction processes are occurring with constant stirring. For example, if a straight chain amino acid has a long carbon chain, it will have a greater heat value than shorter carbon chain compounds. A gas-collecting bag was utilized to see the amounts of gas formed, as measured by a gas

meter, while also having a gas determination instrument.⁹⁷ Therefore, this study greatly parallels the research performed here in my research by using the same type of calorimeter, so results should be highly comparative.

Various other studies on amino acids alone have been performed to determine their specific thermal decomposition behaviors. Simmonds *et al.* (1972) looked at the thermal decomposition of aliphatic monoamino-monocarboxylic acids observing that the major pyrolysis products were amines. Continuous fragmentation can occur yielding secondary reaction products; this suggests that each amine can lose two hydrogen molecules and form its corresponding nitrile. Furthermore, aldehydes and ketones have been seen as pyrolysis products too, but fragmentation into small inorganic gases like CO₂, NH₃, and H₂O prove to have the highest likelihood of formation.⁹⁸ Rodante, Marrosu, and Catalani (1992) solely looked at 13 standard amino acids using TGA and DSC simultaneously in order to perform their thermal analysis and compare their kinetic parameters. Final characterization was based on the following properties: initial decomposition temperature, total decomposition enthalpy, and activation energy. It was hypothesized that the two employed methods alone could help to characterize the amino acids based on their shapes leading to similar thermograms, however this is not always the situation. In fact they are very different for the majority of groupings, except where side chains containing rings are strongly influencing the thermal decomposition of the overall amino acid.⁹⁹

It's also been suggested by Ratcliff, Medley, and Simmonds (1974) that α -amino acids having α -alkyl groups lose ammonia, form an α -lactone, and produce a ketone via an S_Ni reaction. Alternatively, β -amino acids lose ammonia to form unsaturated acids. In

either case, reactions seem to occur through zwitterion formation.¹⁰⁰ Another study by Li *et al.* (2007) dealt with the specific pyrolysis of glycine and glycyglycine using TG-FTIR. Since amino acids make up proteins and the biomass resources for fuels are anticipated to contain proteins, it's important to determine the temperatures at which pyrolysis gases form based on the protein's amino acid composition. Even though many amino acids only exhibit one major weight loss, glycine appears to have three steps of weight loss, referring to it having several pyrolysis reactions. Hence, different amino acids are expected to undergo pyrolysis via different pathways. Additionally, the following pyrolysis gases, CO₂, NH₃, H₂O, CO, HNCO, and HCN, were found to be present in FTIR product analysis. Intermolecular secondary reactions contribute to the production to CO₂, while H₂O forms through condensation reactions. There is a quick NH₃ release in the initial step, while CO and HCN are both produced by further decomposition of HNCO.¹⁰¹

Gil *et al.* (2007) observed amino acid radical cation fragmentation to determine if this is caused by an influence of side chains inherent to the structure.¹⁰² Intramolecular hydrogen bonding is an essential component of understanding amino acid structure and reactivity. Even removal of an electron from these compounds can cause them to become more basic or acidic, which makes it difficult to determine how they are affected by processes like oxidation and reduction. Observations were made using a theoretical computational approach.¹⁰² Alexandrova and Jorgensen (2011) delved into the mechanisms and rates of glycine's spontaneous decomposition.¹⁰³ Ab initio and DFT calculations were performed to determine which mechanism of glycine decomposition in water is most likely to occur. This is interesting to note, since the spontaneous

decarboxylation of amino acids is considered to be one of the slowest reactions; it is a much more difficult process than cleaving amide bonds in polypeptides. This study found that direct decarboxylation of glycine in an aqueous solution is most likely to occur with deamination and hydrolytic routes being noncompetitive.¹⁰³ Stover *et al.* (2012) looked at L-amino acid acidities in the gas phase through computational prediction at the DFT level of theory in coordination with molecular orbital (MO) theory. Even though all of the amino acids in solution are zwitterions, those in the gas phase are not. Since the pK_a 's of these compounds are roughly the same in both cases, the zwitterionic form of the backbone doesn't appear to affect the pK_a 's of the side chains. Furthermore, a higher pK_a indicates a more stable species, which corresponds to stronger hydrogen bonding.¹⁰⁴ All of the above theoretical findings will be taken into comparison purposes within the current work.

A different experimental approach was taken to study sulfur-containing amino acids, as these may have different properties than the non-sulfur-containing compounds. One experiment observed the kinetics of thermal decomposition for D,L-methionine, L-cysteine, and L-cystine, by looking at the composition of each of the substances formed during the thermolysis of the starting amino acid. It was found that the primary gaseous products through decomposition of methionine are CO_2 and CH_3SH , while both cysteine and cystine have products of H_2S and CO_2 . Additionally, their decomposition rates increase from methionine to cysteine to cystine with their activation energies being close to one another.¹⁰⁵ Roux *et al.* (2010) performed a study on sulfur-containing amino acids observed L-cysteine, its corresponding dimer L-cystine, and L-cysteine-derived radicals, along with the specific dissociation energies for S-S, S-H, and C-S bonds. With cysteine

being the only amino acid containing a reactive thiol side group, it is strongly nucleophilic, which makes it important to an enzyme's active sites. Oxidation causes cysteine to form cystine, which is structurally important in various proteins. Therefore, understanding the thermodynamics of all of these compounds becomes highly important as they are linked to many biochemical processes. DSC, isoperibolic rotating bomb calorimetry, the Knudsen effusion technique, and computational chemistry were all applied in this specific project.⁸⁷

Although only three dipeptides were studied here due to their high cost, prior thermal analysis work has been done on a variety of the dipeptides. Rodante, Marrosu, and Catalani (1992) compared the dipeptides to the respective amino acids that made them up using TGA and DSC measurements. It was indicated that the dipeptides are much less stable than their individual amino acids with methyl groups being an important component for dipeptide decomposition in the solid state when it's common to each pair. Furthermore, dipeptides having aromatic or polar side-chains were found to have a higher thermal stability.¹⁰⁶

The fibrates were another class of compounds studied in the bomb calorimetry research, and they were already discussed briefly in the prior section on NMR analysis. Therefore, they will not be discussed here any further. Borneol and camphor are almost analogous structures to one another with oxidation of borneol forming camphor. Therefore, these are interesting compounds to compare to one another, as it is possible to extract the energy required for this mechanistic transformation to take place. In fact, an oxidation reaction can convert borneol to the compound from which camphor is derived. Both of these are in a class of compounds referred to as isoprenoids, which have a fused

tricyclic ring structure. Interestingly, camphor and borneol were both used as an ancient pharmaceutical cold remedy in traditional Chinese medicine as they produced similar effects due to their almost homologous structures.¹⁰⁷

Low acyl gellan gum was a polysaccharide studied in this research and is a hydrocolloid produced by the microbial organism *Sphingomonas elodea*. Gellan gum has been approved for use by the FDA in 1992 for food. It has a straight chain primary polymer structure with β -D-glucose, β -D-glucuronic acid, and α -L-rhamnose repeating monosaccharide units in a 2:1:1 molar ratio.¹⁰⁸ The high acyl gellan gum variety can be deacylated to form low acyl gellan gum when it is exposed to alkali metals at high temperatures. The low acyl variety is soluble in hot or cold water, is heat stable, and has a molecular weight between 2 and 3×10^5 Daltons. Since this form of the gellan gum does not have the acyl groups that are characteristic of high acyl gellan gum, it tends to be hard, non-elastic, and brittle in its gel form. This gel is formed when it's cooled to lower temperatures with cations present. Moreover, gels made of the low acyl kind are not thermally reversible, but this makes them more stable. Since it's a carbohydrate polymer, it can be easily degraded through strong oxidizers along with mixtures of oxidizing and reducing agents.^{108, 109} By studying low acyl gellan gum along with its individual units, one can obtain valuable information as to why it is such a stable compound and possibly what specific properties it has that could be applied to other compounds in the future.

Another polymer, cellulose, was observed as well, since it's considered to be the most abundant organic compound on Earth. This is a component of wood, other lignocellulosic plants, cotton, and fibers as examples. Cellulose is a long chain polymer having crystalline and amorphous regions due to its anhydroglucose units. These are

arranged in a roughly parallel position to one another having strong intra- and intermolecular hydrogen bonding between opposite hydroxyl groups; therefore, this gives it the identity of a structural polymer. Furthermore, cellulose has a high degree of polymerization along with a partial crystalline structure, so it's only dissolvable in a select number of solvents, such as strong acids and bases.¹¹⁰ Rocha *et al.* (2013) discussed levoglucosan, which is an intermediate in the breaking down of cellulose; it's highly important in char formation. This specific approach utilized static bomb calorimetry, DSC, FT-IR, Knudsen effusion methodology, and computational chemistry. This Knudsen mass-loss effusion technique allows for calculating the standard molar enthalpies of sublimation using the Clausius-Clapeyron equation. Therefore, many comparisons can be made between the analysis of cellulose and the work done on levoglucosan.¹¹¹

Additionally, starch was a third polymer that has been studied in this project. Starch is a polysaccharide that is white, granular, and organic, with subunits being joined together in α -1,4- linkages. In animals, starch is broken down into its individual sugar components as an energy source for tissues. Starch is composed of amylose and amylopectin, which are two carbohydrate polymers that are synthesized by enzymes in plants. Both amylose and amylopectin consist of glucose units, however amylose has a linear structure while amylopectin is branched.¹¹² Plastic is the final polymer that was researched here, but it is not certain which form of plastic is actually being analyzed. The most likely source is polypropylene, however calculations will only be performed on what is known about this compound. This means that only plastic's ΔU value can be determined within this thesis.

The other classes of compounds that are observed in this thesis all have a variety of characteristics that make them unable to be completely compared to what's already in the literature. However, an overview of some of the characteristics and thermal properties of similar compounds will be discussed here. A few compound classes have solely carbon, hydrogen, and oxygen present within them structurally, so functional groups with those corresponding elements can impact the thermochemistry of compounds differently. Amaral *et al.* (2015) discussed the observation of hydroxy and methoxy groups in naphthaldehyde-based compounds, while having a focus on estimating standard molar enthalpies, entropies, and Gibbs energies through combustion calorimetry, vapor pressure measurements, and computational approaches.⁸⁸

Ribeiro da Silva, Lobo Ferreira, and Cimas (2011) used very similar experimental methods to study the molecular energetics to benzyloxyphenol isomers. Phenolic compounds are extremely important in many facets of chemistry, as they can serve as antioxidants in oxidative degradation of organic molecules, while also being widely used in various products like lube oil additives, nylon, explosives, pesticides, and as a raw material for use in the production of aspirin. The point of this project was to gather information on gas-phase acidities and basicities, proton and electron affinities, and dissociation enthalpies within the hydroxyl bond.¹¹³ Ribeiro da Silva, Ferrao, and Alves da Silva (1999) noted the molar enthalpies for 2-methylpropanoic acid, 2,2-dimethylpropanoic acid, and 3-methylbutanoic acid, which all contain carboxylic acid moieties. Their method used pure samples and a static bomb calorimeter to obtain data.¹¹⁴ The results from some of the more applicable results from these research projects will be

compared to the calculated observations found here in the results portion to see if any notable trends may be present.

A few other studies observed nitrogen-containing compounds and how this element affects the thermochemistry of certain molecules, specifically when the nitrogen is within a ring structure. Galvao *et al.* (2014) used 4(3H)-pyrimidinone, since this is an extremely stable molecule due to its keto-enol tautomeric equilibrium feature. Using static bomb calorimetry in the solid state, Knudsen effusion in the gaseous state, and computational chemistry, isodemic reactions could be conceived while taking into account the enthalpic properties of hydroxypyridines and pyrimidine.¹¹⁵ Santos and Ribeiro da Silva (2009) specifically studied the energetics of 2-pyrrolicarboxylic acid and 1-methyl-2-pyrrolicarboxylic acid using the same methods as the prior research. These are both five-membered aromatic nitrogen-containing heterocycles that have importance within pharmaceuticals, natural products, and other potential materials.¹¹⁶ Experimental values for ΔU and ΔH from both articles can be compared to those similar compounds within this work to determine if all heterocycles having both nitrogen and carbon atoms within their rings also have similar energetic properties. Additionally, this may help with the abstraction of potential hydrogen bond energies within these types of compounds.

Finally, Lobo Ferreira and Ribeiro da Silva (2011) discussed the thermochemistry of 2,4-, 2,6-, and 3,5-dibromophenol isomers in order to better understand their structural and energetic properties. Bromophenols are naturally produced by sea animals and algae, since they are detected in marine sediment. This study used an isoperibolic rotating bomb combustion calorimeter, a Knudsen effusion apparatus to measure vapor pressure, and a

Calvet high temperature microcalorimeter to find enthalpies of sublimation. Additionally, a computational approach was taken using DFT and B3LYP levels of theory to compare experimental results. Although there was a difference in the experimental and computational work results from this 2011 study, a standard stability of enthalpies for computationally measured data was found, indicating that the most stable isomer overall was 2,5-dibromophenol.¹¹⁷ Even though the research presented within this thesis does not involve brominated compounds, a good analysis of how bromine affects various factors, including hydroxyl bond energetics, can be observed and may be of great importance to future work.

5.3 Experimental Methods

Even though the majority of thermochemical experiments are carried out at constant pressure, heats of combustion experiments are performed at a constant volume.⁹¹ Specifically, a constant volume bomb calorimeter having an adiabatic jacket is used in this study. The jacket is meant to act as an insulator by theoretically not allowing a heat change within the calorimeter pail. Constant adjustments are made between the temperature of the jacket and that of the bucket during an experiment. Since the calorimeter pail contains the “bomb” and water, the temperature of the water should be the same as that of the pail due to the action of the jacket.¹¹⁷ Therefore, the system will be in equilibrium. This means that the calculations that would otherwise be required with other jacketing systems aren't necessary here.⁹⁰ The thick walls of the “bomb” also ensure that combustion will take place at a constant volume. This kind of set-up allows

for no expansion to occur, no work to be done by the reacting system, and the heat produced can be attributed to the internal energy change.

The apparatus consists of a metal bucket that holds the water in which the bomb is submerged, a thermometer, a stirrer, and the internal “bomb” complex filled with oxygen at high pressure. Moreover, additional utensils such as a press to form pellets, oxygen gas tank, and ignition unit, machinery operating the stirrer, and recording device for data collection are used. The stirring rate shouldn't be more than 40 revolutions per minute with a current of 3 or 4 amperes to heat the wire and ultimately ignite the compound.⁸⁸ Additionally, around thirty atmospheres of pressure of oxygen gas should be used to fill the “bomb” for every trial. For this experiment, the utensils and instrumentation used are from the Parr Instrumentation Company including the bomb calorimetry apparatus, ignition unit for 115 Volts, mold and press, fuse wire, precision thermometer and temperature display unit. One great advantage to using the Parr brand calorimeter is its self-sealing nickel-alloy bomb, which has a lead inserted into an insulated terminal and another contacting the calorimeter pail.¹¹⁸ The oxygen tank is a Praxair In brand with Parr attachment. The recording instrument is a Fisher band, Fisher Recordall series 5000.

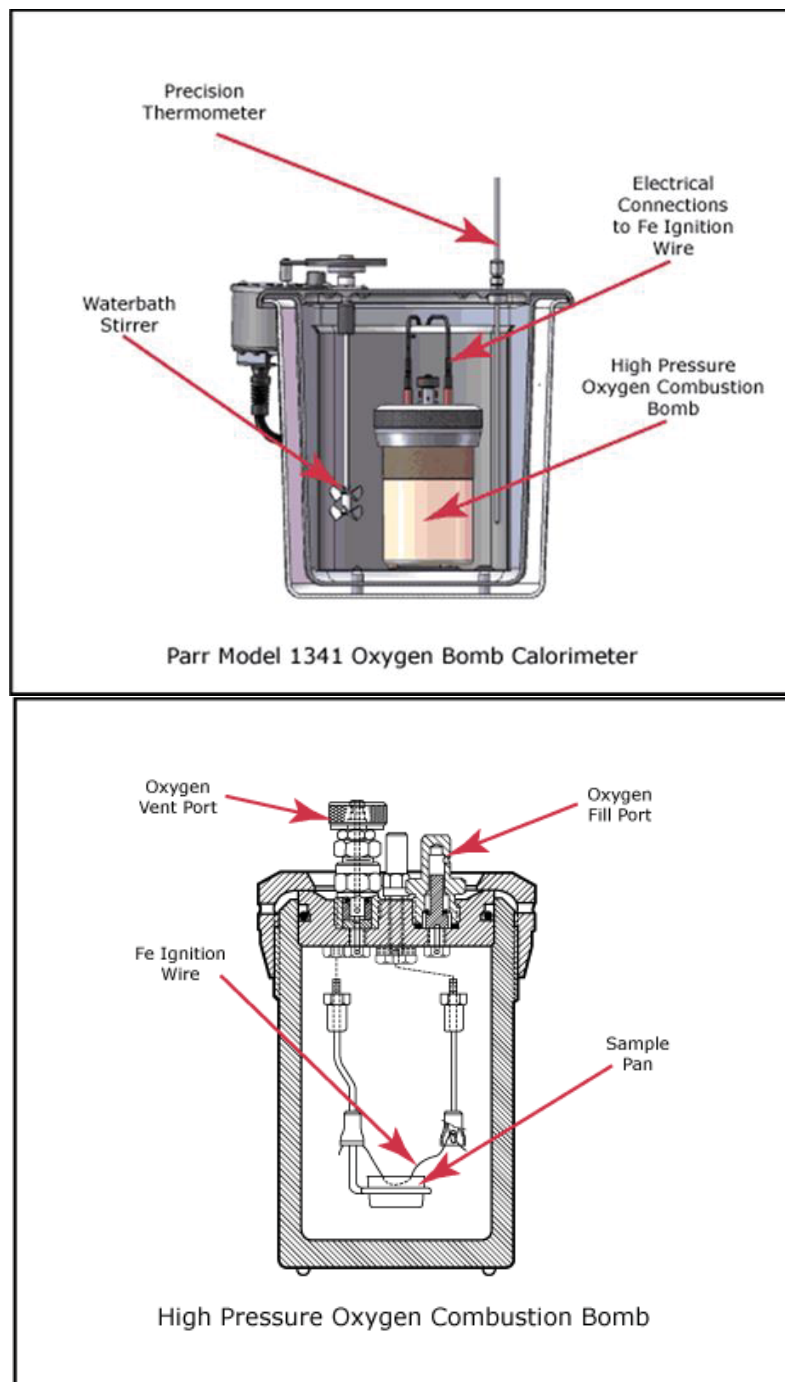


Figure 5.2 General Set-up of a Bomb Calorimeter¹¹⁹

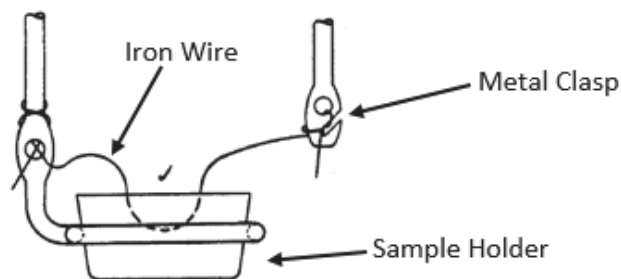


Figure 5.3 Close-Up Illustration of Sample Holder and Fuse Wire¹⁰⁷

The following method is based on the previously reported established procedures.^{92, 118} Initially, the recorder and temperature display were turned on and adjusted to the desired temperature range. Next, a pellet was made by approximately weighing the material before making the pellet when testing compounds in ratios with benzoic acid. These were accurately weighed and recorded after molding for all trials using an analytical balance. The compound was molded into a small pellet to ensure complete combustion of the entire compound, however for some samples this was impossible. Therefore, these samples containing loose substances were very carefully placed in the holding unit. Next, the weight of iron wire was recorded. After initial weight measurements were taken, the bomb complex could be assembled. The pellet was placed into the small holding unit with the fuse wire suspended over the pellet barely touching. The inner bomb unit could be assembled and sealed with care. External air was removed and pure oxygen was passed from the oxygen tank into the “bomb” until the barometer on the oxygen tank read about thirty atmospheres. Then, two liters of distilled water were measured in a volumetric flask and placed in the pail apparatus followed by the actual “bomb” being placed into the water pail. Ensuring no bubbles were in the

apparatus, the ignition leads were plugged into the “bomb,” and the top cover was placed over the apparatus. If bubbles were seen, it was purged again with oxygen; however, if this action did not aid in stopping the bubbles’ formation, the o-rings within the “bomb” were replaced. Upon proper closure of the top cover, the drive belt could be assembled with the stirrer in the “on” position and the recorder could be turned “on” to start.

Measurements could then begin to be taken with five to six initial temperatures being recorded on the chart paper manually every thirty seconds. This allowed for a fairly accurate baseline drift rate and eventual determination of the initial ignition temperature. The ignition button could then be pressed; this allowed the wire to be heated by the electrical current causing it to ignite and fall onto the pellet. The pellet could then begin to combust. Proper ignition was confirmed through movement of the recorder pen away from the baseline creating a curve. Once the reaction proceeded toward completion, which was indicated by a leveling off of the curve, temperatures were recorded and the maximum temperature achieved was noted. Upon this observation, the apparatus could be disassembled with the water removed and the oxygen gas released from the main inner apparatus. Finally, the remaining wire was accurately weighed and recorded, and calculations could be performed. It’s important that only the main pieces of wire were weighed and not the iron globules that might have formed; inclusion of these pieces would lead to inaccurate results. This was performed in triplicate for each compound; in cases with mixtures of each unknown and benzoic acid, measurements were carried out in triplicate at each ratio. The final calculated results could then be compared to one another with an average being taken while also being compared to other compounds and previous findings through other methods.

Each time that measurements were performed, one benzoic acid trial was completed for every three trials of compound. This ensured that any variation was eliminated and that an accurate value was obtained for the heat capacity of the calorimeter, or C_{cal} . Any changes within the assembly of the calorimeter (i.e. the base of the calorimeter, top circuit portion for ignition) required a new determination for the C_{cal} value to guarantee accuracy.

Various compounds were studied in this aspect of the research project, as this method of inquiry doesn't appear to have been performed before to this extent based on the literature search. Bomb calorimetry gives an interesting approach, as possible combustion reaction mechanisms can be thought up but not confirmed; however, some compounds have countless conceivable reactions. These are listed within their individual sections and lay the ground work for future studies on this topic. There may be other reactions that are plausible for some of the compounds studied here but have been omitted for simplicity.

5.4 Results

A full sample calculation for determining ΔU and ΔH values will be shown for trial one of borneol prior to providing all of the potential combustion reactions and tabular results for all compounds. Figure 5.4 is the data graph from which all calculations were made for this specific trial of camphor and the calculations with known values follow this figure.

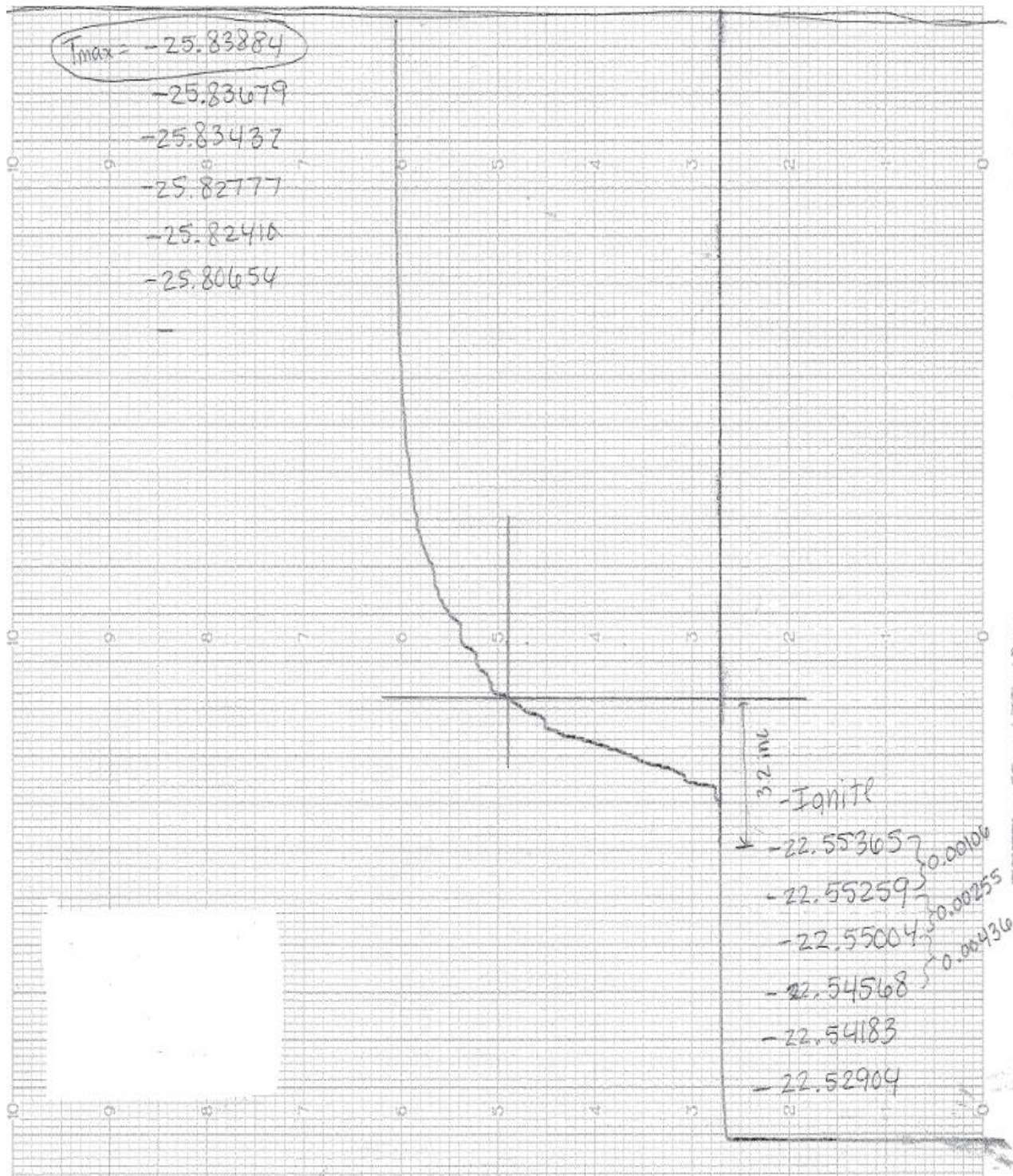


Figure 5.4 Data Graph for Trial One of Borneol

Sample Calculation for Borneol:

$$\text{Pellet Weight} = \mathbf{0.8428 \text{ g}}$$

$$\text{Wire Weight} = 0.0156 \text{ g}$$

$$\text{Excess Wire Weight} = 0.0044 \text{ g}$$

$$\text{Weight of Wire Used in Combustion} = 0.0156 \text{ g} - 0.0044 \text{ g} = \mathbf{0.0112 \text{ g}}$$

$$C_{\text{cal}} = 10.592 \text{ kJ/}^\circ\text{C}$$

$$\frac{dT}{dt} = \frac{0.00106 + 0.00255 + 0.00436}{3} = \mathbf{0.00266 \text{ }^\circ\text{C/increment}}$$

$$2/3 * (T_{\text{max}} - T_{\text{ref}}) = 2/3 * (25.83884 \text{ }^\circ\text{C} - 22.55365 \text{ }^\circ\text{C}) = 2.190126667 \text{ }^\circ\text{C} = \mathbf{2.20 \text{ }^\circ\text{C}}$$

$$T_i = T_{\text{ref}} + (dT/dt) * n_{\text{inc}} = 22.55365 \text{ }^\circ\text{C} + (0.00266 \text{ }^\circ\text{C/inc}) * (3.2 \text{ inc}) = \mathbf{22.562162 \text{ }^\circ\text{C}}$$

$$\Delta T = T_{\text{max}} - T_{\text{ref}} = 25.83884 \text{ }^\circ\text{C} - 22.562162 \text{ }^\circ\text{C} = \mathbf{3.277 \text{ }^\circ\text{C}}$$

$$q_v = C_{\text{cal}} * \Delta T = (10.592 \text{ kJ/}^\circ\text{C}) * (3.277 \text{ }^\circ\text{C}) = \mathbf{34.710 \text{ kJ}}$$

$$\Delta U = \frac{q_v - (\Delta U_{\text{Fe}} * \text{Mass}_{\text{Fe}})}{\text{Mass}_{\text{Borneol}}} = \frac{34.710 \text{ kJ} + (6.68 \text{ kJ/g} * 0.0112 \text{ g})}{0.8428 \text{ g}} = \mathbf{41.273 \text{ kJ/g}}$$

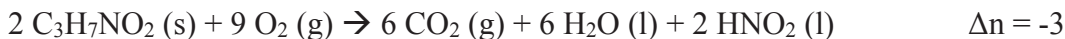
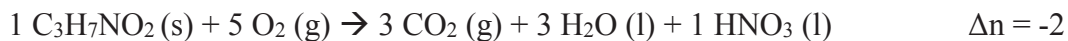
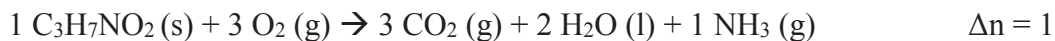
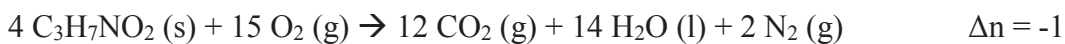
$$\Delta U = 41.273 \text{ kJ/g} * 154.249 \text{ g/mol} = \mathbf{6,366.31 \text{ kJ/mol}} * 1000 = \mathbf{6,366,310 \text{ J/mol}}$$

$$\Delta H = \Delta U + nRT = (6,366,310 \text{ J/mol} + (-4 \text{ mol}) * (8.314 \text{ J/K}) * (298 \text{ K})) / 1000 \\ = \mathbf{6,356.40 \text{ kJ/mol}}$$

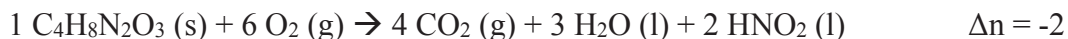
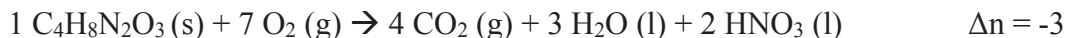
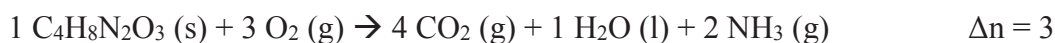
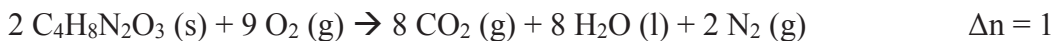
This results section is organized based on each compound's category with the possible combustion reactions listed in alphabetical order of the compound prior to the corresponding list in which it belongs. This was done to ensure that one can view the possible reactions, matching Δn values, and then their calculated energy values in tabular form as well. The inclusion of raw data such as initial temperature and mass has been excluded from this thesis, however the average change in temperature between the

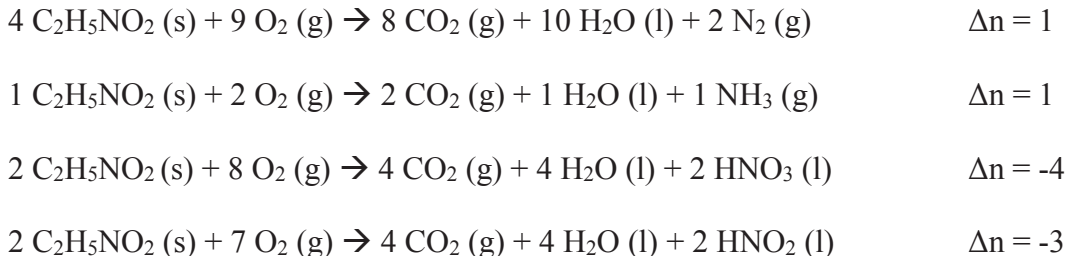
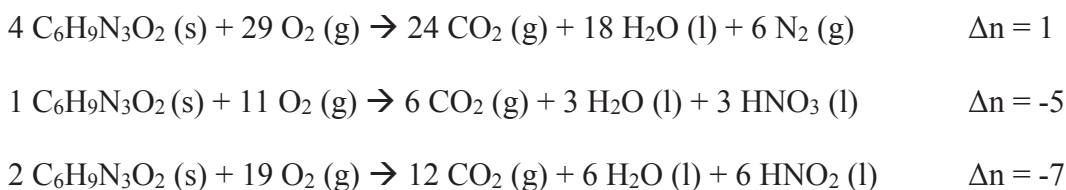
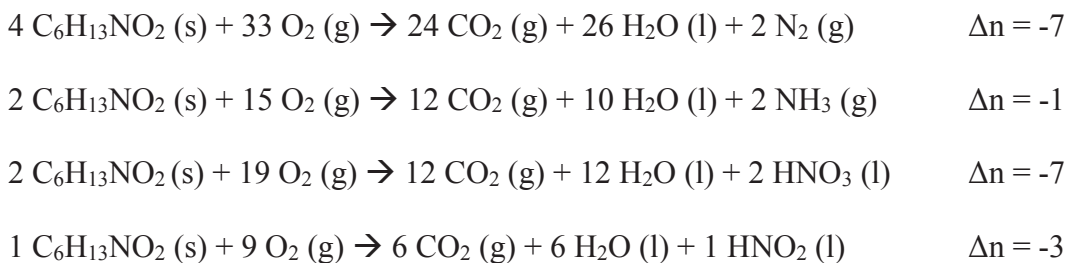
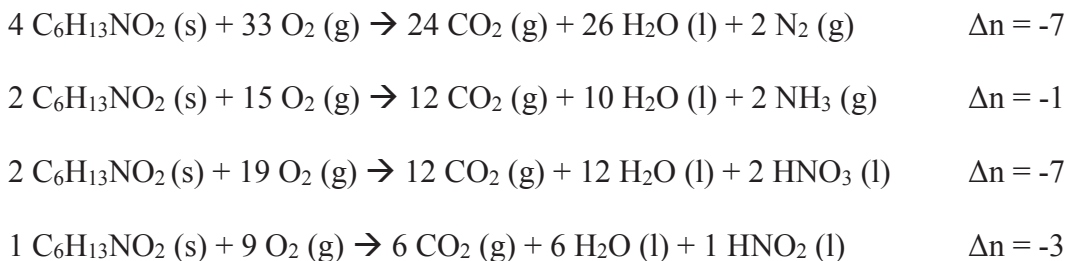
temperature at ignition and the maximum temperature (ΔT) for each has been included within the data tables. The following category order will be used to list the compounds: amino acids, dipeptides, fibrates derivatives, borneol and camphor, benzophenone and biphenyl, assorted analogous compounds, benzimidazole and imidazole, salicylic acid based compounds, low acyl gellan gum and its individual components, three polymers, and finally the *trans*-compounds.

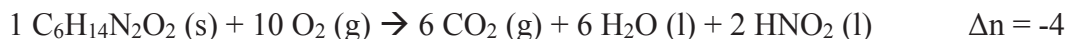
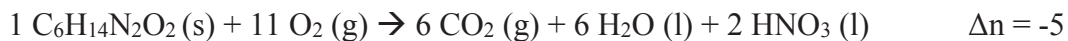
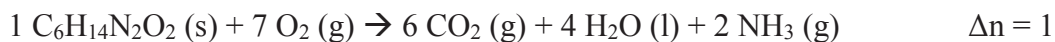
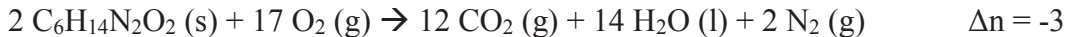
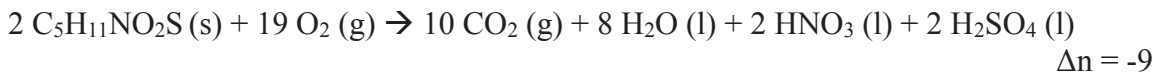
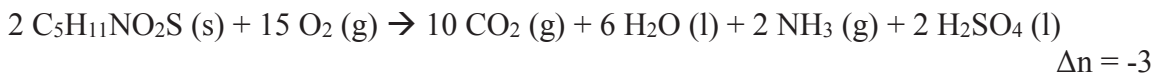
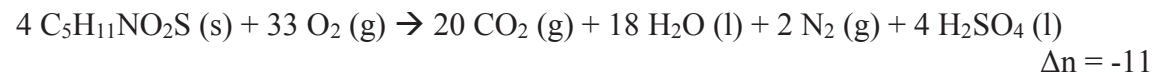
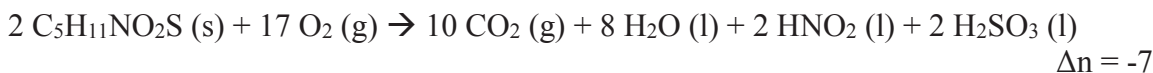
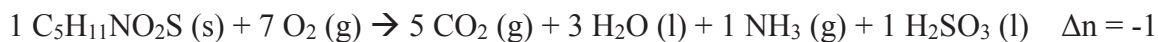
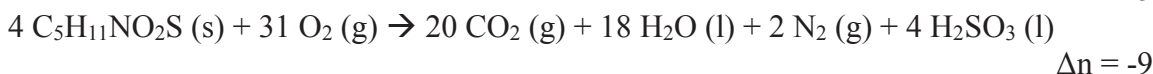
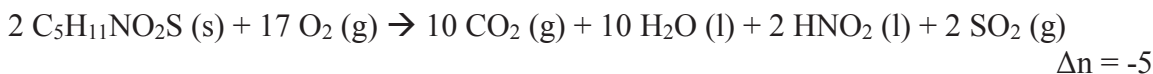
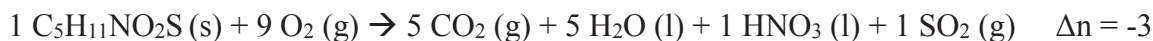
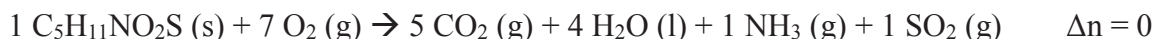
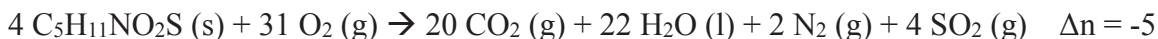
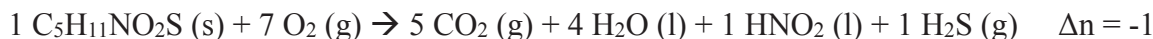
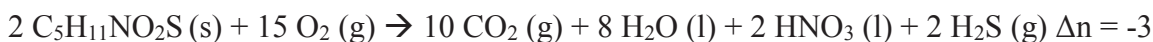
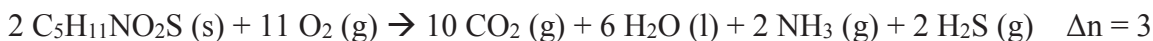
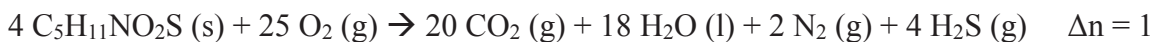
Alanine Possible Combustion Reactions:

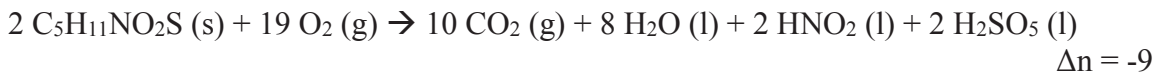
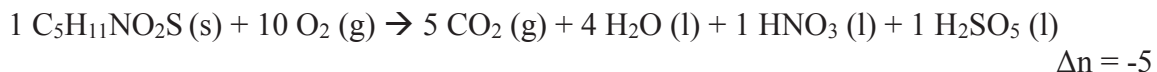
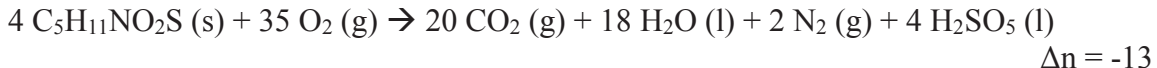
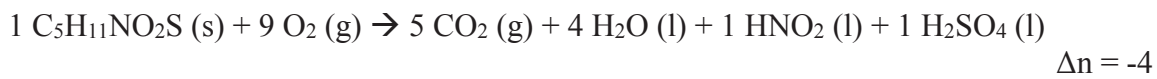


Asparagine Possible Combustion Reactions:

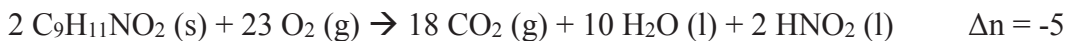
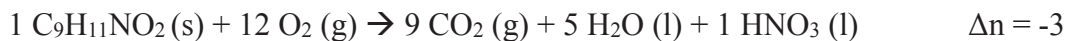
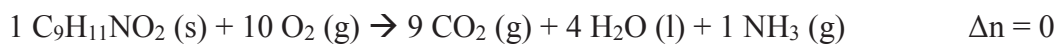
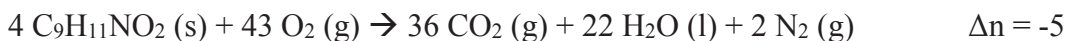


Glycine Possible Combustion Reactions:**Histidine Possible Combustion Reactions:****Isoleucine Possible Combustion Reactions:****Leucine Possible Combustion Reactions:**

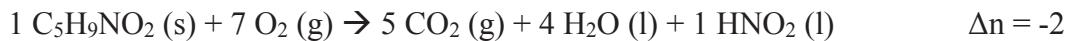
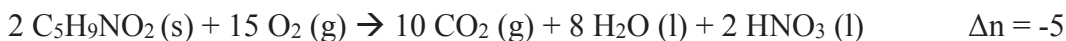
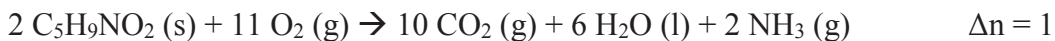
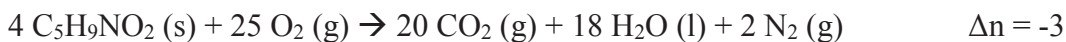
Lysine Possible Combustion Reactions:**Methionine Possible Combustion Reactions:**

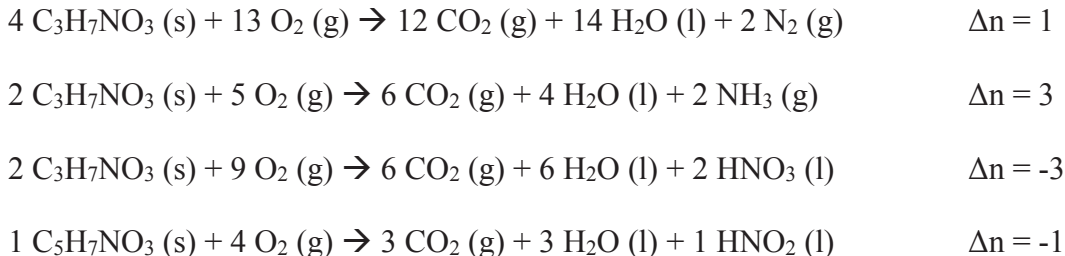
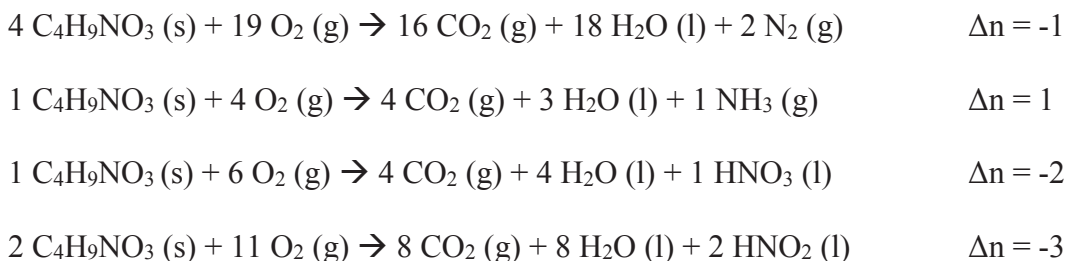
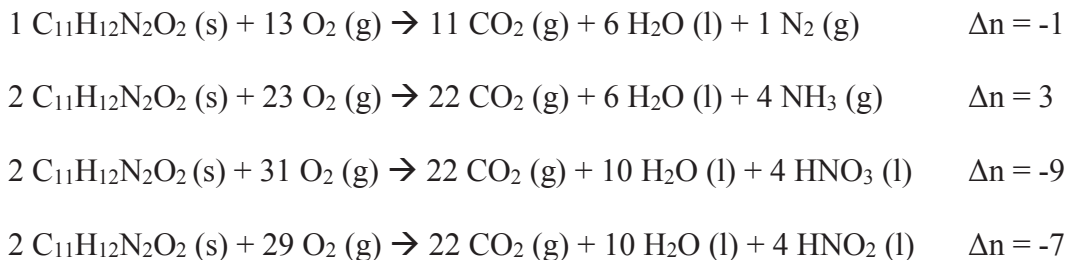
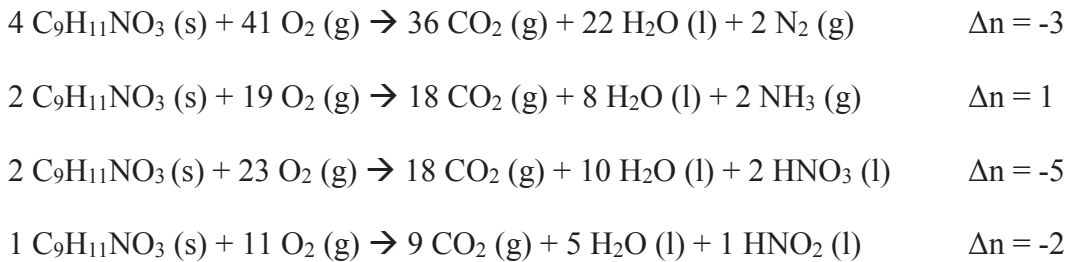


Phenylalanine Possible Combustion Reactions:



Proline Possible Combustion Reactions:



Serine Possible Combustion Reactions:**Threonine Possible Combustion Reactions:****Tryptophan Possible Combustion Reactions:****Tyrosine Possible Combustion Reactions:**

Valine Possible Combustion Reactions:

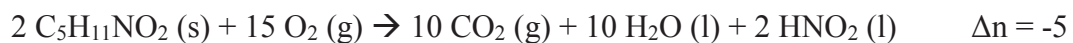
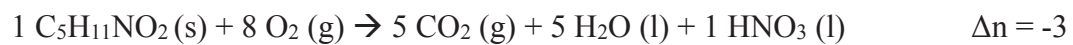
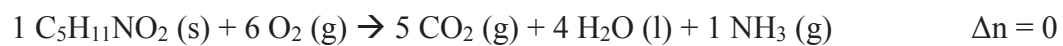
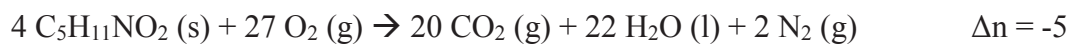
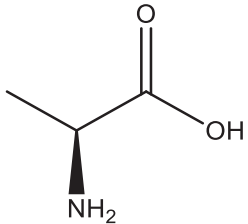
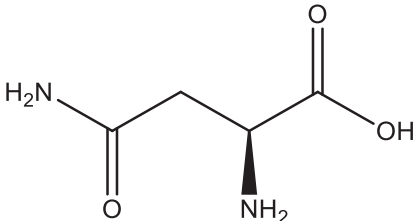
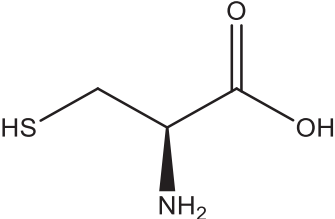
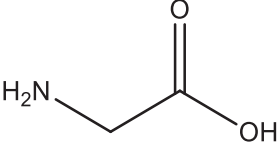
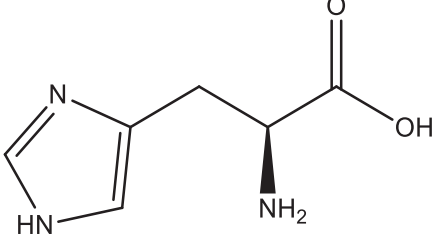
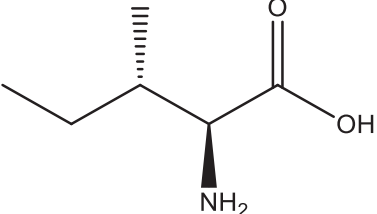
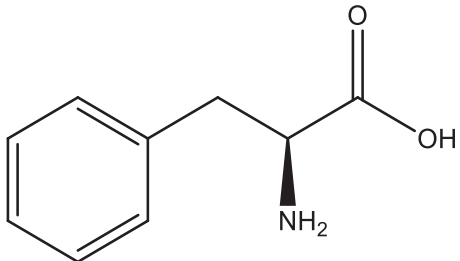
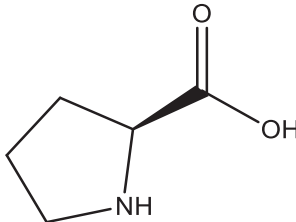
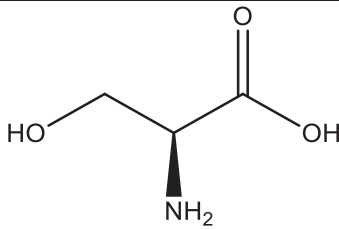
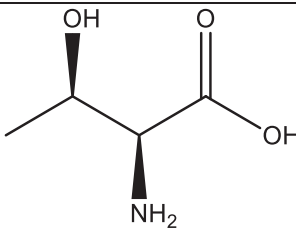


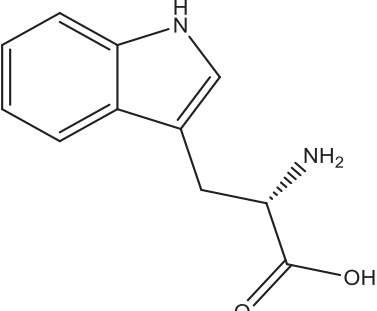
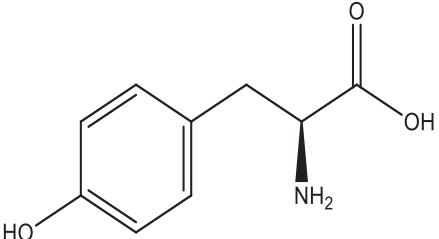
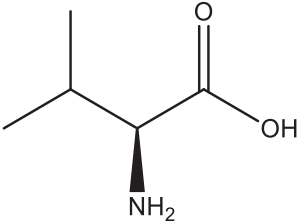
Table 5.1 Average ΔU and ΔH Values of Selected Amino Acids

Compound Information	IUPAC Name	Structure	Average ΔT ($^{\circ}\text{C}$)	Average ΔU (kJ/g)	Δn	Calculated ΔH (kJ/mol)
Alanine $\text{C}_3\text{H}_7\text{NO}_2$ 89.09 g/mol	(<i>S</i>)-2-aminopropanoic acid		2.1428	18.43	-1 1 -2 -3	-1644.71 -1639.75 -1647.19 -1649.66
Asparagine $\text{C}_4\text{H}_8\text{N}_2\text{O}_3$ 132.12 g/mol	(<i>S</i>)-2,4-diamino-4-oxybutanoic acid		1.1443	14.72	1 3 -3 -2	-2678.83 -2673.88 -2688.74 -2686.26

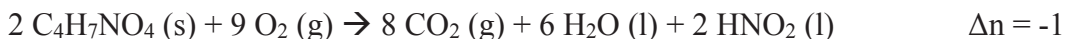
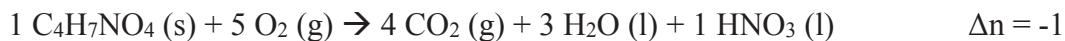
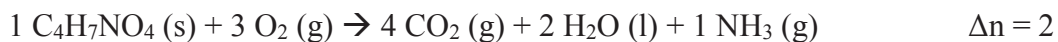
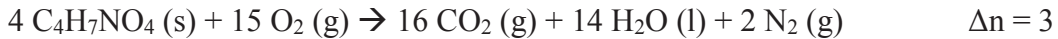
<p>Cysteine C₃H₇NO₂S 121.16 g/mol</p>	<p><i>R</i>-2-amino-3-mercaptopropanoic acid</p>		<p>1.8496</p>	<p>18.66</p>	<p>2 5 -1 0 1 -2 -3 -5 -7 -9 -4</p>	<p>-2256.29 -2248.86 -2263.72 -2261.24 -2258.77 -2266.20 -2268.68 -2273.63 -2275.28 -2283.54 -2271.15</p>
<p>Glycine C₂H₅NO₂ 75.07 g/mol</p>	<p>2-aminoacetic acid</p>		<p>0.9972</p>	<p>12.06</p>	<p>1 -4 -3</p>	<p>-902.85 -915.23 -912.76</p>
<p>Histidine C₆H₉N₃O₂ 155.15 g/mol</p>	<p><i>S</i>-2-amino-3-(1<i>H</i>-imidazol-4-yl)propanoic acid</p>		<p>1.7493</p>	<p>20.98</p>	<p>1 -5 -7</p>	<p>-3254.03 -3268.89 -3273.85</p>
<p>Isoleucine C₆H₁₃NO₂ 131.17 g/mol</p>	<p>(2<i>S</i>,3<i>S</i>)-2-amino-3-methylpentanoic acid</p>		<p>2.4597</p>	<p>27.02</p>	<p>-7 -1 -3</p>	<p>-3562.76 -3547.90 -3552.85</p>

<p>Leucine C₆H₁₃NO₂ 131.17 g/mol</p>	<p>(<i>S</i>)-2-amino-3-methylpentanoic acid</p>		1.7798	23.15	-7 -1 -3	-3053.89 -3039.03 -3043.98
<p>Lysine C₆H₁₄N₂O₂ 146.19 g/mol</p>	<p>(<i>S</i>)-2,6-diaminohexanoic acid</p>		1.2080	18.45	-3 1 -5 -4	-3378.07 -3368.16 -3383.02 -3380.54
<p>Methionine C₅H₁₁NO₂S 149.21 g/mol</p>	<p>(<i>S</i>)-2-amino-4-(methylthio)butanoic acid</p>		1.6311	23.40	1 3 -3 -1 -5 0 -9 -4 -7 -11 -13 -2	-3489.71 -3484.75 -3499.62 -3494.66 -3504.57 -3492.19 -3511.18 -3499.62 -3507.05 -3516.14 -3516.96 -3506.23

Phenylalanine $C_9H_{11}NO_2$ 165.19 g/mol	(S)-2-amino-3-phenylpropanoic acid		2.6584	27.48	-5 0 -3	-4551.35 -4538.96 -4546.39
Proline $C_5H_9NO_2$ 115.13 g/mol	(S)-pyrrolidine-2-carboxylic acid		1.6902	23.97	-3 1 -5 -2	-2766.46 -2756.55 -2771.41 -2763.98
Serine $C_3H_7NO_3$ 105.09 g/mol	(S)-2-amino-3-hydroxypropanoic acid		1.3580	14.07	1 3 -3 -1	-1476.43 -1471.47 -1486.34 -1481.38
Threonine $C_4H_9NO_3$ 119.12 g/mol	(2S,3R)-2-amino-3-hydroxybutanoic acid		1.4760	17.95	-1 1 -2 -3	-2140.91 -2135.95 -2143.39 -2145.86

<p>Tryptophan $C_{11}H_{12}N_2O_2$ 204.23 g/mol</p>	<p>(<i>S</i>)-2-amino-3-(1<i>H</i>-indol-3-yl)propanoic acid</p>		1.8675	26.81	<p>-1 3 -9 -7</p>	<p>-5477.10 -5467.19 -5496.92 -5491.96</p>
<p>Tyrosine $C_9H_9NO_3$ 181.19 g/mol</p>	<p>(<i>S</i>)-2-amino-3-(4-hydroxyphenyl)propanoic acid</p>		1.4134	21.09	<p>-3 1 -5 -2</p>	<p>-3830.19 -3820.28 -3835.15 -3827.71</p>
<p>Valine $C_5H_{11}NO_2$ 117.15 g/mol</p>	<p>(<i>S</i>)-2-amino-3-methylbutanoic acid</p>		2.5859	25.29	<p>-5 0 -3</p>	<p>-2974.74 -2962.35 -2969.78</p>

Aspartic Acid Possible Combustion Reactions:



Glutamic Acid Possible Combustion Reactions:

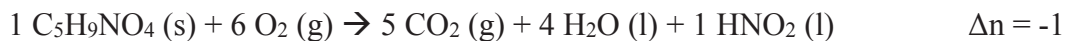
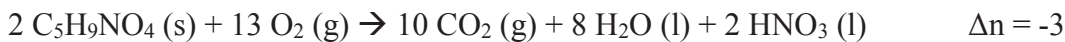
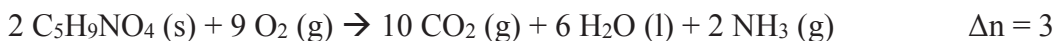
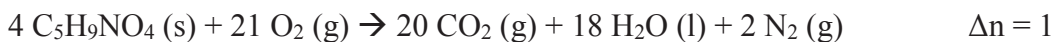


Table 5.2 Average ΔU and ΔH Values of Aspartic and Glutamic Acids in a 2:1 Compound to Benzoic Acid Ratio

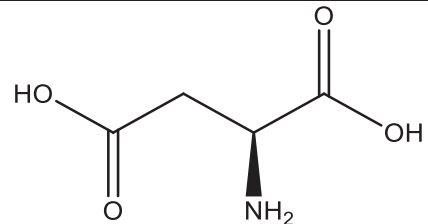
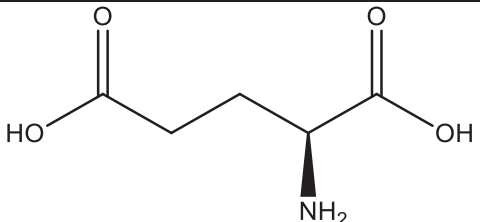
Compound Information	IUPAC Name	Structure	Average ΔT ($^{\circ}\text{C}$)	Average ΔU (kJ/g)	Δn	Calculated ΔH (kJ/mol)
Aspartic Acid $\text{C}_4\text{H}_7\text{NO}_4$ 133.10 g/mol	(<i>S</i>)-2-aminosuccinic acid		1.4788	38.94	3 2 -1	-5175.40 -5177.88 -5185.31
Glutamic Acid $\text{C}_5\text{H}_9\text{NO}_4$ 147.13 g/mol	(<i>S</i>)-2-aminopentanedioic acid		1.7089	42.26	1 3 -3 -1	-6213.72 -6208.76 -6223.63 -6218.67

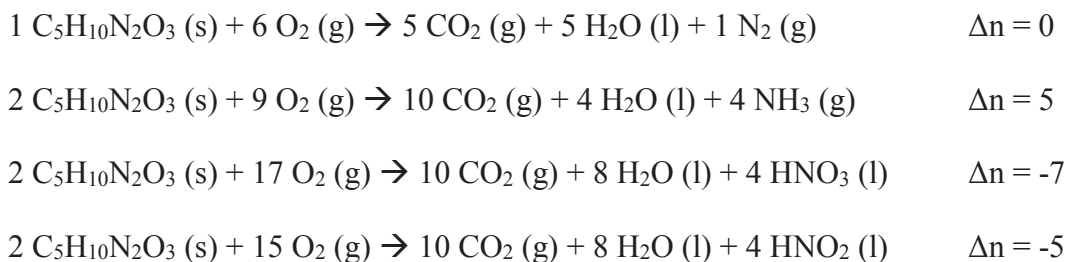
Table 5.3 Average ΔU and ΔH Values of Aspartic and Glutamic Acids in a 1:1 Compound to Benzoic Acid Ratio

Compound	Average ΔT ($^{\circ}\text{C}$)	Average ΔU (kJ/g)	Δn	Calculated ΔH (kJ/mol)
Aspartic Acid	1.8793	65.99	3	-8808.23
			2	-8778.72
			-1	-8786.15
Glutamic Acid	2.0267	68.95	1	-10140.47
			3	-10135.51
			-3	-10150.38
			-1	-10145.42

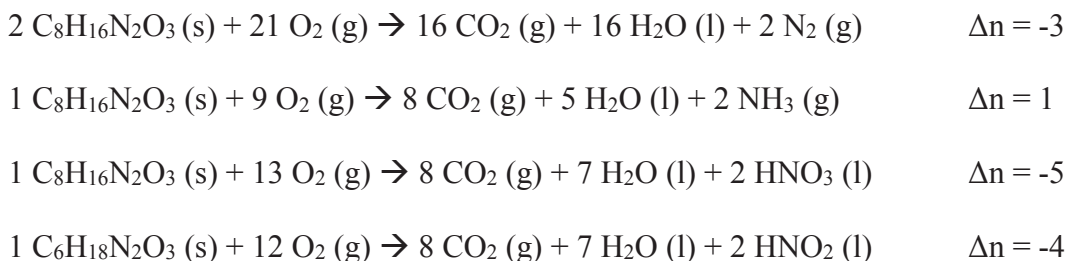
Table 5.4 Average ΔU and ΔH Values of Aspartic and Glutamic Acids in a 1:2 Compound to Benzoic Acid Ratio

Compound	Average ΔT ($^{\circ}\text{C}$)	Average ΔU (kJ/g)	Δn	Calculated ΔH (kJ/mol)
Aspartic Acid	1.8959	119.16	3	-15852.18
			2	-15854.66
			-1	-15862.09
Glutamic Acid	2.1506	122.30	1	-17987.47
			3	-17982.52
			-3	-17997.382
			-1	-17992.43

Ala-Gly Possible Combustion Reactions:



Gly-Leu Possible Combustion Reactions:



Gly-Val Possible Combustion Reactions:

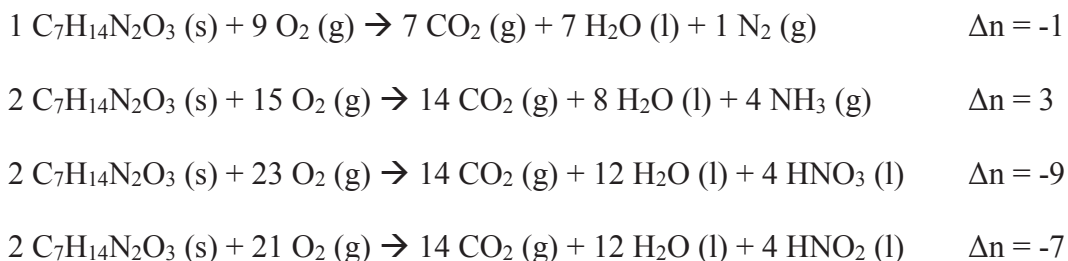


Table 5.5 Average ΔU and ΔH Values of Dipeptides

Compound Information	IUPAC Name	Structure	Average ΔT (°C)	Average ΔU (kJ/g)	Δn	Calculated ΔH (kJ/mol)
Ala-Gly $C_5H_{10}N_2O_3$ 146.1 g/mol	(S)-2-(2-aminopropanamido)acetic acid		1.3148	18.22	0 5 -7 -5	-2662.19 -2649.80 -2679.53 -2674.58
Gly-Leu $C_8H_{16}N_2O_3$ 188.22 g/mol	(S)-2-(2-aminoacetamido)-4-methylpentanoic acid		0.7256	16.92	-3 1 -5 -4	-3192.90 -3182.99 -3197.85 -3195.38
Gly-Val $C_7H_{14}N_2O_3$ 174.2 g/mol	(S)-2-(2-aminoacetamido)-3-methylbutanoic acid		1.3596	17.89	3 -1 -9 -7	-3109.36 -3119.27 -3139.09 -3134.13

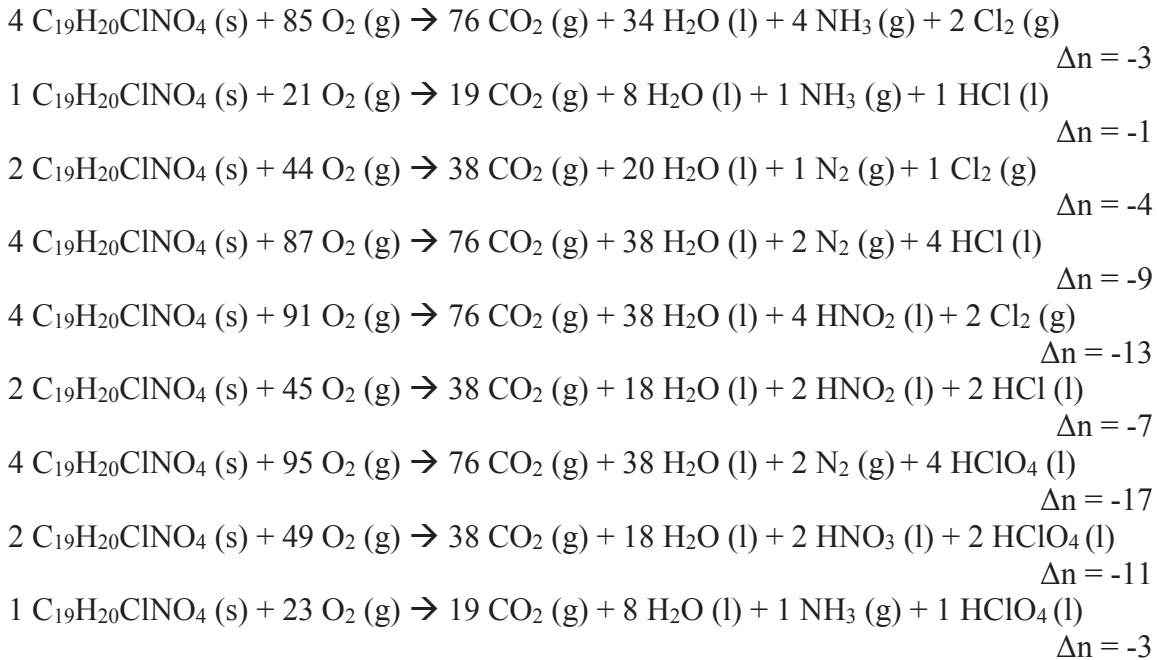
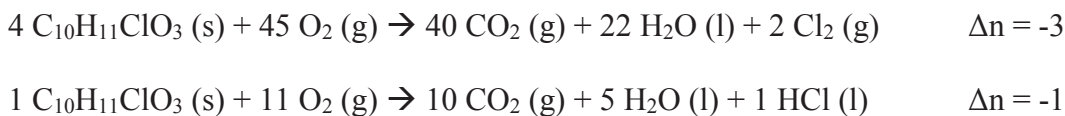
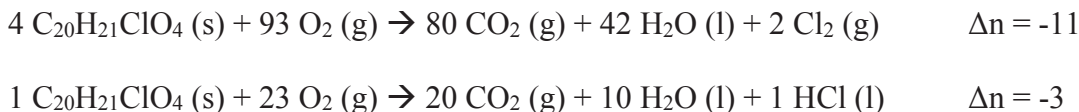
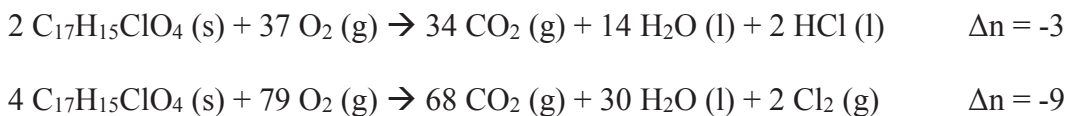
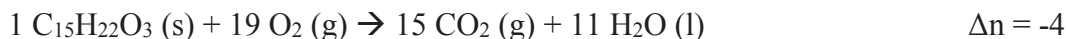
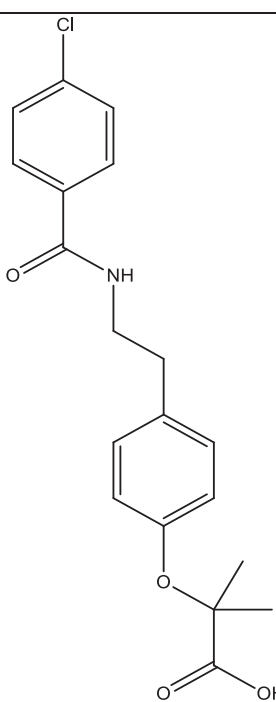
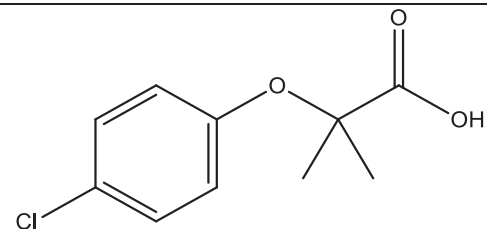
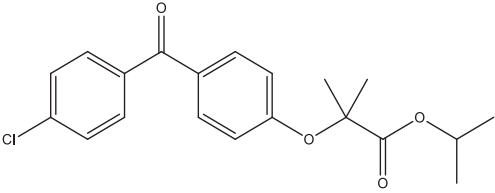
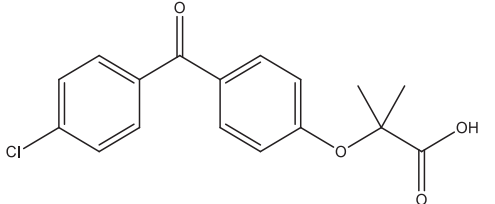
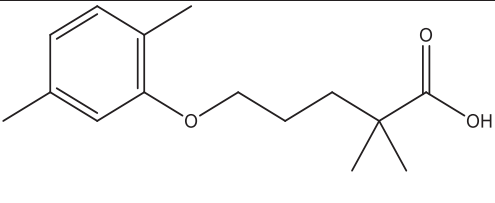
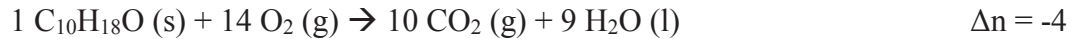
Bezafibrate Possible Combustion Reactions:**Clofibrilic Acid Possible Combustion Reactions:****Fenofibrate Possible Combustion Reactions:****Fenofibrilic Acid Possible Combustion Reactions:****Gemfibrozil Combustion Reaction:**

Table 5.6 Average ΔU and ΔH Values of Fibrate Derivative Compounds

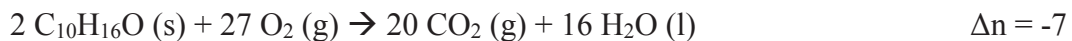
Compound Information	IUPAC Name	Structure	Average ΔT (°C)	Average ΔU (kJ/g)	Δn	Calculated ΔH (kJ/mol)
Bezafibrate C ₁₉ H ₂₀ ClNO ₄ 361.82 g/mol	2-(4-(2-(4-chlorobenzamido)ethyl)phenoxy)-2-methylpropanoic acid		1.3172	26.40	-3 -1 -4 -9 -13 -7 -17 -11	-9561.24 -9556.29 -9563.72 -9576.11 -9586.02 -9571.15 -9595.93 -9581.06
Clofibric Acid C ₁₀ H ₁₁ ClO ₃ 214.65 g/mol	2-(4-chlorophenoxy)-2-methylpropanoic acid		2.1817	23.82	-3 -1	-5119.73 -5114.78

<p>Fenofibrate $C_{20}H_{21}ClO_4$ 360.83 g/mol</p>	<p>Isopropyl 2-(4-(4-chlorobenzoyl)phenoxy)-2-methylpropanoate</p>		<p>2.4756</p>	<p>27.44</p>	<p>-11 -3</p>	<p>-9928.20 -9871.75</p>
<p>Fenofibric Acid $C_{17}H_{15}ClO_4$ 318.76 g/mol</p>	<p>2-(4-(4-chlorobenzoyl)phenoxy)-2-methylpropanoic acid</p>		<p>1.6309</p>	<p>28.33</p>	<p>-3 -9</p>	<p>-9037.83 -9052.70</p>
<p>Gemfibrozil $C_{15}H_{22}O_3$ 250.33 g/mol</p>	<p>5-(2,5-dimethylphenoxy)-2,2-dimethylpentanoic acid</p>		<p>2.2596</p>	<p>33.59</p>	<p>-4</p>	<p>-8419.70</p>

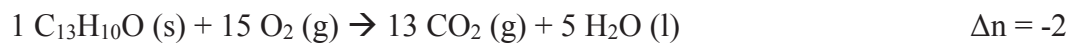
Borneol Combustion Reaction:



Camphor Combustion Reaction:



Benzophenone Combustion Reaction:



Biphenyl Combustion Reaction:

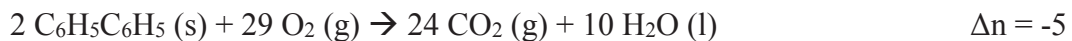


Table 5.7 Average ΔU and ΔH Values of Borneol and Camphor

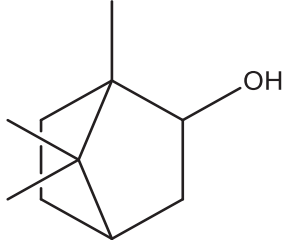
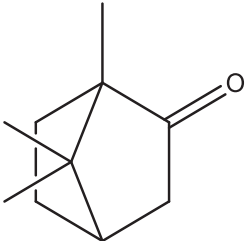
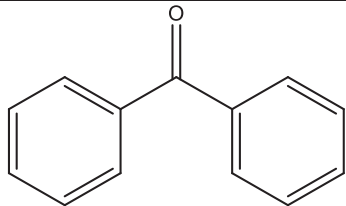
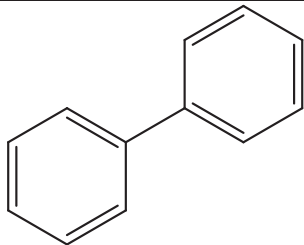
Compound Information	IUPAC Name	Structure	Average ΔT (°C)	Average ΔU (kJ/g)	Δn	Calculated ΔH (kJ/mol)
Borneol C ₁₀ H ₁₈ O 146.1 g/mol	1,7,7-trimethylbicyclo[2.2.1]heptan-2-ol		3.3941	40.36	-4	-6235.64
Camphor C ₁₀ H ₁₆ O 152.23 g/mol	1,7,7-trimethylbicyclo[2.2.1]heptan-2-one		3.6239	39.48	-7	-6027.80

Table 5.8 Average ΔU and ΔH Values of Benzophenone and Biphenyl

Compound Information	IUPAC Name	Structure	Average ΔT ($^{\circ}\text{C}$)	Average ΔU (kJ/g)	Δn	Calculated ΔH (kJ/mol)
Benzophenone $\text{C}_{13}\text{H}_{10}\text{O}$ 182.22 g/mol	N/A		2.9525	35.96	-2	-6558.39
Biphenyl $\text{C}_6\text{H}_5\text{C}_6\text{H}_5$ 154.21 g/mol	1,1'-biphenyl		4.2690	40.13	-5	-6200.53

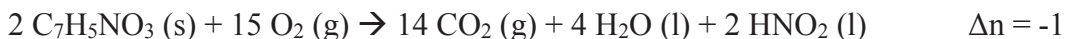
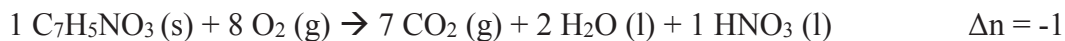
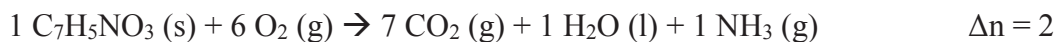
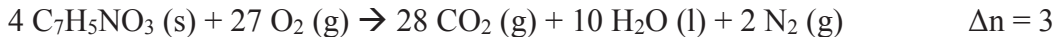
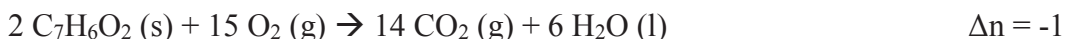
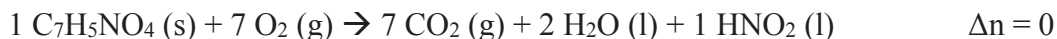
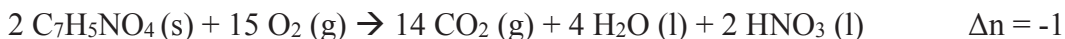
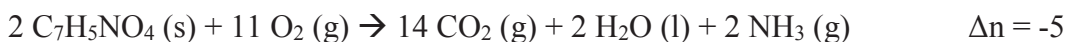
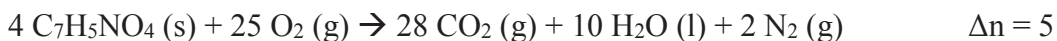
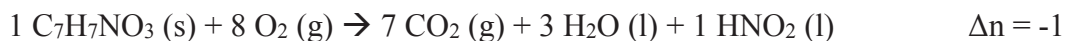
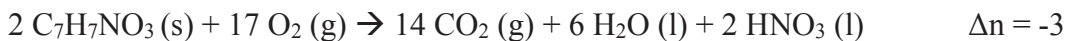
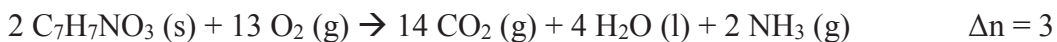
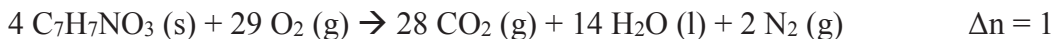
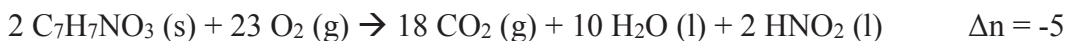
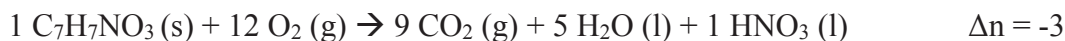
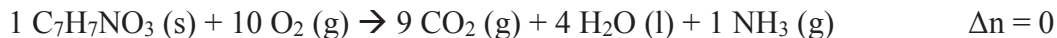
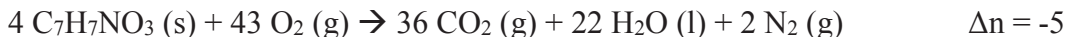
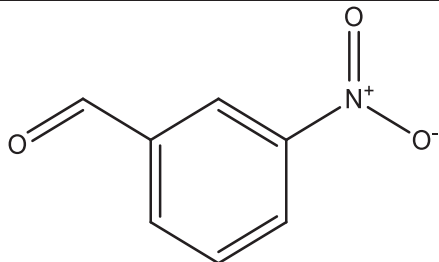
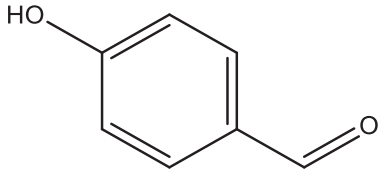
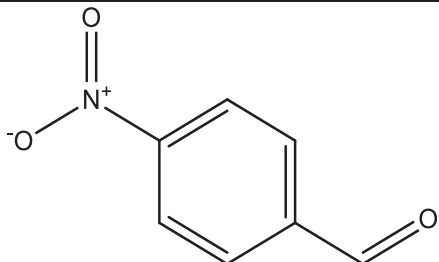
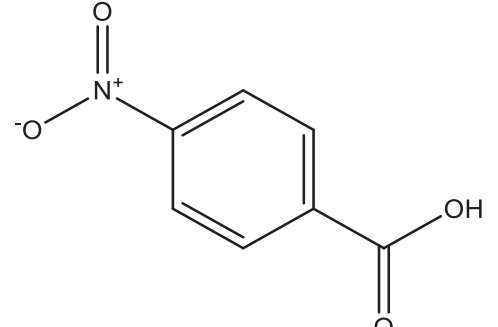
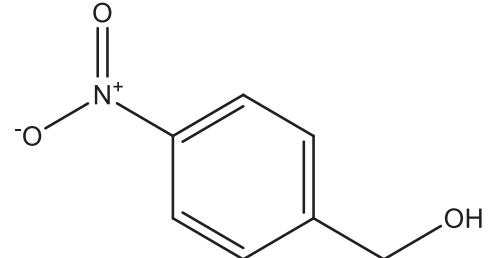
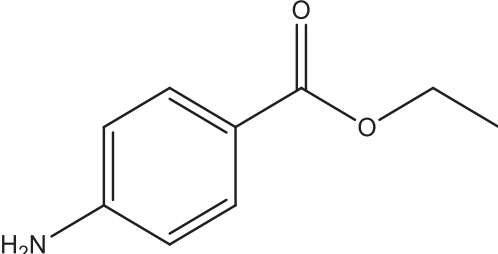
3-Nitrobenzaldehyde and 4-Nitrobenzaldehyde Possible Combustion Reactions:**4-Hydroxybenzaldehyde Combustion Reaction:****4-Nitrobenzoic Acid Possible Combustion Reactions:****4-Nitrobenzyl Alcohol Possible Combustion Reactions:****Ethyl 4-Aminobenzoate Possible Combustion Reactions:**

Table 5.9 Average ΔU and ΔH Values of Assorted Analogous Compounds

Compound Information	IUPAC Name	Structure	Average ΔT ($^{\circ}\text{C}$)	Average ΔU (kJ/g)	Δn	Calculated ΔH (kJ/mol)
3-Nitrobenzaldehyde $\text{C}_7\text{H}_5\text{NO}_3$ 151.12 g/mol	N/A		1.7136	20.22	3 2 -1	-3047.82 -3050.30 -3057.73
4-Hydroxybenzaldehyde $\text{C}_7\text{H}_6\text{O}_2$ 122.12 g/mol	N/A		2.0746	21.73	-1	-2656.49
4-Nitrobenzaldehyde $\text{C}_7\text{H}_5\text{NO}_3$ 151.12 g/mol	N/A		2.0714	22.84	3 2 -1	-3444.64 -3447.12 -3454.55

<p>4-Nitrobenzoic Acid $C_7H_5NO_4$ 167.12 g/mol</p>	<p>N/A</p>		<p>1.7058</p>	<p>16.92</p>	<p>5 -5 -1 0</p>	<p>-2814.94 -2839.72 -2829.81 -2827.33</p>
<p>4-Nitrobenzyl Alcohol $C_7H_7NO_3$ 153.14 g/mol</p>	<p>(4-nitrophenyl)methanol</p>		<p>2.5476</p>	<p>23.15</p>	<p>1 3 -3 -1</p>	<p>-3542.53 -3537.58 -3552.44 -3547.49</p>
<p>Ethyl-4-Aminobenzoate $C_9H_{11}NO_2$ 165.19 g/mol</p>	<p>N/A</p>		<p>2.5025</p>	<p>28.56</p>	<p>-5 0 -3</p>	<p>-4729.99 -4717.60 -4725.03</p>

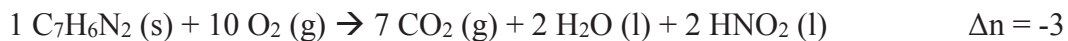
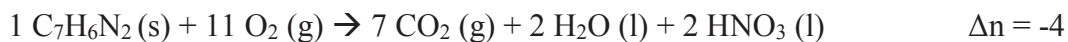
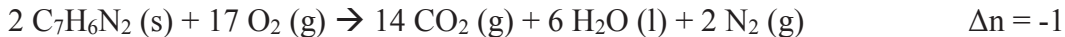
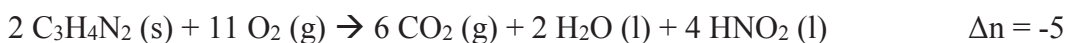
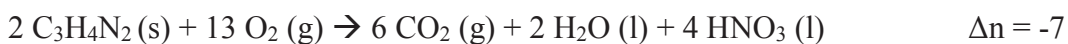
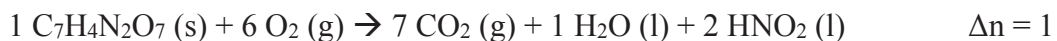
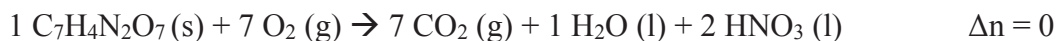
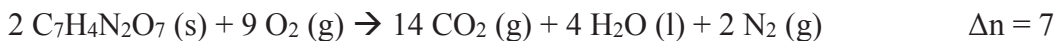
Benzimidazole Possible Combustion Reactions:**Imidazole Possible Combustion Reactions:****3,5-Dinitrosalicylic Acid Possible Combustion Reactions:****Acetylsalicylic Acid Combustion Reaction:****Salicylic Acid Combustion Reaction:**

Table 5.10 Average ΔU and ΔH Values of Benzimidazole and Imidazole

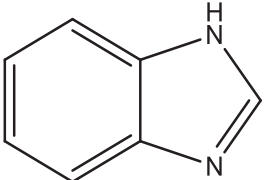
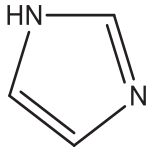
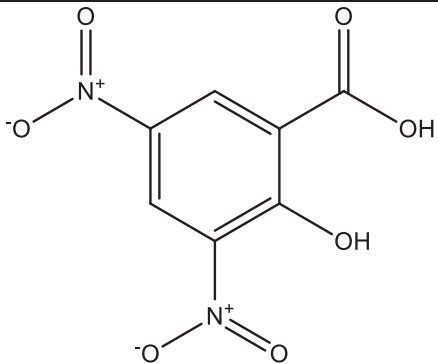
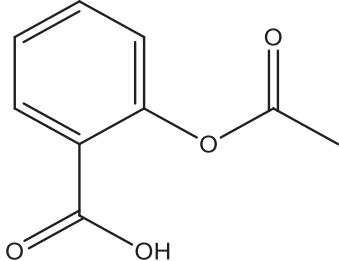
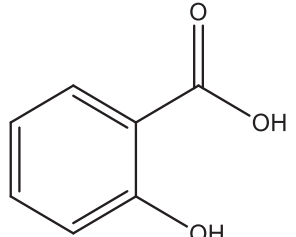
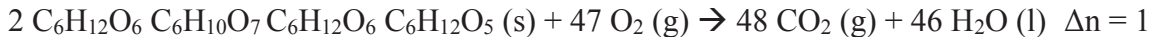
Compound Information	IUPAC Name	Structure	Average ΔT ($^{\circ}\text{C}$)	Average ΔU (kJ/g)	Δn	Calculated ΔH (kJ/mol)
Benzimidazole $\text{C}_7\text{H}_6\text{N}_2$ 118.14 g/mol	1 <i>H</i> -benzo[<i>d</i>]imidazole		2.3758	29.31	-1 -4 -3	-3464.65 -3472.09 -3469.61
Imidazole $\text{C}_3\text{H}_4\text{N}_2$ 68.08 g/mol	1 <i>H</i> -imidazole		2.4432	26.92	0 -7 -5	-1832.85 -1850.19 -1845.24

Table 5.11 Average ΔU and ΔH Values of Salicylic Acid Based Compounds

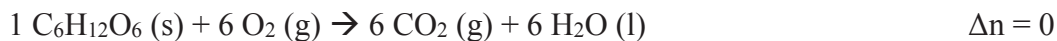
Compound Information	IUPAC Name	Structure	Average ΔT ($^{\circ}\text{C}$)	Average ΔU (kJ/g)	Δn	Calculated ΔH (kJ/mol)
3,5-Dinitrosalicylic Acid: Benzoic Acid (2:1) $\text{C}_7\text{H}_4\text{N}_2\text{O}_7$ 228.12 g/mol	2-hydroxy-3,5-dinitrobenzoic acid		1.5082	37.30	7 0 1	-8490.88 -8508.22 -8505.75
3,5-Dinitrosalicylic	“	“	1.6914	60.96	7	-13887.78

Acid: Benzoic Acid (1:1)					0 1	-13905.12 -13902.64
3,5-Dinitrosalicylic Acid: Benzoic Acid (1:2)	“	“	2.0631	117.79	7 0 1	-26852.11 -26869.45 -26866.97
Acetylsalicylic Acid $C_9H_8O_4$ 180.16 g/mol	2-acetoxybenzoic acid		2.6252	21.60	0	-3890.63
Salicylic Acid $C_7H_6O_3$ 138.12 g/mol	2-hydroxybenzoic acid		2.7642	21.82	0	-3014.16

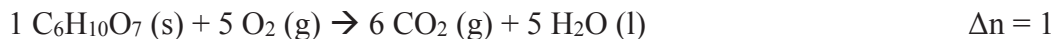
One Unit of Low Acyl Gellan Gum Combustion Reaction:



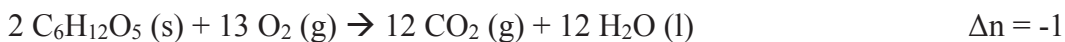
Glucose Combustion Reaction:



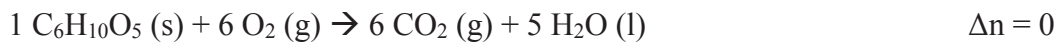
Glucuronic Acid Combustion Reaction:



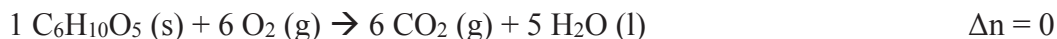
Rhamnose Combustion Reaction:



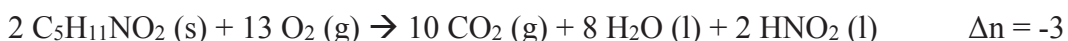
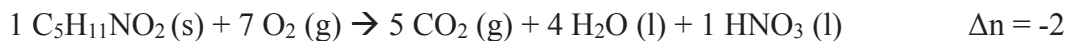
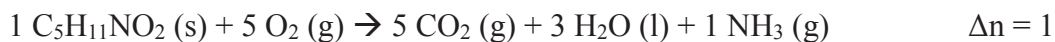
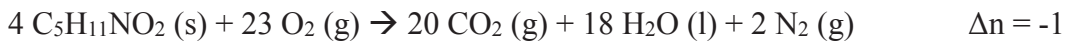
Cellulose Fiber Combustion Reaction:



One Unit of Starch Combustion Reaction:



***trans*-4-Hydroxy-L Proline Possible Combustion Reactions:**



***trans*-Cinnamic Acid Combustion Reaction:**

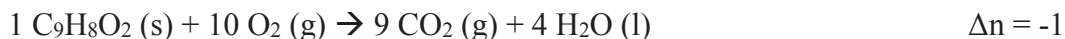


Table 5.12 Average ΔU and ΔH Values of Low Acyl Gellan Gum and Individual Components in a 2:1 Compound to Benzoic Acid Ratio

Compound Information	IUPAC Name	Structure	Average ΔT ($^{\circ}\text{C}$)	Average ΔU (kJ/g)	Δn	Calculated ΔH (kJ/mol)
Low Acyl Gellan Gum C ₆ H ₁₂ O ₆ C ₆ H ₁₀ O ₇ C ₆ H ₁₂ O ₆ C ₆ H ₁₂ O ₅ 718.0 g/mol	[D-Glc(β 1 \rightarrow 4)D-Glc(β 1 \rightarrow 4)D-Glc(β 8 \rightarrow 8)L-Rha(α 1 \rightarrow 3)] _n		1.0567	40.68	1	-19469.06
Glucose C ₆ H ₁₂ O ₆ 180.16 g/mol	(2R,3S,4R,5R)-2,3,4,5,6-pentahydroxyhexanal		1.8608	42.44	0	-5097.25
Glucuronic Acid C ₆ H ₁₀ O ₇ 194.14 g/mol	(2R,3S,4S,5R)-2,3,4,5-tetrahydroxy-6-oxohexanoic acid		1.4867	38.90	1	-5032.35

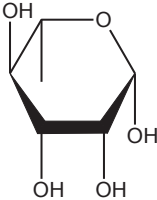
Rhamnose C ₆ H ₁₂ O ₅ 164.16 g/mol	(2S,3S,4R,5R)- 2,3,4,5- tetrahydroxyhexanal		1.9331	43.24	-1	-4734.21
---	---	--	--------	-------	----	----------

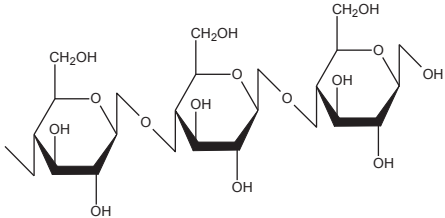
Table 5.13 Average ΔU and ΔH Values of Low Acyl Gellan Gum and Individual Components in a 1:1 Compound to Benzoic Acid Ratio

Compound	Average ΔT (°C)	Average ΔU (kJ/g)	Δn	Calculated ΔH (kJ/mol)
Low Acyl Gellan Gum	1.1759	67.41	1	-48395.57
Glucose	2.1596	69.28	0	-12481.71
Glucuronic Acid	1.8403	65.45	1	-12703.60
Rhamnose	2.0866	69.78	-1	-11457.71

Table 5.14 Average ΔU and ΔH Values of Low Acyl Gellan Gum and Individual Components in a 1:2 Compound to Benzoic Acid Ratio

Compound	Average ΔT (°C)	Average ΔU (kJ/g)	Δn	Calculated ΔH (kJ/mol)
Low Acyl Gellan Gum	1.9244	120.20	1	-86303.20
Glucose	2.3448	121.73	0	-21930.65
Glucuronic Acid	1.9278	118.98	1	-23097.23
Rhamnose	2.1046	123.38	-1	-20256.08

Table 5.15 Average ΔU and ΔH Values of Cellulose, Plastic, and Starch Polymers

Compound Information	IUPAC Name	Structure	Average ΔT ($^{\circ}\text{C}$)	Average ΔU (kJ/g)	Δn	Calculated ΔH (kJ/mol)
Cellulose: Benzoic Acid (2:1) $\text{C}_6\text{H}_{10}\text{O}_5$ (1 unit) 162.16 g/mol	(3R,4S,5S,6R)-2- [(2R,3S,4R,5R)-4,5-dihydroxy- 2-(hydroxymethyl)-6- [(2R,3S,4R,5R,6S)-4,5,6- trihydroxy-2- (hydroxymethyl)oxan-3- yl]oxyoxan-3-yl]oxy-6- (hydroxymethyl)oxane-3,4,5- triol		1.0368	43.32	0	-7024.10
Cellulose: Benzoic Acid (1:1)	“	“	1.3212	69.61	0	-11199.22
Cellulose: Benzoic Acid (1:2)	“	“	1.6331	123.24	0	-19984.43
Plastic Rings: Benzoic Acid (2:1)	-	-	2.3999	73.55	-	-
Plastic Rings: Benzoic Acid (1:1)	-	-	2.3433	101.06	-	-
Plastic Rings: Benzoic Acid (1:2)	-	-	1.6101	153.67	-	-

Starch C ₆ H ₁₀ O ₅ (1 unit) 162.16 g/mol	(2R,3S,4S,5R,6R)-2-(hydroxymethyl)-6-[(2R,3S,4R,5R,6S)-4,5,6-trihydroxy-2-(hydroxymethyl)oxan-3-yl]oxyoxane-3,4,5-triol		1.3836	15.71	0	-2548.11
--	---	--	--------	-------	---	----------

Table 5.16 Average ΔU and ΔH Values of *trans*-4-Hydroxy-L-Proline and *trans*-Cinnamic Acid

Compound Information	IUPAC Name	Structure	Average ΔT (°C)	Average ΔU (kJ/g)	Δn	Calculated ΔH (kJ/mol)
<i>trans</i> -4-Hydroxy-L-Proline C ₅ H ₁₁ NO ₂ 131.13 g/mol	(2S,4R)-4-hydroxypyrrolidine-2-carboxylic acid		2.4036	19.73	-1 1 -2 -3	-2589.47 -2584.51 -2591.95 -2594.43
<i>trans</i> -Cinnamic Acid C ₉ H ₈ O ₂ 148.16 g/mol	cinnamic acid		2.4709	26.55	-1	-3935.40

5.5 Discussion

When relating values within each section of compounds that were studied, it's important to note that the most accurate comparison comes with ΔH values, as these have units of kJ/mol. If the ΔU values were to be used for comparison purposes, issues may arise regarding the validity of assessment, as this is measured in kJ/g, and different compounds obviously have different masses. Therefore, these values can be converted into kJ/mol for proper evaluation. Furthermore, ΔH values are calculated with the change in moles, or Δn ; this requires the knowledge of combustion reactions for each species. Determining these reactions can be a difficult task, since there's no true way to do this using solely a bomb calorimeter. Therefore, the calculations performed in this thesis are based on the most likely occurrences of what reactions may occur in these situations. This is not to say that other reactions cannot occur; however for simplicity, only the main possibilities will be included in this thesis to have calculations based on them for general comparison purposes.

The meaning of the values shown in the results section should be explained before a valid discussion can be performed. Exothermic reactions, like combustion, lower the internal energy of a system by releasing heat to the surroundings outside of the system, indicated by a negative value for ΔH . This is measured as an increase in the temperature of the surroundings. If more heat is released leading to a more negative ΔH value, the compound is considered to be more stable because it takes more energy to break the bonds of the compound into its main individual components. First, a comparison of compounds will be discussed within each set in this section giving reasons why different compounds may provide different ΔH values based on their chemical structures. Then,

there will be a comparison of the sets of compounds with one another and a description of how one may deduce the specific energies of certain functional groups. Data from the studied compounds can be compared to similar compounds found in the literature when applicable as previously mentioned.

Eighteen amino acids were studied in this thesis so each will be discussed and compared to ones having similar structures and comparable ΔH values. They will be discussed from the compounds requiring the least amount of energy for combustion to those needing the most. Since glycine is the simplest amino acid, it follows that this amino acid would require the least amount of energy among the eighteen amino acids to combust at roughly 910 kJ/mol. A literature value for this compound found it to be 978 kJ/mol, which is a 7.2% difference.⁹⁷ Serine is next at about 1480 kJ/mol followed by alanine at 1645 kJ/mol; this leads to a difference of less than 200 kJ/mol between them. The literature values for serine and alanine are 1446 kJ/mol and 1607 kJ/mol, respectively. Values calculated in this research project are a bit higher for both compounds by only 2.3% in each case.⁹⁷ The methyl group of alanine is electron donating and more stable than the hydroxyl group of serine, which is electron withdrawing and allows for easier combustion. Additionally, it's possible that serine is partially more oxidized than alanine and hence, serine regains less energy for faster oxidation. Since both glycine and alanine have been mentioned within the discussion, one prior study by Gil *et al.* (2007) could shed light on how these two amino acids specifically combust. In both compounds, ionization is found on the primary amine group with hydrogen bonds being altered due to planarity of that group. Therefore, this causes an increased acidity

and strengthening of intramolecular hydrogen bonds. This can lead to more energy being needed for combustion than may be expected.¹⁰²

Threonine has a combustion energy of about 2,140 kJ/mol and cysteine has one at 2,260 kJ/mol giving about a 120 kJ/mol difference. The sulfhydryl group of cysteine is replaced by the hydroxyl of serine so it's expected that these compounds are very similar energy-wise. A study in the literature by Roux *et al.* (2010) specifically observed cysteine using a rotating bomb calorimeter and found it's enthalpy of combustion to be anywhere from 2,248 to 2,267 kJ/mol.⁸⁷ The value found in this thesis, being 2,260 kJ/mol, does fall within this range and can further confirm the validity of the study. Since this research found that serine has a lower combustion energy than cysteine, it can be concluded that less energy may be necessary to break the oxygen (C-O) bond over the sulfur bond due to their sizes. It's interesting to note that there is a difference in the combustion energy between the two of about 800 kJ/mol which is relatively large considering the fact that the compounds are chemically very similar to one another. Threonine and serine have different orientations of their functional groups in space so that orientation difference can account for the roughly 660 kJ/mol more combustion energy needed to break threonine over serine.

Asparagine and proline are next in this sequence at about 2,680 kJ/mol and 2,765 kJ/mol, respectively. This results in an energy difference of less than 100 kJ/mol, however these two are very different amino acids and can't very well be compared to one another based on their chemical structures. Had glutamine been performed, a good comparison could have been made between it and asparagine, however availability of the instrument prevented this from occurring. Valine is next in the combustion energy

sequence at 2,970 kJ/mol followed by leucine at 3,045 kJ/mol leading to a 75 kJ/mol difference. This finding makes sense because the only difference between these two amino acids is that leucine has an extra carbon in its chain. Therefore, the 75 kJ/mol combustion energy difference observed here can be attributed to the alkyl group. Ribeiro da Silva, Ferrao, and Alves da Silva (1999) performed a study observing 2-methylpropanoic acid, 2,2-dimethylpropanoic acid, and 3-methylbutanoic acid. The last of these is very similar to valine, except valine exhibits a primary amine on the free carbon closest to the carboxylic acid.¹¹³ A difference of 4.7% exists between these compounds, which makes sense since the extra 137 kJ/mol might account for the $-NH_2$ group of valine. The other two compounds have slightly smaller heats of formation, however they don't structurally resemble any of the compounds observed in this thesis. Histidine was found to have a combustion energy of about 3,260 kJ/mol, while lysine was found to have one at 3,375 kJ/mol which is a difference of 175 kJ/mol between them. Histidine's value can be compared to the 3,212 kJ/mol value found in the literature, leading to a 1.5% difference between them. Additionally, Yang *et al.* (1999) found a value for lysine's combustion energy to be 3,275 kJ/mol, which gives a 3.0% difference compared to what's found here.⁹⁷ Histidine has a bit more strain which may lead to easier combustion while lysine is more stable, and this can account for the 175 kJ/mol difference between them.

Next, methionine and isoleucine were found to have a difference of 55 kJ/mol, since their combustion energies were calculated to be about 3,500 kJ/mol and 3,555 kJ/mol, respectively. Yang *et al.* (1999) computationally calculated methionine's combustion energy to be 3,245 kJ/mol; this gives a 7.6% difference in values between

this study and the findings from their 1999 study for methionine.⁹⁷ This is much higher than the other comparisons, however this could be due to methionine's sulfur moiety causing different interactions. Methionine contains five carbons, a sulfur within the carbon chain, an ester, and a primary amine; isoleucine has an extra carbon, a carboxylic acid functional group, and a primary amine as well but no sulfur is present here. Since sulfur is greatly electron withdrawing, this characteristic may cause it to break easier than the extra alkyl group in isoleucine which can account for this small difference in the combustion between these two compounds. The final three amino acids in this combustion energy sequence are tyrosine with about 3,830 kJ/mol, phenylalanine with 4,540 kJ/mol, and tryptophan with 5,480 kJ/mol. These three are much more difficult to break apart and take more energy to combust than any other amino acid studied in this thesis. All three of these compounds are very different from one another and are spread apart energy-wise by roughly 1,600 kJ/mol across all of them.

Tyrosine has a hydroxyl serving as an electron withdrawing group in the para-position on the benzene ring, which may cause it to break more easily than the others. Yang *et al.* (1999) provides a literature value for tyrosine's combustion energy that is computationally found to be 4,417 kJ/mol, which is a 14.2% difference between what is calculated in this project compared to the literature value.⁹⁷ This is the highest percent difference found across all amino acids studied in this bomb calorimetry experiment. Phenylalanine is more stable in this capacity and Yang *et al.* (1999) shows it to have a 4,634 kJ/mol combustion energy.⁹⁷ This results in a difference of 2.0%. Tryptophan is the most complex amino acid tested in this study, so it was expected to require a higher

amount of energy to combust which was confirmed by having a 5,483 kJ/mol combustion energy value.

Two amino acids that were studied but have not been discussed thus far are aspartic acid and glutamic acid. Neither of these combusted on their own which is most likely caused by the carboxylic acid groups located on the main chain and side chain of each molecule. When molecules such as these are highly oxidized, combustion issues may arise. Therefore, these were mixed in the specified ratios with benzoic acid. The only difference between the two compounds is that there are five carbons in glutamic acid and only four in aspartic acid. Since a true combustion value for each compound by itself is unable to be determined, each ratio of the individual compound can be compared to one another with an expectation that aspartic acid would require less energy to combust. This was expected, since aspartic acid contains one less methyl group. This means that less energy would need to be expended, which was found to be the case.

Next, the dipeptides that were studied will be examined. Ala-Gly, Gly-Leu, and Gly-Val all have a primary amine, ketone, secondary amine, and carboxylic acid group. The main difference can be seen in the carbon chain length in each scenario. Gly-Leu has on average the most negative ΔH value, meaning that it is the most stable compound among the three. This is followed closely by Gly-Val, then Ala-Gly is the most easily combustible dipeptide studied here. Gly-Leu has eight carbons meaning there are more bonds needed to break and more energy is needed for this process. Gly-Val contains seven carbons and should require slightly less energy than Gly-Leu to combust which is consistent with the finding. In fact, the difference in combustion energies between Gly-Leu and Gly-Val was found to be roughly 70 kJ/mol, which can directly correspond to an

additional $-\text{CH}_2$ group in the Gly-Leu dipeptide. Rodante, Marrosu, and Catalani (1992) concluded that methyl groups in the solid phase are extremely important to overall thermal stability which is shown here.¹⁰⁶ Additionally, it's noted that the amide bond is very strong, and therefore it is usually the last bond to break in dipeptides. Since Ala-Gly has the least number of carbons in its chain and is the simplest dipeptide among the three, it makes sense that it would combust the easiest.

The fibrates studied here include bezafibrate, clofibric acid, fenofibrate, fenofibric acid, and gemfibrozil. Bezafibrate has nineteen carbons within it and needs about 9,500 kJ/mol of energy to combust. This value is only second highest to fenofibrate, which has twenty carbons and needs roughly 9,900 kJ/mol for complete combustion to occur. Therefore, the extra carbon and corresponding hydrogens between these two compounds may account for about 400 kJ/mol of energy. There may be a variety of other factors that allow for this difference as well, but it seems like the difference in carbons make the most sense in this situation. Fenofibric acid contains three less carbons than fenofibrate so 900 kJ/mol less energy is necessary to break the bonds of fenofibric acid than fenofibrate. The isopropyl group of fenofibrate becomes a carboxylic acid functional group in fenofibric acid; therefore, this type of conversion requires 900 kJ/mol less energy. Gemfibrozil is made up of fifteen carbons, so it makes sense that this compound has the second least amount of energy needed for combustion. Finally, clofibric acid is the simplest fibrate studied here containing only ten carbons, and therefore needs the least amount of energy to break apart. Therefore, based on these findings, there is a possibility that the number of carbons does dictate the amount of energy necessary for combustion; however, more research needs to be performed to confirm this assumption.

Borneol and camphor were two compounds studied in this research project that belong to a class by themselves. Both of these compounds are bicyclic, however the only structural difference is that a hydroxyl group in borneol is oxidized to a ketone in camphor. It was found that camphor has a more negative ΔH value by roughly 121 kJ/mol. This finding makes sense, as the ketone bond is stronger and should require more energy to break apart. The hydroxyl group of borneol breaks easier due to the hydrogen being readily able to have more interactions and not being as stable of a compound as camphor.

Next, benzophenone and biphenyl were grouped together since they are very similar structurally. The main difference is that benzophenone has a ketone group and corresponding extra carbon compared to biphenyl. Therefore, one should expect benzophenone to have a more negative ΔH value meaning that more energy may be needed for combustion to occur. This was confirmed experimentally by calculating that about 350 kJ/mol more energy is necessary to break apart benzophenone compared to biphenyl. This value can be used to account for the ketone group's energy within the compound.

An assortment of nitrogen containing compounds that are very analogous to one another were considered here as well. The most energy was needed to combust ethyl-4-aminobenzoate probably because of its ester group and nine carbons along with the primary amine group. This was followed by 4-nitrobenzyl alcohol and 4-nitrobenzaldehyde, respectively which had an energy combustion difference of roughly 100 kJ/mol. This means that it takes an extra 100 kJ/mol to combust an alcohol when compared to an aldehyde on the same compound. Next in this trend is 4-

nitrobenzaldehyde followed by 3-nitrobenzaldehyde with a difference of about 400 kJ/mol. Therefore, the former compound here is more stable and needs a greater energy input to combust. This finding can be attributed to the meta- versus para- positioning of the aldehyde group. The para- position of the aldehyde within 4-nitrobenzaldehyde is more stable since it's further away from the nitro group. Additionally, electron withdrawing groups such as aldehydes should be placed in the ortho- or para- position to increase the stability; in the case of 3-nitrobenzaldehyde, the aldehyde is located meta- to the nitro substituent on the ring leading to instability. In this set of six compounds, the second easiest compound to combust is 4-nitrobenzoic acid and the one requiring the least amount of energy is 4-hydroxybenzaldehyde by roughly 170 kJ/mol. It's possible that the carboxylic acid, being an electron withdrawing group, allows for easier combustion than the previously stated compounds, like 3-nitrobenzaldehyde, 4-nitrobenzaldehyde, and ethyl-4-aminobenzoate. Furthermore, 4-hydroxybenzaldehyde contains two electron withdrawing groups, and although they're in para- positions to one another, this leads to an easier combustion than the other compounds in this category.

Benzimidazole and imidazole are highly similar structurally with the main imidazole ring being fused to a benzene ring in benzimidazole. It was found that a roughly 1,600 kJ/mol difference existed between benzimidazole and imidazole with benzimidazole needing more energy to fully combust. This finding implies the role of the benzene ring in benzimidazole has extremely high stability. Since all other structural features are the same between the two compounds,

The current study focused on derivatives of the salicylic acid class of compounds using the bomb calorimeter. For 3,5-dinitrosalicylic acid, ratios of this compound with

benzoic acid needed to be performed in order for full combustion to occur. This is most likely due to its tetra-substituted benzene ring that's highly oxidized because the other two compounds in this section are only bi-substituted. Due to this situation, it would become inaccurate to make a comparison between 3,5-dinitrosalicylic acid and the other two compounds. There is a roughly 875 kJ/mol difference in combustion energy between acetylsalicylic acid and salicylic acid with acetylsalicylic acid requiring more energy to combust. Therefore, the conversion from hydroxyl to ester takes about 875 kJ/mol of energy to form.

Low acyl gellan gum and its individual components, glucose, glucuronic acid, and rhamnose, were studied in this section as well. All four compounds in this set needed to be mixed with benzoic acid in order to have complete combustion. The results align across all ratios for the individual sugars. Rhamnose required the least amount of energy to combust followed by glucose and then glucuronic acid, which needed the most energy to breakdown. Rhamnose requires the least energy most likely due to it being less oxygenated than the other sugars. Also, the carboxylic acid group of glucuronic acid might have been the reason why it needed the most energy to combust. Since low acyl gellan gum consists of two glucose subunits and one each of glucuronic acid and rhamnose, adding the combustion energies of these species in each ratio gives the approximate value for the low acyl gellan gum ratio. However, the calculated values were found to be a bit higher than the experimental combustion of the gum itself. This is most likely caused by its linkage and extra number of hydrogens within each sugar itself compared to the low acyl gellan gum compound.

Cellulose, plastic rings, and starch were grouped together due to their polymeric nature and general uses. Interestingly, the cellulose and plastic rings weren't able to fully combust on their own but starch did not need the addition of benzoic acid to combust. It should be noted that the plastic rings can't truly be compared at this point, since there's uncertainty as to whether this is polypropylene or another material and there's no access to the equipment necessary to determine its identity. This means that only the ΔU value for plastic could be calculated and that the possible combustion reaction's parameters, Δn values, and ΔH could not be determined. Therefore, it cannot be compared here to the fullest extent at this time. However, based on its ΔU value, it can be assumed that if similar Δn values were determined and it has a related size to the others, plastic would need a larger amount of energy to combust than either cellulose or starch. By structurally comparing cellulose and starch, starch consists of a repeating monomer while cellulose is a repeating dimer. Therefore, the repeating dimer should require more energy to combust, and this may be why cellulose needed benzoic acid to aid in its combustion while starch did not. In general, it would be a stretch to make conclusions relating these three compounds as more information is needed for a valid comparison.

Finally, two compounds were studied that didn't truly fit into any of the other stated categories and were grouped together based on their complexities and trans-structural feature. Both *trans*-4-hydroxyl-L-proline and *trans*-cinnamic acid contain carboxylic acid groups. However *trans*-4-hydroxyl-L-proline contains nitrogen, an extra hydroxyl, and five carbons, while *trans*-cinnamic acid has a benzene ring, double bond, and nine carbons. The combustion energy of *trans*-cinnamic acid is roughly 1,300 kJ/mol more than that of *trans*-4-hydroxyl-L-proline. Most likely, *trans*-cinnamic acid required

more energy to combust because of the energy that's necessary to break the double bond along with the stable benzene ring.

Comparisons amongst all compounds and more so between the characterized groups themselves can provide useful information on generalizing assumptions. Each group looked at compounds of comparable structure, functionality, or purpose and reflects their similarities. The dipeptides showed differing values than each individual amino acid that was contained within them, and the addition of each to one another was a lower value in Ala-Gly but a higher value in Gly-Leu and Gly-Val. This is an interesting finding that needs to be researched further before conclusions can be drawn as to why this is the case. The fibrates all fell within the 8,000 to 9,000 kJ/mol range except for clofibric acid which was substantially lower. This compound is much smaller than the others though and may account for this difference. The nitrogen-containing compounds had very similar combustion energies to numerous amino acids which makes sense due to some of their similar structures. Biphenyl and benzophenone showed higher values than most amino acids, but since both have two benzene rings within them, it's not a stretch to see why this occurs. Unfortunately, not many values were found in the literature to compare with all of these compounds, since many don't appear to have been tested before using this bomb calorimetry method.

5.6 Future Work

There are a few aspects of this project that could be improved upon for future work. For example, the calorimeter in use was approximately 25 years old and the recorder was almost double that age. Therefore, with all older pieces of equipment being

utilized, there becomes a need to confirm the results and data with instrumentation produced today. Additionally, although fifty compounds were able to be analyzed in triplicate, it would have been advantageous to observe all of the amino acids and not just the selected ones that I was able to finish with my time constraint on the instrument. Furthermore, a more thorough comparison of the values obtained here to those found through other methods of determining values for ΔH can give greater insight into the validity and accuracy of the method.

Another aspect of this project that could be improved upon involves the actual set-up of the bomb calorimeter. Combustion reactions that are included are the best guesses as to what may be happening once each compound combusts, however they are by no means completely accurate. In order to obtain the true reaction, a mass spectrometer would need to be attached to the calorimeter to determine the composition of compounds that are formed upon combustion. This would give the components of the final products and give a definitive combustion reaction.

Chapter 6: Conclusions and Future Studies on Hydrogen Bonding Energies

The overall purpose of this thesis was met, since the ability to measure hydrogen bonds with their corresponding energies was attempted through the stated, varied methods. All three projects showed that both visualizing hydrogen bonds and quantifying them can be performed in a variety of ways, allowing for the ability of multiple approaches to be executed in order to solve the same general research problem. Determining hydrogen bond energies proves to be a basic research inquiry; however, it has diverse applications and is very important in many aspects of science, for example when designing drugs. The analytical and theoretical techniques utilized in this thesis lay a decent groundwork for other comparisons regarding the evolution of hydrogen bond energy patterns and future studies involving similar compounds using different procedures or even unlike compounds using the same procedure.

Many future research projects can be based off the work already performed here and elsewhere by providing a way to compare results and organize experiments. For example, the diverse ways in which aspartic and glutamic acids in their potassium chloride matrices were measured qualitatively has never been attempted to be characterized until this point. This description will provide great potential for all future studies on similar topics. Also, the exact NMR procedure employed in that research project did not exist prior to my study. Additionally, the eleven sub-categories within the bomb calorimetry project can be explored further using other methods to confirm and strengthen the validity of the results. All future work should include characterization of more bonds and potential patterns in energies using the methods completed here and others from the literature.

Appendix A: Supplementary Material from Praveen Bandrupalli's Thesis entitled "Thermal Analysis of Decomposition Reactions of Aspartic and Glutamic Acids in Potassium Chloride Matrix"

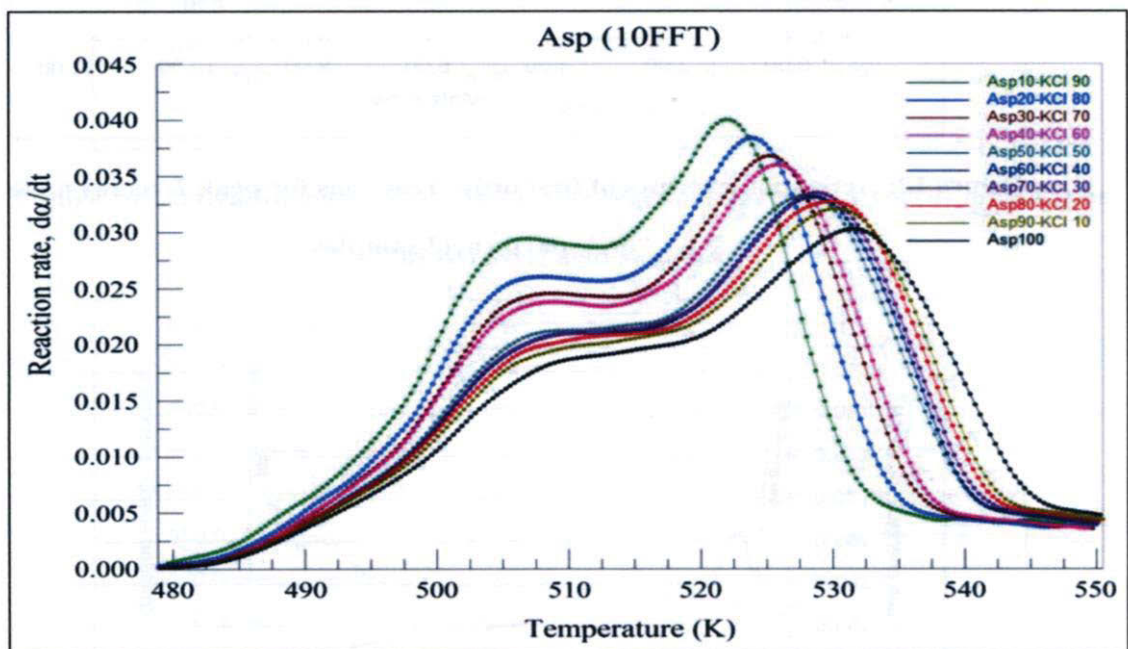


Figure A.1 Overlay of PSI Plots of Reaction Rate Profiles of Aspartic Acid Samples versus Temperature

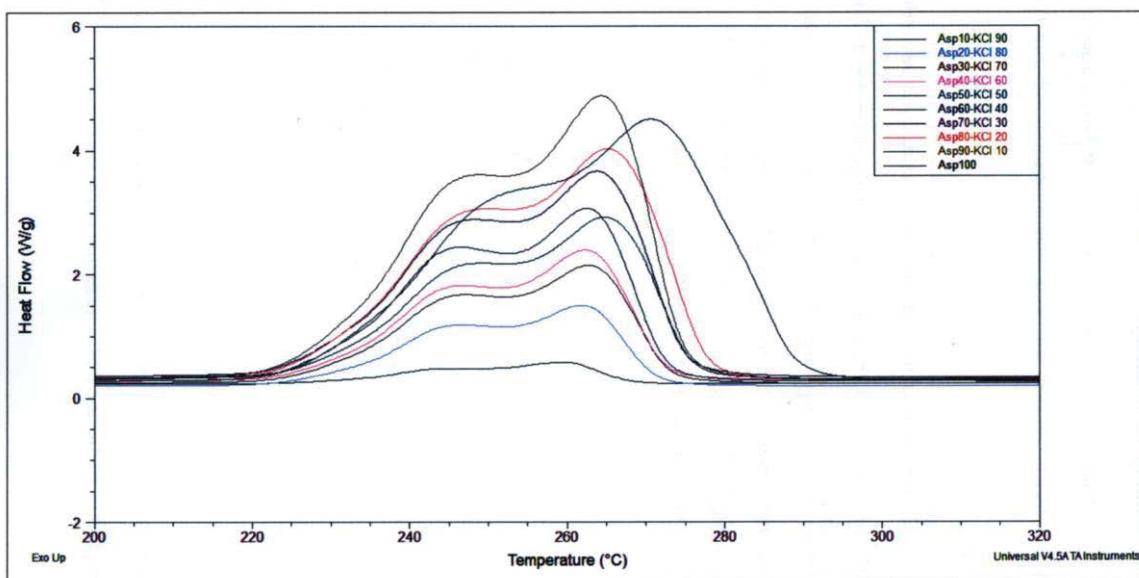


Figure A.2 Overlay of DSC Plots of Aspartic Acid Samples Showing Heat Flow versus Temperature

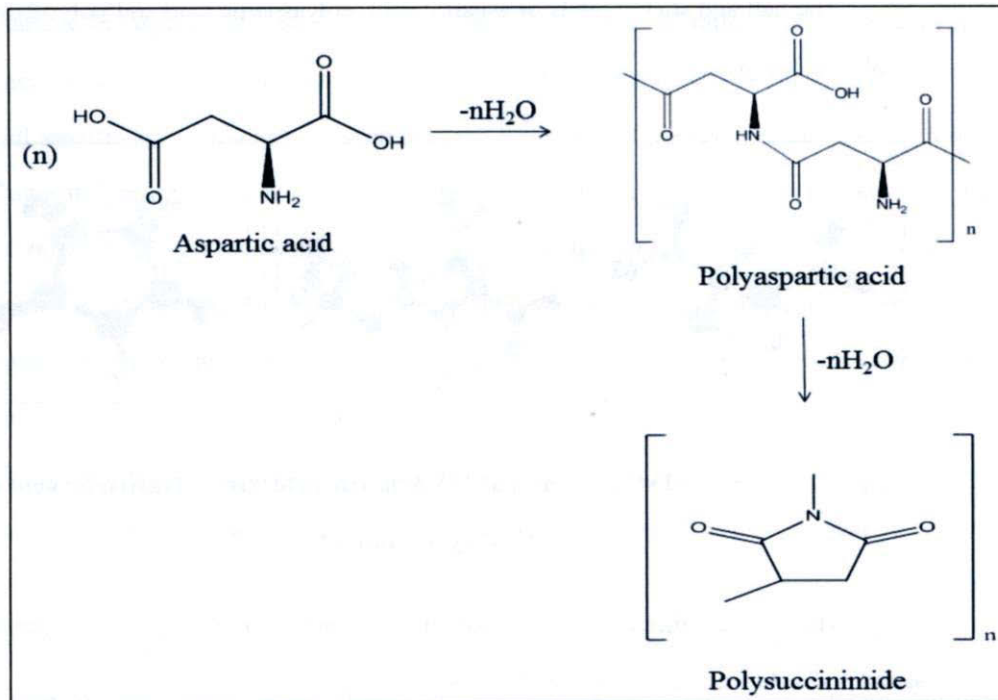


Figure A.3 Proposed Thermal Decomposition Reactions of Aspartic Acid Samples

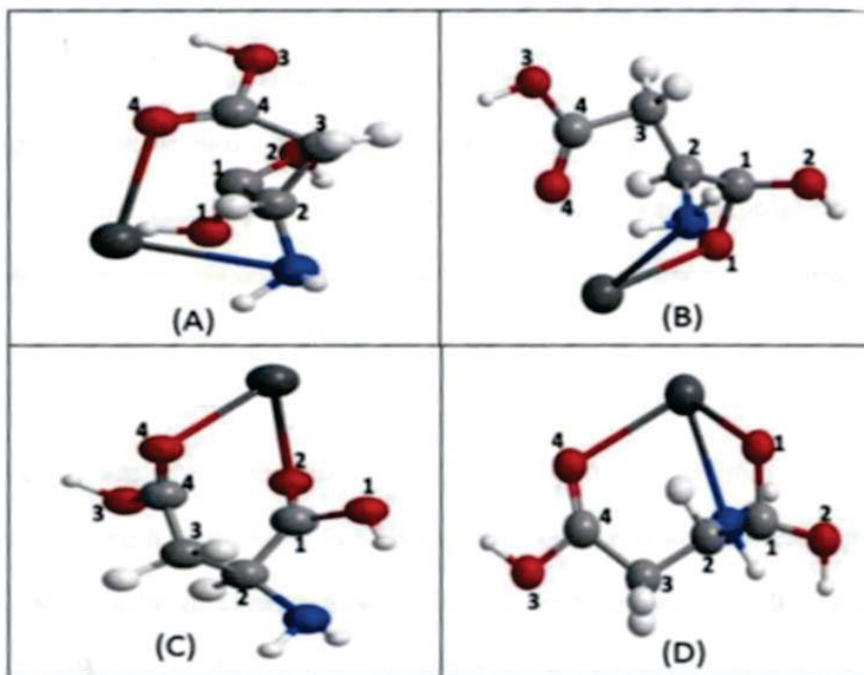


Figure A.4 Possible Binding modes of K^+ ion to Aspartic Acid Ligand Referring to Asp A through Asp D

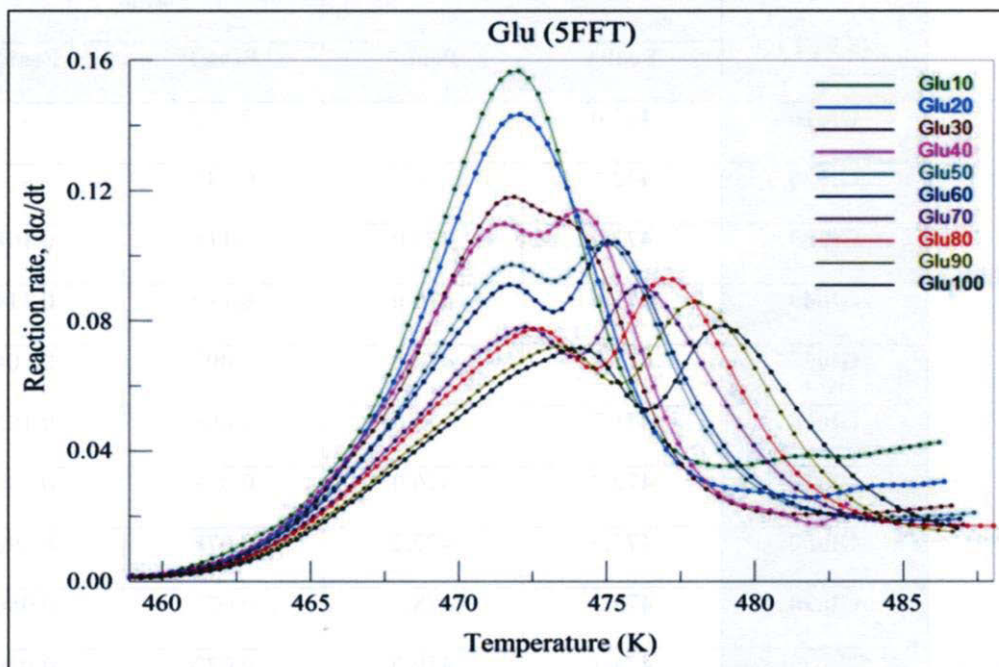


Figure A.5 Overlay of PSI Plots of Reaction Rate Profiles of Glutamic Acid Samples versus Temperature

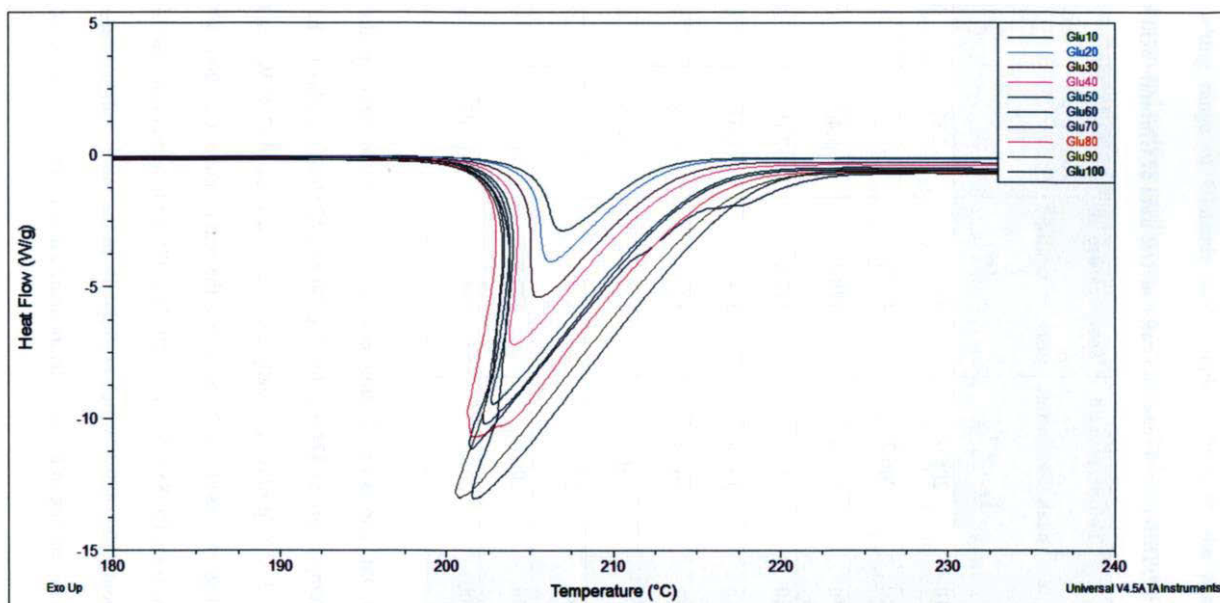


Figure A.6 Overlay of DSC Plots of Glutamic Acid Samples Showing Heat Flow versus Temperature

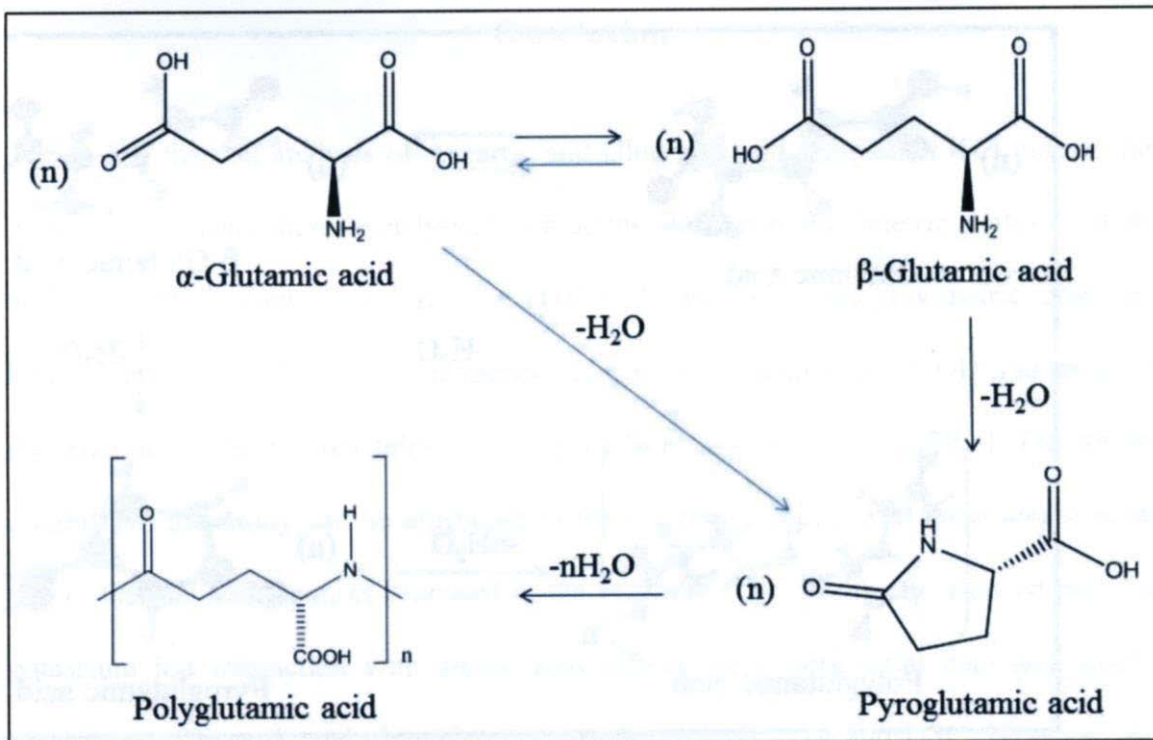


Figure A.7 Proposed Thermal Decomposition Reactions of Glutamic Acid Samples

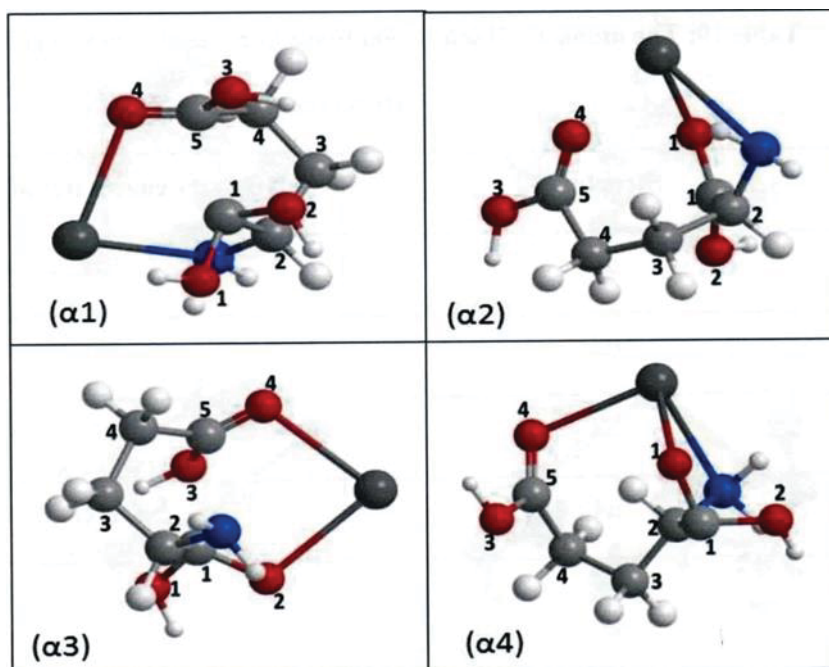


Figure A.8 Possible Binding modes of K^+ ion to Glutamic Acid Ligand Referring to Glu 1 through Glu 4

Appendix B: Use of Spartan '04 Computer Program Input and Output

The Spartan '04 computer program was utilized in this project. Input required correctly drawing the molecular structure and then minimizing the overall energy of the molecule. Calculations could then be set up through a prompt box. Below is an example of what appears on the screen upon selecting “setup” and “calculations” and how you may change different parameters with the drop-down arrows.

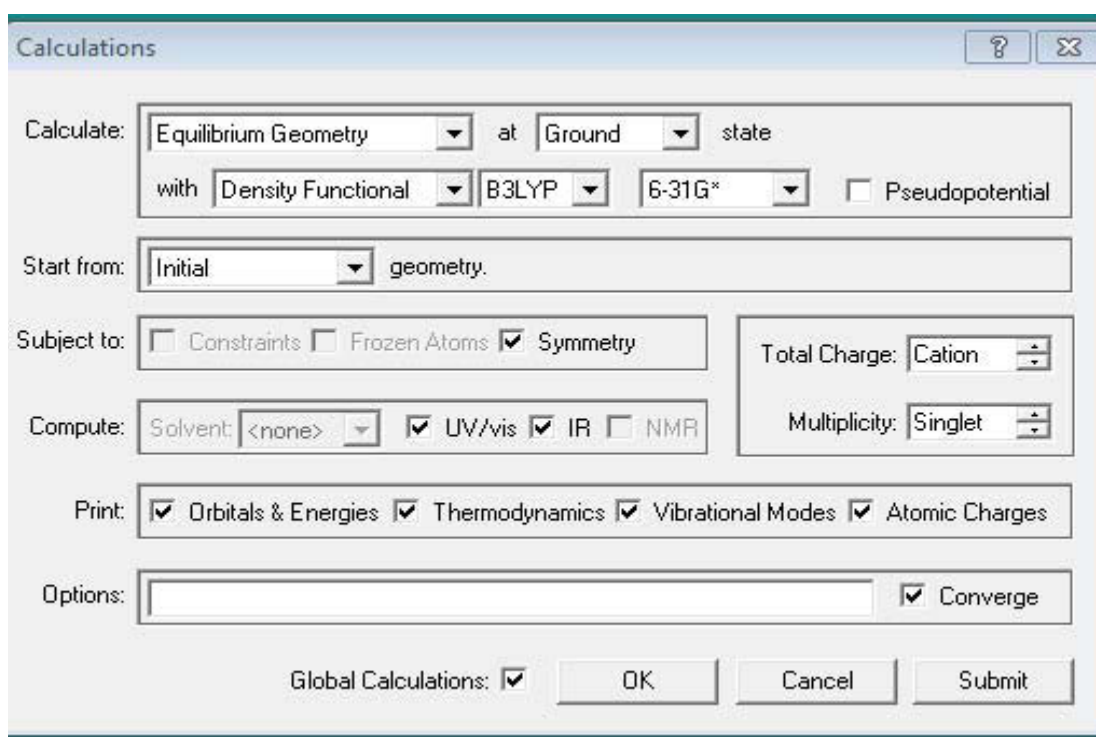


Figure B.1 Example of Spartan '04 Calculations Prompt Box

After clicking submit and naming the file, the molecule will undergo the theoretical calculations according to the basis set and other parameters that were selected. Upon completion of the successful run, the output of the process can be observed by choosing “display” then “output.” The document that appears provides all of the

necessary information to perform any theoretical calculative analysis on the molecule of interest. For the simplicity of this thesis, I will only provide images of the molecules built before the run using minimized energy and then after the runs from both the Hartree-Fock and Density Functional calculations. The pictures below were taken directly from the Spartan '04 computer program and were only manipulated by including the numbering of bonds corresponding to those in Chapter 3 of this thesis. For simplicity, only the minimized energy form of each complex will be shown below since bond numbering does not change after performance of calculations.

Works Cited

1. Etter, M.C. Encoding and Decoding Hydrogen-Bond Patterns of Organic Compounds. *Acc. Chem. Res.* 1990, 23, 120-126.
2. Abraham, R.J.; Aboitiz, N.; Merrett, J.; Sherborne, B.; Whitcombe, I. Conformational analysis. Part 34. An NMR investigation of the conformational equilibrium and intramolecular hydrogen bonding in nipecotic acid derivatives. *J. Chem. Soc., Perkin Trans.* 2000, 2, 2382-2392.
3. Perrin, C.L.; Burke, K.D. Variable-Temperature Study of Hydrogen-Bond Symmetry in Cyclohexene-1,2-dicarboxylate Monoanion in Chloroform-d. *J. Am. Chem. Soc.* 2014, 136, 4355-4362.
4. Sá Barreto, F.C. Ferroelectric phase transitions and the Ising model. *Braz. J. Phys.* 2000, 30 (4), 778-782.
5. Carey, F.A. *Organic Chemistry*. 7th Ed. New York: McGraw Hill Higher Education, 2008. 790-821.
6. Reed, C.A. Myths about the Proton. The Nature of H⁺ in Condensed Media. *Acc. Chem. Res.* 2013, A-I.
7. Doan, V.; Koppe, R.; Kasai, P.H. Dimerization of Carboxylic Acids and Salts: An IR Study in Perfluoropolyether Media. *J. Am. Chem. Soc.* 1997, 119, 9810-9815.
8. Chaudhari, S.R.; Suryaprakash, N. Probing acid-amide intermolecular hydrogen bonding by NMR spectroscopy and DFT calculations. *J. Mol. Struct.* 2012, 1016, 163-168.
9. Walsh, P.L.; Maverick, E.; Chiefari, J.; Lightner, D.A. Acid-Amide Intermolecular Hydrogen Bonding. *J. Am. Chem. Soc.* 1997, 119, 3802-3806.
10. Meyer, J.S.; Quenzer, L.F. *Psychopharmacology: Drugs, the Brain, and Behavior*. 2nd Ed. Sunderland, MA: Sinauer Associates, Inc. 2013. 4-7, 21-22, 25-28.
11. Remenar, J.F.; Morissette, S.L.; Peterson, M.L.; Moulton, B.; MacPhee, J.M.; Guzman, H.R.; Almarsson, O. Crystal Engineering of Novel Cocrystals of a Triazole Drug with 1,4-Dicarboxylic Acids. *J. Am. Chem. Soc.* 2003, 125, 8456-8457.
12. Su, H-F.; Xue, L.; Li, Y-H.; Lin, S-C.; Wen, Y-M.; Huang, R-B.; Xie, S-Y.; Zheng, L-S. Probing Hydrogen Bond Energies by Mass Spectrometry. *J. Am. Chem. Soc.* 2013, 135, 6122-6129.

13. Blanksby, S.J.; Barney Ellison, G. Bond Dissociation Energies of Organic Molecules. *Acc. Chem. Res.* 2003, 36, 255-263.
14. Yang, X.; Ong, T.C.; Michaelis, V.K.; Heng, S.; Huang, J.; Griffin, R.G.; Myerson, A.S. Formation of organic molecular nanocrystals under rigid confinement with analysis by solid state NMR. *Cryst. Eng. Comm.* 2014, 16, 9345-9352.
15. Choi, S-S.; Ko, J-E. Dimerization reactions of amino acids by pyrolysis. *J. Anal. Appl. Pyrolysis.* 2010, 89, 74-86.
16. Wolfs, I.; Desseyn, H.O. Hydrogen bond patterns in solid state carboxylic acids. Vibrational study of the hydrogen bond patterns in oxamic, malonamic and succinamic acid. *Spectrochim. Acta, Part A.* 1995, 51, 1601-1615.
17. Nandi, C.K.; Hazra, M.K.; Chakraborty, T. Vibrational coupling in carboxylic acid dimers. *J. Chem. Phys.* 2005, 123, (124310) 1-7.
18. Kibet, J.K.; Khachatryan, L.; Dellinger, B. Molecular Products from the Thermal Degradation of Glutamic Acid. *J. Agri. Food Chem.* 2013, 61, 7696-7704.
19. Manning, M.C.; Patel, K.; Borchardt, R.T. Stability of protein pharmaceuticals. *Pharm. Res.* 1989, 6, 903-907.
20. He, L.J.; Fan, J.F.; Tang, M. DFT Study of Gaseous Conformers of Aspartic Acid. *J. Theor. Comput. Chem.* 2010, 9 (III), 687-700.
21. Voet, D.; Voet, J.; Pratt, C. *Fundamentals of Biochemistry.* Third Edition. 2008. Wiley. Print.
22. Shogren, R.L.; Willett, J.L.; Westmoreland, D.; Gonzalez, S.O.; Doll, K.M.; Swift, G. Properties of copolymers of aspartic acid and aliphatic dicarboxylic acids prepared by reactive extrusion. *J. Appl. Polym. Sci.* 2008, 110 (6), 3348-3354.
23. Wu, H.; Reeves-McLaren, N.; Jones, S.; Ristic, R.I.; Fairclough, J.P.A.; West, A.R. Phase Transformations of Glutamic Acid and Its Decomposition Products. *Cryst. Growth Des.* 2010, 10, 988-994.
24. Goldberg, V.M.; Lomakin, S.M.; Todinova, A.V.; Shchegolikhin, A.N.; Varfolomeev, S.D. Regulation of Solid-Phase Polycondensation of L-Aspartic Acid. *Dokl. Phys. Chem.* 2009, 429, 252-254.
25. Goldberg, V.M.; Todinova, A.V.; Shchegolikhin, A.N.; Varfolomeev, S.D. Kinetic Parameters for Solid Phase Polycondensation of L-Aspartic Acid:

- Comparison of Thermal Gravimetric Analysis and Differential Scanning Calorimetry Data. *Polym. Sci.* 2011, 53 (I-II), 10-15.
26. Bandarupalli, P.K. Thermal Analysis of Decomposition Reactions of Aspartic and Glutamic Acids in Potassium Chloride Matrix. MS Thesis. Youngstown State University (1424), 2013. Print.
 27. Kovacs, J.; Nagy Kovacs, H.; Konyves, I.; Csaszar, J.; Vajda, T.; Mix, H. Chemical Studies of Polyaspartic Acid. University of Budapest, 1961, 26, 1084-1091.
 28. Heaton, A.L.; Armentrout, P.B. Thermodynamics and Mechanism of the Deamidation of Sodium-Bound Asparagine. *J. Am. Chem. Soc.* 2008, 130, 10227-10232.
 29. Sang-aroon, W.; Ruangpornvisuti, V. Conformational study of cationic, zwitterionic, anionic species of aspartic acid, water-added forms and their protonation. A DFT method. *J. Mol. Struct.: Thermochem.* 2006, 758, 181-187.
 30. Lehmann, M.S.; Koetzle, T.F.; Hamilton, W.C. Precision neutron diffraction structure determination of protein and nucleic acid components. VIII: the crystal and molecular structure of the β -form of the amino acid L-glutamic acid. *J. Cryst. Mol. Struct.* 1972, 2, 225-233.
 31. Wu, H.; Reeves-McLaren, N.; Pokorny, J.; Yarwood, J.; West, A.R. Polymorphism, Phase Transitions, and Thermal Stability of L-Pyroglutamic Acid. *Cryst. Growth Des.* 2010, 10, 3141-3148.
 32. Heaton, A.L.; Moision, R.M.; Armentrout, P.B. Experimental and Theoretical Studies of Sodium Cation Interactions with the Acidic Amino Acids and Their Amide Derivatives. *J. Phys. Chem. A.* 2008, 112, 3319-3327.
 33. Heaton, A.L.; Ye, S.J.; Armentrout, P.B. Experimental and Theoretical Studies of Sodium Cation Complexes of the Deamidation and Dehydration Products of Asparagine, Glutamine, Aspartic Acid, and Glutamic Acid. *J. Phys. Chem A.* 2008, 112, 3328-3338.
 34. Van Holst, J.; Kersten, S.R.A.; Hogendoorn, K.J.A. Physicochemical Properties of Several Aqueous Potassium Amino Acid Salts. *J. Chem. Eng. Data.* 2008, 53, 1286-1291.
 35. Dunbar, R.C.; Steill, J.D.; Oomens, J. Encapsulation of Metal Cations by the PhePhe Ligand: A Cation- π Ion Cage. *J. Am. Chem. Soc.* 2011, 133, 9376-9386.
 36. Citir, M.; Hinton, C.S.; Oomens, J.; Steill, J.D.; Armentrout, P.B. Infrared Multiple Photon Dissociation Spectroscopy of Cationized Histidine: Effects of

- Metal Cation Size on Gas-Phase Conformation. *J. Phys. Chem. A.* 2012, 116, 1532-1541.
37. Swiderski, G.; Wojtulweski, S.; Kalinowska, M.; Swislocka, R.; Lewandowski, W. Effect of alkali metal ions on the pyrrole and pyridine π -electron systems in pyrrole-2-carboxylate and pyridine-2-carboxylate molecules: FT-IR, FT-Raman, NMR and theoretical studies. *J. Mol. Struct.* 2011, 993, 448-458.
 38. Atkins, P.; de Paula, J. *Physical Chemistry*. 9th Ed. New York: W.H. Freeman and Company, 2010. 54-65, 524-550, 700-701. Print.
 39. *Raman Spectroscopy Basics*. Princeton Instruments. 1-5.
 40. Harris, D.C. *Quantitative Chemical Analysis*. 8th Ed. New York: W.H. Freeman and Company, 2010. 515-518. Print.
 41. *Raman Knowledge: Theory of Raman Scattering, Components of a Raman Spectrometer*. B&W Tek Inc., 2014.
 42. Carey, P.R. *Biochemical Applications of Raman and Resonance Raman Spectroscopies*. New York: Academic Press, 1982. 48-57. Print.
 43. Colthup, N.B.; Daly, L.H.; Wiberley, S.E. *Introduction to Infrared and Raman Spectroscopy*. 2nd Ed. New York: Academic Press, 1975. 111-114, 365-370. Print.
 44. *Introduction to Fourier Transform Infrared Spectrometry*. Thermo Nicolet Corporation. 2001, 1-8.
 45. Smith, B.C. *Fundamentals of Fourier Transform Infrared Spectroscopy*. 2nd Ed. Taylor and Francis Group, LLC: CRC Press, 2011. 8-23, 56-57, 66. Print.
 46. Dutrow, B.L.; Clark, C.M. *X-ray Powder Diffraction (XRD)*. *Geochemical Instrumentation and Analysis*. 1-2.
 47. Fultz, B.; Howe, J. *Transmission Electron Microscopy and Diffractometry of Materials*, Graduate Texts in Physics. Springer. 2013. 1-12, 21-30, 48.
 48. Grebenkemper, J. *Powder X-ray Diffraction*. UC Davis ChemWiki. 1-3.
 49. Hehre, W.J. *A Guide to Molecular Mechanics and Quantum Chemical Calculations*. Print, 17-52.
 50. Hesse, M.; Meier, H.; Zeeh, B. *Spectroscopic Methods in Organic Chemistry*. New York: Georg, Thieme, Verlag, Stuttgart, 1997. 48-55, 66-67, 136-141. Print.

51. Sang-aroon, W.; Ruangpornvisuti, V. Conformational Analysis of Alkali Metal Complexes of Aspartate Dianion and Their Interactions in Gas Phase. *J. Mol. Graphics Modell.* 2007, 26, 342-351.
52. Jiang, W.; Tiefenbacher, K.; Ajami, D.; Rebek Jr., J. Complexes within Complexes: Hydrogen Bonding in Capsules. *Chem. Sci.* 2012, 3, 3022-3025. And *J. R. Soc. Chem.* 2012, S1-S18.
53. Efimov, A.V.; Brazhnikov, E.V. Relationship between intramolecular hydrogen bonding and solvent accessibility of side-chain donors and acceptors in proteins. *FEBS Lett.* 2003, 554, 389-393.
54. Wuthrich, K.; Shulman, R.G.; Peisach, J. High-Resolution Proton Magnetic Resonance Spectra of Sperm Whale Cyanometmyoglobin. *Proc. Natl. Acad. Sci. U.S.A.* 1968, 60, 373-380.
55. Shipman, S.T.; Douglass, P.C.; Yoo, H.S.; Hinkle, C.E.; Mierzejewski, E.L.; Pate, B.H. Vibrational dynamics of carboxylic acid dimers in gas and dilute solution. *Phys. Chem. Chem. Phys.* 2007, 9, 4572-4586.
56. Miller, D.B.; Spence, D, J. Clinical Pharmacokinetics of Fibric Acid Derivatives (Fibrates). *Clin. Pharmacokinet.* 1998, 34, 2, 155-162.
57. FIELD study investigators. Effects of long-term fenofibrate therapy on cardiovascular events in 9795 people with type 2 diabetes mellitus (the FIELD study): randomized controlled trial. *Lancet.* 2005, 366, 1849-1861.
58. Benitta, T. Asenath; Balendiran, G. K.; James, C. Vibrational Spectral Studies of Gemfibrozil. *AIP Conf. Proc.* 2008, 1075, 218.
59. Shah, I.; Barker, J.; Barton, S.J.; Naughton, D.P. A Novel Method for Determination of Fenofibric Acid in Human Plasma using HPLC-UV: Application to a Pharmacokinetic Study of New Formulations. *J. Anal. Bioanal. Tech.* S12, 1-4.
60. Rath, N.P.; Haq, W.; Balendiran, G.K. Fenofibric acid. *Acta. Cryst.* 2005, 61, 81-84.
61. Balendiran, G.K.; Rath, N.; Kotheimer, A.; Miller, C.; Zeller, M.; Rath, N.P. Biomolecular Chemistry of Isopropyl Fibrates. *J. Pharm. Sci.* 2012, 101 (4), 1555-1569.
62. Structure Determinations of IR and NMR Spectroscopy. *Sustain Chemistry.* 1-20.
63. Edwards, J.C. Principles of NMR. Process NMR Associates, LLC. 1998-2008.

64. Gottlieb, H.E.; Kotlyar, V.; Nudelman, A. NMR Chemical Shifts of Common Laboratory Solvents as Trace Impurities. *J. Org. Chem.* 1997, 62, 7512-7515.
65. McConnell, H.M. Reaction Rates by Nuclear Magnetic Resonance. *J. Chem. Phys.* 1958, 28, 3, 430-431.
66. Chen, J-S.; Shirts, R.B. Iterative Determination of the NMR Monomer Shift and Dimerization Constant in a Self-Associating System. *J. Phys. Chem.* 1985, 89, 1643-1646.
67. Mora, A.J.; Avila, E.E.; Delgado, G.E.; Fitch, A.N.; Brunelli, M. Temperature effects on the hydrogen-bond patterns in 4-piperidinecarboxylic acid. *Acta. Cryst.* 2005, 61, 96-102.
68. Balendiran, G.K.; Sawaya, M.R.; Schwarz, F.P.; Ponniah, G.; Cuckovich, R.; Verma, M.; Cascio, D. The Role of Cys-298 in Aldose Reductase Function. *J. Biol. Chem.* 2011, 286, 8, 6336-6344.
69. Zvereva, E.E.; Vandyukova, I.I.; Vandyukov, A.E.; Katsyuba, S.A.; Khamatgalimov, A.R.; Kovalenko, V.I. IR and Raman spectra, hydrogen bonds, and conformations of N-(2-hydroxyethyl)-4,6,-dimethyl-2-oxo-1,2-dihydropyrimidine (drug Xymedone). *Russ. Chem. Bull. Int'l Ed.* 2012, 61 (VI), 1199-1206.
70. Brougham, D.F.; Horsewill, A.J.; Ikram, A.; Ibberson, R.M.; McDonald, P.J.; Pinter-Krainer, M. The correlation between hydrogen bond tunnelling dynamics and the structure of benzoic acid dimers. *J. Chem. Phys.*, 1996, 105, 979-982.
71. Demsar, A.; Kosmrlj, J.; Petricek, S. Variable-Temperature Nuclear Magnetic Resonance Spectroscopy Allows Direct Observation of Carboxylate Shift in Zinc Carboxylate Complexes. *J. Am. Chem. Soc.* 2002, 124, 3951-3958.
72. Tensmeyer, L.G.; Ainsworth, C. Proton Magnetic Resonance Studies of Pyrazoles. 1966, 31, 1878-1883.
73. Denisov, G.S.; Gindin, V.A.; Golubev, N.S.; Ligay, S.S.; Shchepkin, D.N.; Smimov, S.N. NMR study of proton location in strongly hydrogen bonded complexes of pyridine as influenced by solvent polarity. *J. Mol. Liq.* 1995, 67, 217-234.
74. Watterson, S.; Hudson, S.; Svard, M.; Rasmuson, A.C. Thermodynamics of fenofibrate and solubility in pure organic solvents. *Fluid Phase Equilib.* 2014, 367, 143-150.
75. Naito, M.; Souda, H.; Koori, H.; Komiya, N.; Naota, T. Binuclear *trans*-Bis(β -iminoaryloxy)palladium (II) Complexes Doubly Linked with Pentamethylene

- Spacers: Structure-Dependent Flapping Motion and Heterochiral Association Behavior of the Clothespin-Shaped Molecules. *Chem. Eur. J.* 2014, 20, 6991-7000.
76. Castilla, A.M.; Conn, M.M.; Ballester, P. Synthesis and binding studies of two new macrocyclic receptors for the stereoselective recognition of dipeptides. *Beilstein J. Org. Chem.* 2010, 6 (5), 1-15.
 77. Kimtys, L.L.; Balevicius, V.J. Self-Association of Carboxylic Acids As Studied by ¹H NMR Spectroscopy. *Adv. Mol. Rel. and Int. Proc.* 1979, 15, 151-161.
 78. Kimtys, L.; Mikulskis, P. A Proton Magnetic Resonance Study of Hydrogen Bonding and Self-Association Processes of Trimethylacetic Acid. *J. Magn. Reson.* 1975, 20, 475-483.
 79. Ajami, D.; Tolstoy, P.M.; Dube, H.; Odermatt, S.; Koeppe, B.; Guo, J.; Limbach, H.-H.; Rebek Jr.; J. Encapsulated Carboxylic Acid Dimers with Compressed Hydrogen Bonds. *Angew. Chem. Int. Ed.* 2011, 50, 528-531.
 80. Alvarado, E. *Vnmrj Training Guide*. University of Michigan. 2011, 1-23.
 81. *Glas-Col: Tools for Scientists. Inflatable Glove Chamber with Handy-Glide Closure*. 2008.
 82. Vicic, D.A.; Jones, G.D. *Experimental Methods and Techniques: Basic Techniques. (NMR Spectroscopy of Air-Sensitive Compounds, Glovebag and Glovebox Techniques)*. 2007, 210-214.
 83. *Use of Variable Temperature on Bruker NMR Spectrometers*. 2013, 1-6.
 84. Wei, Y. *1D Proton NMR on Bruker NMR*. Rockefeller University. 1-16.
 85. Miller, Chad. *Characterization of Novel Aldose Reductase Inhibitors and Their Binding Modes Using Spectroscopic and Computational Methods*. MS Thesis. Youngstown State University (1207), 2010. Print.
 86. Kotheimer, Amanda. *Design, Synthesis, and Characterization of Novel Chiral Inhibitors for Aldose Reductase*. MS Thesis. Youngstown State University (1245), 2010. Print.
 87. Roux, M.V.; Foces-Foces, C.; Notario, R.; Ribeiro da Silva, M.A.V.; Ribeiro da Silva, M.D.M.C.; Santos, A.F.L.O.M.; Juaristi, E. Experimental and Computational Thermochemical Study of Sulfur-Containing Amino Acids: L-Cysteine, L-Cystine, and L-Cysteine-Derived Radicals, S-S, S-H, and C-S Bond Dissociation Enthalpies. *J. Phys. Chem. B.* 2010, 114, 10530-10540.

88. Amaral, L.M.P.F.; Freitas, V.L.S.; Goncalves, J.F.R.; Barbosa, M.; Chickos, J.S.; Ribeiro da Silva, M.D.M.C. The influence of the hydroxy and methoxy functional groups on the energetic and structural properties of naphthaldehyde as evaluated by both experimental and computational methods. *Struct. Chem.* 2015, 26, 137-149.
89. Atwater, W.O.; Snell, J.F. Description of a Bomb-Calorimeter and Method of its Use. *J. Am. Chem. Soc.* 1903, XXV (7), 659-699.
90. Introduction to Bomb Calorimetry. Parr Instrument Company. 2007.
91. Muthurajan, H.; Sivabalan, R.; Talawar, M.B.; Anniyappan, M.; Venugopalan, S. Prediction of heat of formation and related parameters of high energy materials. *J. Hazard. Mater. A.* 2006, 133, 30-45.
92. Garland, C.W.; Nibler, J.W.; Shoemaker, D.P. *Experiments in Physical Chemistry.* McGraw-Hill. 2003, 7th edition, 145-151.
93. Dickinson, H.C. *Bull. Natl. Bur. Stand.* 1914, 11, 189.
94. Sharma, R.K.; Chan, W.G.; Hajaligol, M.R. Product compositions from pyrolysis of some aliphatic α -amino acids. *J. Anal. Appl. Pyrolysis.* 2006, 75, 69-81.
95. Chiavari, G.; Galletti, G.C. Pyrolysis-gas chromatography/mass spectrometry of amino acids. *J. Anal. Appl. Pyrolysis.* 1992, 24, 123-137.
96. Rozenberg, M.Sh. IR spectra and hydrogen bond energies of crystalline acid salts of carboxylic acids. *Spectrochim. Acta, Part A.* 196, 52, 1559-1563.
97. Yang, X.W.; Liu, J.R.; Gao, S.L.; Hou, Y.D.; Shi, Q.Z. Determination of combustion energies of thirteen amino acids. *Thermochim. Acta.* 1999, 329, 109-115.
98. Simmonds, P.G.; Medley, E.E.; Ratcliff Jr., M.A.; Shulman, G.P. Thermal Decomposition of Aliphatic Monoamino Monocarboxylic Acids. *Anal. Chem.* 1972, 44, 2060-2066.
99. Rodante, F.; Marrosu, G.; Catalani, G. Thermal analysis of some α -amino acids with similar structures. *Thermochim. Acta.* 1992, 194, 197-213.
100. Ratcliff Jr., M.A.; Medley, E.E.; Simmonds, P.G. Pyrolysis of Amino Acids. Mechanistic Considerations. *J. Org. Chem.* 1974, 39 (11), 1481-1490.

101. Li, J.; Wang, Z.; Yang, X.; Hu, L.; Liu, Y.; Wang, C. Evaluate the pyrolysis pathway of glycine and clycylclysine by TG-FTIR. *J. Anal. Appl. Pyrolysis*. 2007, 80, 247-253.
102. Gil, A.; Simon, S.; Rodriguez-Santiago, L.; Bertran, J.; Sodupe, M. Influence of the Side Chain in the Structure and Fragmentation of Amino Acids Radical Cations. *J. Chem. Theory Comput.* 2007, 3, 2210-2220.
103. Alexandrova, A.N.; Jorgensen, W.L. On the Mechanism and Rate of Spontaneous Decomposition of Amino Acids. *J. Phys. Chem. B.* 2011, 115, 13624-13632.
104. Stover, M.L.; Jackson, V.E.; Matus, M.H.; Adams, M.A.; Cassady, C.J.; Dixon, D.A. Fundamental Thermochemical Properties of Amino Acids: Gas-Phase and Aqueous Acidities and Gas-Phase Heats of Formation. *J. Phys. Chem. B.* 2012, 116, 2905-2916.
105. Yablokov, V.A.; Vasina, Ya.A.; Zelyaev, I.A.; Mitrofanova, S.V. Kinetics of Thermal Decomposition of Sulfur-Containing Amino Acids. *Russ. J. Gen. Chem.* 2009, 6, 1141-1145.
106. Rodante, F.; Marrosu, G.; Catalani, G. Thermal analysis of different series of dipeptides. *Thermochim. Acta.* 1992, 197, 147-160.
107. The Enthalpy of Formation of Camphor by Bomb Calorimetry. Colby College. PDF, 1-8.
108. Mao, R.; Tang, J.; Swanson, B.G. Texture properties of high and low acyl mixed gellan gels. *Carbohydr. Polym.* 2000, 41, 331-338.
109. Kelcogel Gellan Gum. CPKelco: A Huber Company. Applied Bioscience Consultants and Distributors. 2007, 5th edition, 1-28.
110. Wang, H. H. Cellulose and Pulp. *Forests and Forest Plants (Vol. II). Encyclopedia of Life Support Systems.*
111. Rocha, I.M.; Galvao, T.L.P.; Sapei, E.; Ribeiro da Silva, M.D.M.C.; Ribeiro da Silva, M.A.V. Levoglucosan: A Calorimetric, Thermodynamic, Spectroscopic, and Computational Investigation. *J. Chem. Eng. Data.* 2013, 58, 1813-1821.
112. Lewis, B.A. Starch. *Encyclopedia of Food and Culture.* The Gale Group Inc. Encyclopedia.com. 2003, 1-2.
113. Ribeiro da Silva, M.A.V.; Lobo Ferreira, A. I.M.C.; Cimas, A. Experimental and Computational Study on the Molecular Energetics of Benzyloxyphenol Isomers. *J. Chem. Thermodyn.* 2011, 43, 1857-1864.

114. Ribeiro da Silva, M.A.V.; Ferrao, M.L.C.C.H.; Alves da Silva, A.M.R.O. Standard molar enthalpies of formation of three branched alkyl carboxylic acids. *J. Chem. Thermodyn.* 1999, 31, 1129-1134.
115. Galvao, T.L.P.; Rocha, I.M.; Sapei, E.; Ribeiro da Silva, M.D.M.C.; Ribeiro da Silva, M.A.V. Energetic Study of 4(3H)-Pyrimidinone: Aromaticity of Reactions, Hydrogen Bond Rules, and Support for an Anomeric Effect. *J. Phys. Chem. A.* 2014, 118, 3360-3366.
116. Santos, A.F.L.O.M.; Ribeiro da Silva, M.A.V. Experimental and Computational Study on the Molecular Energetics of 2-Pyrrolicarboxylic Acid and 1-Methyl-2-pyrrolicarboxylic Acid. *J. Phys. Chem. A.* 2009, 113, 9741-9750.
117. Lobo Ferreira, A. I.M.C.; Ribeiro da Silva, M.A.V. Thermochemical Study of Three Dibromophenol Isomers. *J. Chem. Thermodyn.* 2011, 43, 227-234.
118. Leskiw, B.D.; Mettee, H.D. Experiment 6: Heats of Combustion. *Physical Chemistry Laboratory*. McGraw-Hill, 2012. Print.
119. Enthalpy of Combustion via Calorimetry. *Physical Chemistry (chem 75)*. Trustees of Dartmouth College. 2010.